THE UNIVERSITY *of* EDINBURGH

The role of the Neurofascins in targeting voltage-gated sodium channels in myelinated nerves

Ao Zhang

Ph.D.

University of Edinburgh

Centre for Neuroregeneration

2013

DECLARATION

I declare that this thesis and the work described in it are my own except where indicated and have not been submitted for any other degree.

Ao Zhang
Aug 14, 2013

ACKNOWLEDGEMENTS

I would like to thank my supervisor, Professor Peter J. Brophy for his support and excellent supervision over the course of this work. I am very grateful for all past and current members of the Brophy lab for helpful discussions, outstanding advice and technical assistance, particularly Dr. Barbara Zonta and Dr. Anne Desmazieres. I also express my gratitude to Diane Sherman, Matthew Grove, Qiushi Li, Stuart Fleming, Heather Anderson and Veronica Brivio for help and encouragement.

Special thanks also go to Dr. Liliana Minichiello for the discussions of my animal works and Professor David Price for guiding me on the study of the development of cerebellum.

I thank The China Scholarship Council (CSC) for funding my PhD work. Finally, I want to thank my family for giving me the freedom and support to pursue my dreams in life.

LIST OF FIGURES

LIST OF TABLES

ABBREVIATIONS

AIS	Axon Initial Segment
bp	base pairs
CAP	compound action potential
CAM	Cell-adhesion molecule
cDNA	complementary DNA
CNS	Central nervous system
CPN	cerebellar plate neuroepithelium
d	days
DIV	Days *in vitro*
DTT	Dithiothreitol
EDTA	Ethylene diamine tetracetic acid
ES	Embryonic day
FITC	Fluorescein isothiocyanate
h	hour
HCl	Hydrochloric acid
HRP	Horseradish peroxidase
Ig	Immunoglobulin
kb	kilobases
kD	kiloDalton
K_v	Voltage-gated potassium channels
K^+	potassium ion
LB	Luria-Bertani medium
mA	milli-ampere
MAG	Myelin associated glycoprotein
MBP	Myelin Basic Protein
min	minutes
mm	millimeter
mM	millimolar
mRNA	messenger RNA
MS	Multiple sclerosis
Na^+	sodium ion
Na_v	Voltage-gated sodium channels
NF	Neurofilament
Nfasc	Neurofascin
ng	nanogram
NTZ	and nuclear transitory zone
OCT	Optimal cutting temperature
OSP	Oligodendrocyte specific protein
P	Post-natal day
P0	Myelin protein zero
PAGE	Polyacrylamide gel electrophoresis
PB	Phosphate buffer
PBS	Phosphate buffer saline
PC	Purkinje cell
PCR	Polymerase chain reaction
PFA	Paraformaldehyde

PLP	Proteolipid protein
PMSF	Phenylmethanesulphonylfluoride
PNS	Peripheral Nervous System
RLS	rhombic lip migratory stream
s	seconds
SC	Schwann cell
SDS	Sodium dodecyl sulfate
TAE	Tris-acetate-EDTA
TESPA	3'Amino propyl tri ethoxy silane
TRIS	trishydroxymethylaminomethane
TRITC	Tetramethylrhodamine isothiocyanate
µm	micron
µl	microliter
VZ	ventricular zone

Abstract

The nodes of Ranvier are short, periodical interruptions in the myelin sheath of myelinated axons, at which voltage-gated sodium channels are highly concentrated. The correct targeting of sodium channels to the nodes of Ranvier permits rapid propagation of action potentials in myelinated axons. The nodes of Ranvier contain a unique set of ion channels, cell-adhesion molecules, and cytoplasmic adaptor proteins.

Neurofascins are cell adhesion molecules of the immunoglobulin superfamily and previous work has shown they are involved in the assembly of the node of Ranvier. The *Neurofascin* (*Nfasc*) gene is subject to extensive alternative splicing. RT-PCR studies have suggested that there were several different Neurofascin (Nfasc) transcripts. Thus far, research on the Neurofascins has concentrated on two isoforms, Nfasc186 and Nfasc155, which are expressed in neurons and glia respectively. A third Neurofascin isoform, Nfasc140, lacking the Mucin domain and two of the fibronectin repeats was originally identified in the laboratory of V. Bennett. However, neither the location nor function of this protein was known.

By RT-PCR I successfully cloned the Nfasc140 cDNA and determined its domain composition, which was confirmed by a series of Western blots using domain-specific antibodies. The developmental expression of Nfasc140 revealed that it is the predominate isoform of Neurofascin during the embryonic stage. Using cell-type-specific conditional Neurofascin knock-out mice, I have also found that Nfasc140 is a neuronal isoform, like Nfasc186.

I have used transgenic mouse lines to characterize the location and function of Nfasc140. Like Nfasc186, Nfasc140 is targeted to the nodes of Ranvier and axonal initial segment. Also Nfasc140 alone can reconstitute the nodal complex in Neurofascin knock-out mice in CNS and PNS in the absence of Nfasc186 and Nfasc155. It can also partially restore the electrophysiological function of PNS nerves.

In order to address the role of the paranodes in sodium channel clustering, I generated a new neuronal-Cre-expressing transgenic line which, when bred with floxed *Nfasc* mice, generated early neuronal Neurofascin knock-out mice. Using those animals I have shown that after the ablation of all neuronal Neurofascins, when

only glial Nfasc155 is presented, sodium channels can still target to the nodes of Ranvier in both PNS and CNS. These conditional knock-out mice have a longer life span than pan-Neurofascin knock-out mice. This indicates the importance of paranodal junctions, in addition to nodal neuronal Neurofascins, in clustering sodium channels at the node.

CONTENTS

1. Introduction

1.1 Myelin and Nodes of Ranvier.

The myelin sheath is a greatly extended and modified plasma membrane of glial cells wrapped around the nerve axon (Raine et al., 1984). The non-conductive lipid-rich myelin sheath coats and thus provides insulation for the most part of the axonal surface, increasing electrical resistance and decreasing capacitance between the inside and outside of a nerve fibre (Hartline and Colman, 2007). Nodes of Ranvier are short and periodical interruptions of the myelin sheath, (Morell et al., 1999). Myelin sheaths are formed by two different glial cells: Schwann cells in the vertebrate peripheral nervous system (PNS), named after the German physiologist Theodor Schwann; their counterparts in the central nervous system (CNS) are the oligodendrocytes, first described as mesoglia by William Ford Robertson, an Edinburgh pathologist Dr W.F. Robertson in 1899 (Robertson, 1900). Myelination is found mainly in vertebrates, but an analogous system has been discovered in a few invertebrates, for example in members of the Annelida, Arthropoda and Chordata (Roots, 2009). Not all neurons in vertebrates are myelinated; for example, axons of the neurons comprising the autonomous nervous system are not, in general, myelinated (Simons et al., 2007). Nodes of Ranvier are regularly spaced along the length of myelinated nerve fibres, and enable saltatory conduction in which action potentials appear to "jump" from node to node. Myelin and nodes of Ranvier have allowed the development of complex nervous systems with rapid impulse propagation resulting in, among other things, more rapid and sustained responses in a predator-and-prey environment (Hartline and Colman, 2007; Nave et al., 2010).

1.2 Electrophysiology of axon

1.2.1 Ion Channels and action potential

The action potential (Fig. 1) is a short-lasting event in which the electrical transmembrane potential rapidly rises and falls, following a consistent trajectory. This was first measured in unmyelinated giant axons of squids by Hodgkin & Huxley

(1939). Along the axon a voltage difference between the interior and the exterior of the cell, known as the membrane potential (resting), is established and maintained by sodium-potassium ATP-dependent pumps. The ATP-dependent pumps concentrate Na^+ outside and K^+ inside. Na_v channels possess a sensor mechanism that detects depolarization in transmembrane voltage. Synaptic inputs to a neuron triggering this sensor and promote Na_v opening, and Na^+ flow inward causing membrane depolarization. When membrane depolarization reaches the threshold, a rapid recruitment of Nav leads to the fast depolarizing phase of the action potential. The same raised voltage also causes the sodium channels to become inactivated. At the same time, the raised voltage opens K_v, and K^+ flowing out leads to repolarization. Combined, these changes in Na^+ and K^+ permeability cause the membrane potential to drop quickly back towards to the resting state (Hodgkin & Huxley,1939, Neher et al., 1976, Barnett et al., 2007).

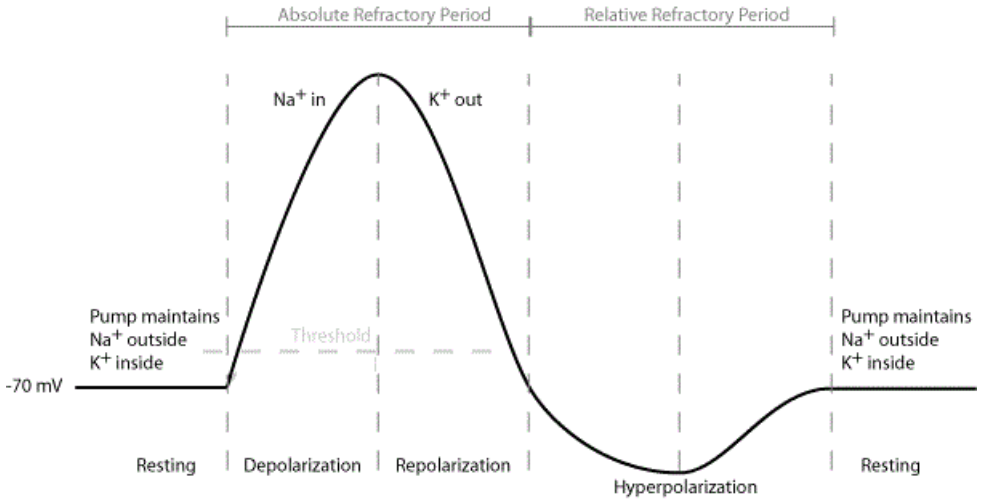

Figure 1. Schematic picture of an idealized action potential (reproduced picture from http://mcat-review.org)

The picture shows the various phases as the action potential passes a point on a cell membrane. Which includes

1. Resting: cell at rest, sodium-potassium pump maintaining resting potential.
2. Depolarization: sodium channels open, positive sodium rushes inside, membrane potential shoots up.
3. Repolarization: potassium channels open, sodium channels close, positive potassium rushes outside, membrane potential drops back down.
4. Hyperpolarization: potassium channels doesn't close fast enough, so the membrane potential actually drops below the resting potential for a

bit.

5. Refractory period: the sodium-potassium pump works to re-establish the original resting state .

1.2.2 Electrophysiology of axon

Nerve conduction velocity depends critically on axon diameter and myelination. Larger diameter axons have a greater total volume for charges to flow through with correspondingly less resistance from the membrane (Arbuthnott et al., 1980).In unmyelinated axons, studies also suggest that conduction velocity can be mediated in other ways. For moderate discharge rates, the conduction speed is determined by the dynamic equilibrium between the slowing effect of cumulative sodium channel inactivation and the speeding effect of Na^+–K^+-ATPase-mediated hyperpolarization (Rang & Ritchie, 1968, Gordon et al. 1990, Morita et al. 1993, Kobayashi et al. 1997, De Col et al., 2008).

In myelinated axons the conduction velocity is affected by the myelin sheath. The myelin sheath wraps around the axon to form a high resistance insulating membrane. Thus, the local currents are unable to leak across the membrane because of the insulating myelin, resulting in their greater penetration down the core of the axon. Action potentials cannot propagate through the membrane in myelinated segments of the axon. However, the current is carried by the axonal cytoplasm, which is sufficient to depolarize the first or second subsequent node of Ranvier. Myelination and the high densities of Na_v at the nodes of Ranvier, allow the action potential to propagate by jumping from node to node by what is called "saltatory conduction" (Huxley et al., 1949, Barnett et al., 2007,). By saltatory conduction the myelinated axon has the ability to increase the speed of conduction, and also nodal conduction results in significant economies of energy and space (Salzer et al., 1997).

1.3 Structure and functions of myelinated axons

1.3.1 Four regions of myelinated axons.

Based on morphology and protein composition, myelinated axons can be divided into four different regions. The node of Ranvier (Fig. 2 blue) is encapsulated by

microvillar processes arising from the outer collar of the Schwann cells in the PNS or by perinodal extensions from astrocytes in the CNS (Butt et al., 1994). The nodes are enriched in voltage-gated sodium channels (Na_v), a density of 25-fold of that along the internode, providing a site for the generation of the action potential (Hille, 2001). Ezrin, radixin and moesin (ERM) belong to a family of actin-binding proteins. In the PNS, the microvilli, which are enriched in ERM, express a unique perinodal matrix thought to be important in node formation and function (Scherer et al., 2011, Melendez-Vasquez et al., 2001, Salzer et al., 2008). In both PNS and CNS, the interaction of nodes of Ranvier with extracellular matrix is crucial for axon formation and myelination (Colognato et al. 2005; Chernousov et al. 2008). Gliomedin is a protein in the ECM, knockdown of Gliomedin can cause the mislocolization of new channels (Feinberg et al., 2011). And also Brevican as a member of ECM in CNS may have a role in regulating the extracellular matrix (Bekku et al., 2009).

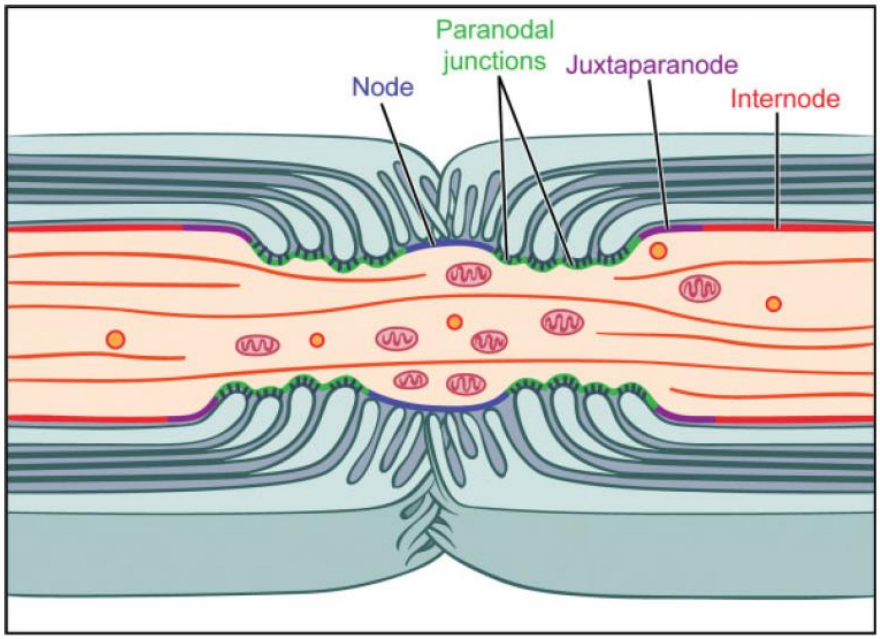

Figure 2. Organization of myelinated PNS fibers (Salzer et al., 2008).
Schematic picture showing the four different regions of a myelinated fibre. Node in the center labelled in blue, flanked by paranodal junctions labelled in green. Juxtaparanodes are in purple next to paranodal junctions. And Internodes are in red which are a continuation of the Juxtaparanode. The size of the node spans from 1–2 µm whereas the internodes can be up to (and occasionally even greater than) 1.5 millimeters long.

The paranodal axoglial junctions (Fig. 2 green) flank either side of the node. The junctions are the site of closest apposition between the myelinating cell and the axonal membranes. In longitudinal sections, a series of loops formed by the glial cells are closely lined around the axolemma; a series of transverse bands can be observed at the axoglial junctions (Peters et al., 1991). Paranodal junctions serve as a diffusion barrier between the nodal area and the juxtaparanodal regions (Fig. 2 purple). Mouse mutants which have defects in the paranodal junctions show relocalization of $K_v1.1$ and $K_v1.2$ channels towards the paranodal region and the diffusion of Na_v channels (Pillai et al., 2009, Rios et al., 2003, Bhat et al., 2011).

The juxtaparanodal regions (Fig. 2 purple), on the outer side of the paranodal junctions, are enriched in hetero-multimers composed of $K_v1.1$, $K_v1.2$, and their cytoplasmic K_v2 subunit, which may stabilize conduction and help to maintain the internodal resting potential and repolarize the membrane during an action potential; but the precise function of K_v channels remains unclear (Wang et al., 1993, Rhodes et al., 1997, Rasband et al., 1998, Zhou et al., 1998, Vabnick et al., 1999).

The segments between nodes of Ranvier are termed internodes (Fig. 2 red), and their outermost parts are in contact with the juxtaparanodal regions (Fig. 2 purple). They are the longest regions of the myelinated fibres and have a low capacitance and high transverse resistance. Compared with the high capacitive load in unmyelinated axons or poorly myelinated internodes, myelinated internodes can enhance the ability of the inward current at one node to depolarize the next nodal membrane without wasting charge and time on discharging the transmembrane capacitance (William et al., 2002).

1.3.2 Protein organization of nodes of Ranvier

To perform their function, nodes of Ranvier are composed of a unique set of molecules.

By immunofluorescent studies, various proteins have been identified at the nodes (Fig. 3A), which include scaffold protein AnkyrinG, cell adhesion molecules

NrCAM and Nfasc186, ion channels Na_v and $K_v3.1b$ and membrane skeleton protein ßIV Spectrin. Also other proteins have been found expressed at the nodal area (Fig. 3A), which include ezrin–radixin–moesin proteins, dystroglycan, proteoglycans, brain link protein 1 and tenascin-R. AnkyrinG is likely to have a very important linking role through possible interaction with other nodal proteins. Immunoprecipitation showed the interaction between Na_v and AnkyrinG which suggested Na_v channels are anchored to AnkyrinG. Mislocalization of Nfasc186, NrCAM was found in AnkyrinG knockout mice and AnkyrinG and $K_v3.1b$ have been co-immunoprecipitated (Srinivasan et al., 1988, Xu et al., 2007, Zhou et al., 1998). This suggests that all four proteins interact with AnkyrinG. AnkyrinG is missing in ßIV-Spectrin knockout mice indicating that AnkyrinG is connected to the cytoskeleton through ßIV-Spectrin (Komada et al., 2002). *In vitro,* all three ezrin–radixin–moesin proteins are expressed predominantly in Schwann cells, notably in their microvilli.

In the PNS, Schwann cell microvilli encapsulate the nodal gap. The ezrin–radixin–moesin proteins are concentrated in the nodal processes of cultured myelinating Schwann cells (Melendez-Vasquez et al., 2001). These data suggested ezrin–radixin–moesin were expressed by Schwann cell microvilli. Dystroglycan was expressed by cultured Schwann cells where it localizes to the outer membrane apposing the basal lamina. Selective deletion of Schwann cell dystroglycan resulted in slowed nerve conduction and nodal changes including reduced sodium channel density and disorganized microvilli (Saito et al., 1999, Saito et al., 2003).

In the CNS extensions from astrocytes and a specialized extracellular matrix (ECM) surround the nodes. In vitro protein expression studies and in vivo immunofluorescent studies, have suggested that the ECM is composed of three chondroitin sulfate proteoglycans (Brevican, phosphacan, and versican V2) (Bartsch et al., 1993, Xiao et al.,1997, Oohashi et al., 2002, Hedstrom et al., 2007). However, their functions at the ECM are still unclear.

At the paranodes (Fig. 3B), the proteins which have been identified by immunofluorescence are Nfasc155, Caspr and Contactin. Their detailed interactions will be explained at section 1.5.1. At the paranodes, Caspr/Contactin from the axolemma together with Nfasc155 from the glial membrane form the Nfasc155-Caspr-Contactin complex (Tait et al., 2000, Zonta etal., 2008). GST-pull down assays and immunoprecipitations showed the cytoplasmic tail of Caspr interacts with the cytoskeletal adaptor protein 4.1B (Denisenko-Nehrbas et al., 2003), providing a potential link with the actin cytoskeleton.

At the juxtaparanodal reign (Fig. 3C) the proteins which have been identified by immunofluorescence are K_v channels, Caspr2 protein 4.1B, PSD95, Tag1 and Connexin 29.

It has been shown Caspr2 binds to the N-terminal FERM domain of protein 4.1R and B through the GNP motif. Protein 4.1B clusters at paranodes and juxtaparanodes during postnatal development. Finally, Caspr2 coimmunoprecipitated with 4.1B from rat brain homogenates. These results suggest that protein 4.1B is associated with Caspr2 at juxtaparanodes, and may constitute a potential link between the paranodal and juxta-paranodal axolemma and the axonal cytoskeleton (Denisenko-Nehrbas et al., 2003). PSD-95 colocalizes precisely with Kv1 potassium channels and Caspr2 at juxtaparanodes, and a macromolecular complex of Kv1 channels and PSD-95 can be immunopurified from mammalian brain and spinal cord. The high density clustering of Kv1 channels and Caspr2 at juxtaparanodes is normal in a mutant mouse lacking juxtaparanodal PSD-95, suggesting that the indirect interaction between Kv1 channels and Caspr2 is maintained in these mutant mice. These data suggested that the primary function of PSD-95 at juxtaparanodes lies outside of its accepted role in mediating the high density clustering of Kv1 potassium channels at these sites (Rasband et al., 2002). In unmyelinated fibers, TAG-1 was still expressed by ensheathing Schwann cells; in mature myelinated fibers of the CNS and PNS, TAG-1 is localized to the juxtaparanodal region, which colocalized with K_v (Traka et al., 2002). Immunofluorescence showed Connexin 29, which localizes at the glial membrane of juxtaparanodal areas. However, its function is unknown.

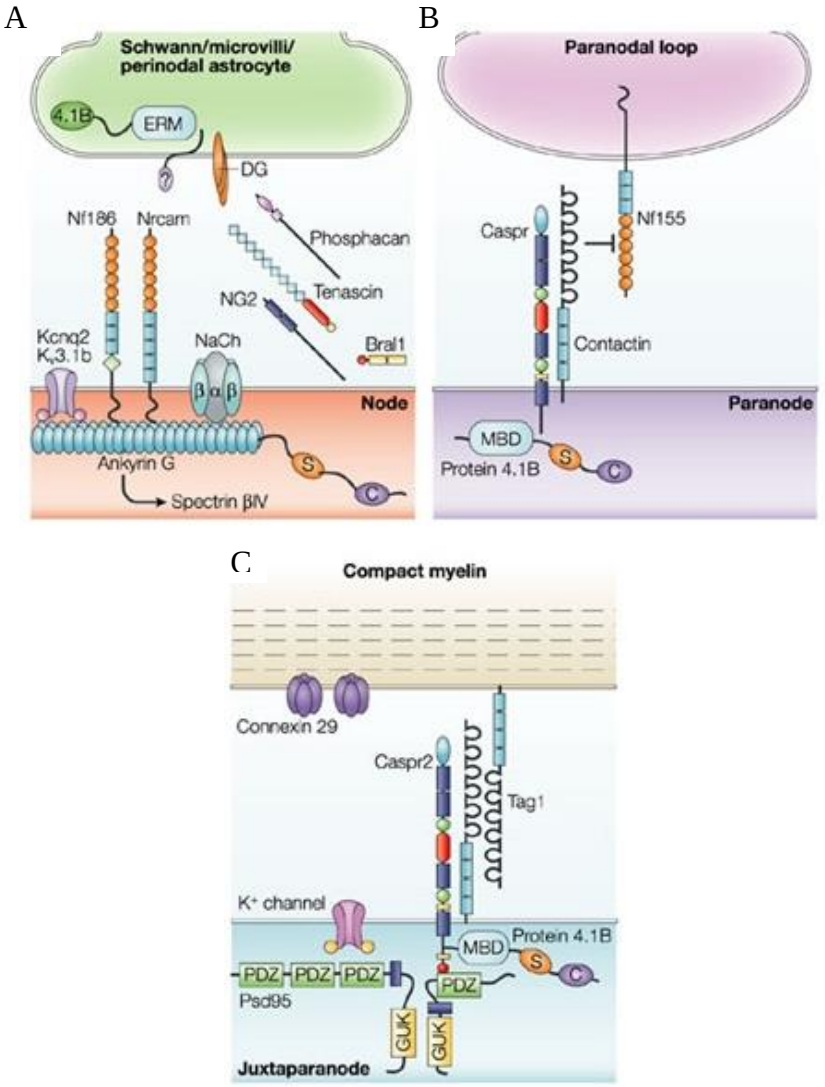

Figure 3. Schematic representation of the molecular organization of the nodal and perinodal regions of a PNS myelinated fiber. (Pictures modified from Poliak et al., 2003).

A. Nodal region in PNS and proteins which are targeted to nodal region. Microvilli of Schwann cells or perinodal astrocytes surround the nodes.
B. Paranodal region in PNS and protein compositions at the paranodes. The paranodal loops from Schwann cells wrap around paranodes.
C. Juxtaparanodal region in PNS and the protein composition at the Juxtaparanodes. Compact myelin sheath wraps around axon.

1.4 Neurofascins

1.4.1 *Neurofascin* gene and isoforms

The *Neurofascin* gene (*Nfasc*) encodes cell adhesion molecules (CAMs) of the immunoglobulin superfamily (Ig-CAMs) that can initiate and maintain the organization of the node of Ranvier. Neurofascins were initially discovered in chick as cell surface molecules involved in the promotion of neurite extension (Rathjen et al., 1987). Meanwhile, the group of Bennett found binding partners of AnkyrinG and identified high molecular mass transmembrane proteins in the nervous system termed ankyrin-binding glycoprotein (ABGP), which are now referred to as Neurofascins (Davis et al., 1993). Neurofascin was also identified in zebrafish (Voas et al., 2009). Thus, Neurofascins are widely expressed in different species.

In the mouse, the *Neurofascin* gene is composed of 34 exons distributed over 72 kilobases (Hassel et al., 1997). Each of the six immunoglobulin (IgG1-6) and five fibronectin type III (FnIIIA-E) domains is encoded by two exons. Neurofascins can also contain a Mucin domain (M). They all contain a single transmembrane region (Tm) and a cytoplasmic domain (IC) (Fig. 4A). PCR analyses showed that *Nfasc* mRNA can undergo extensive mRNA splicing. In mouse, three isoforms of Neurofascin were identified by western blot. They were Nfasc186, Nfasc155 and Nfasc140 (Davis et al., 1993) (Fig. 4B). However, only the domain compositions of Nfasc186 and Nfasc155 were reported (Tait et al., 2000) (Fig. 4A). Also the related NH_2-terminal sequences of Nfasc186, Nfasc155 and Nfasc140 indicated that they are alternatively spliced products of the same pre-mRNA (Davis et al., 1993) (Fig. 4B). Previous studies had suggested that Nfasc186 has a function in the maintenance of the protein complex structures of axo-axonic interactions but recent studies have focused on its role in the assembly of nodes and the stabilization of the protein components of the Axon Initial Segment (AIS) (Hassel et al., 1997, Sherman et al., 2005 Burkarth et al., 2007, Zonta et al., 2008, Kriebel et al., 2011, Zonta et al., 2011).

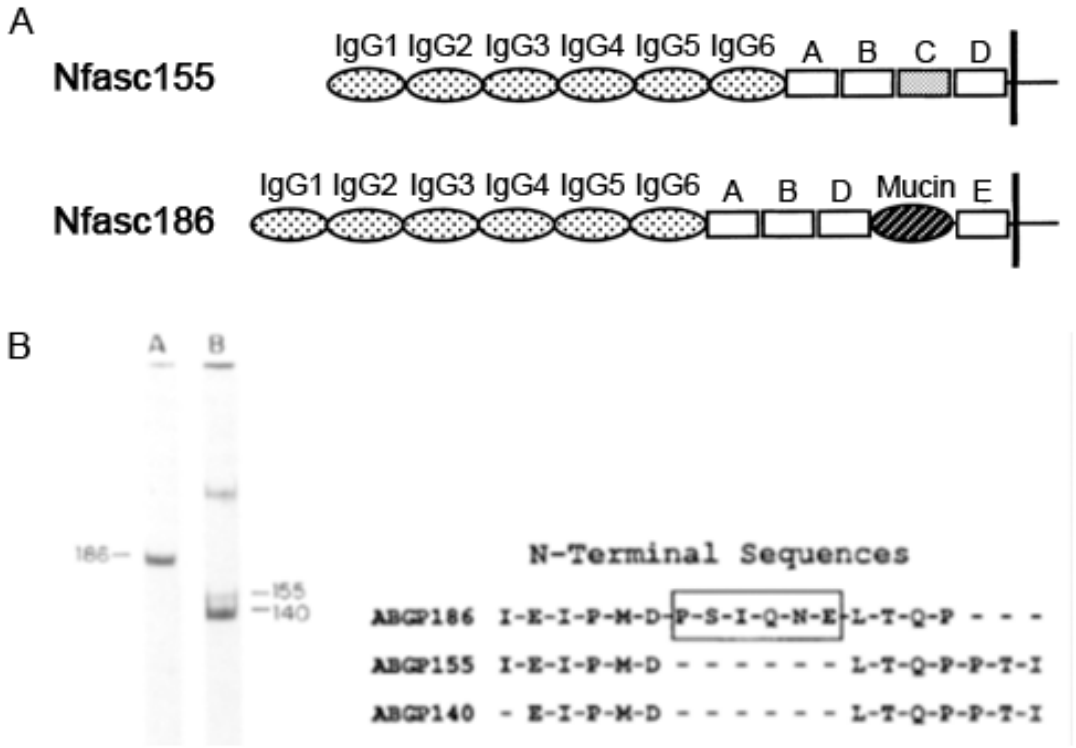

Figure 4. Different isoforms of Neurofascins in mouse (Fig. 4A is modified from Tait et al., 2000; Fig. 4B is from Davis et al., 1993).

A. Only the domain compositions of Nfasc186 and Nfasc155 were identified in rodents. Nfasc155 has a specific FnIIIC domain, Nfasc186 has Mucin and FnIIIE domains (Tait et al., 2000). The domain compositon of Nfasc140 has not been studied in the past.
B. Western blot showing the mobility of Nfasc186, Nfasc155 and Nfasc140 from rat tissue extractions (Davis et al., 1993). Their N-terminal sequences confirmed they are all Neurofascins.

Neurofascin has also been identified in chick and studies on chick suggested more isoforms of Neurofascin could be present in animal tissue. One study has suggested that there could be more than 50 different Neurofascin transcripts (Hassel et al., 1997). This could result in many different isoforms of Neurofascin proteins. However, the proteins which have been identified so far by antibodies are not so diverse. There are four different isoforms of Neurofascin proteins found in chick, Nfasc186, Nfasc180, Nfasc155 and Nfasc166 (Fig. 5) (Hassel et al., 1997, Martin et al., 2012).

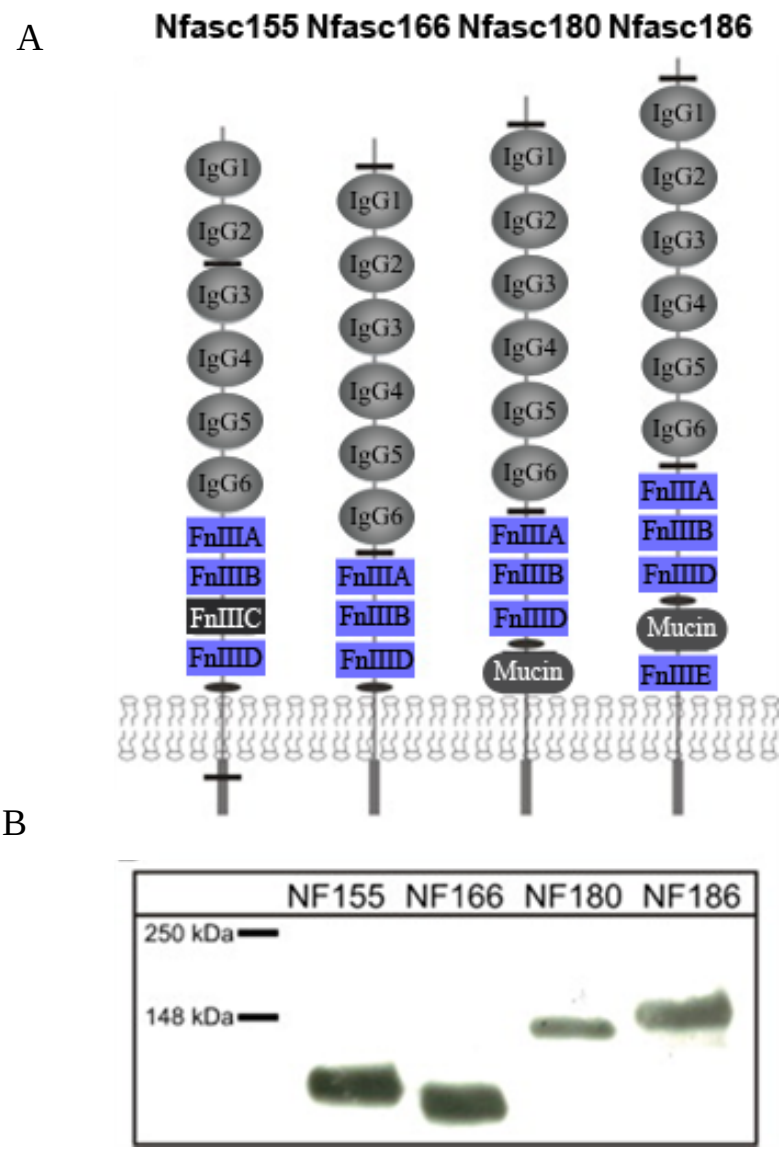

Figure 5. Different isoforms of Neurofascins in chick (Picture modified from Hassel et al., 1997).

A. Schematic representation of the four different isoforms of Neurofascins found in chick. Nfasc155 has specific FnIIIC domain. Nfasc166 does not have unique domains. Nfasc180 has a Mucin domain and is only found in chick. Nfasc186 has the Mucin and FnIIIE domains.
B. Western blot demonstrating the different mobility of those 4 isoforms of Neurofascins.

1.4.2 Role of Nfasc186 and Nfasc155 in clustering Na_v channels.

A key observation concerning the function of the Neurofascins was the demonstration that in the Neurofascin knockout (*Nfasc*$^{-/-}$) mouse Na_v channels are no longer clustered at nodes in the PNS; subsequently it was shown that only a very

small proportion (16%) of nodes have clustered Na_v channels in CNS in the absence of the Neurofascins (Sherman et al., 2005, Zonta et al., 2008).

Both *in vitro* and *in vivo* studies have supported the view that neuronal Nfasc186 has a role in clustering Na_v channels at the nodes of Ranvier. *In vitro*, short hairpin RNA (shRNA) knockdown of Nfasc186 in DRG and Schwann cell co-culture showed Na_v channels fail to cluster at the nodes of Ranvier in PNS (Dzhashiashvili et al., 2007). Meanwhile, the *in vivo* study of Zonta showed when Nfasc186 is expressed in neurons on a Neurofascin knockout mouse background, it is sufficient to restore the Na_v channels in the nodes in PNS (Zonta et al., 2008). Meanwhile, in the CNS, expression of Nfasc186 showed that Na_v channel-positive nodes were restored from less than 20% in knockout mice to more than 90% in transgenic mice expressing only Nfasc186 (Zonta et al., 2008). In another animal model, in which Nfasc155 was deleted, where only Nfasc186 was present, Na_v channels were able to be targeted at the nodes in the PNS supporting the earlier data (Thaxton et al., 2012). From the above observations it is clear that Nfasc186 alone can restore the Na_v channels at the nodes in both PNS and CNS.

On the other hand, the role of Nfasc155 in clustering of nodes has been controversial, and different researchers have come to different conclusions. *In vivo*, in the PNS, Nfasc155 lacking its C-terminus was unable to rescue sodium channel clustering in the absence of Nfasc186 whereas in the CNS it was (Sherman et al., 2005, Zonta et al., 2008). *In vitro*, shRNA knockdown of Nfasc186 in DRG co-culture, which still has glial Nfasc155 showed no sodium clustering (Dzhashiashvili et al., 2007). Which suggested Nfasc155 alone is not sufficient to restore the Na_v channels. Meanwhile, an *in vivo* study of Thaxton, after conditional knockout of Nfasc186, suggested that Nfasc155 alone can not restore Na_v channels clustering at the nodes of Ranvier both in the CNS and PNS (Thaxton et al., 2012). This contradicted the findings of Zonta, at least in the CNS (Zonta et al., 2008). Moreover, a paper of Feinberg et al showed that when Nfasc155 is expressed in Schwann cell-neuron co-culture, sodium channels are targeted to the nodes in the absence of Nfasc186 (Feinberg et al., 2010).

The possible cause of the differences is further discussed in the chapter of conclusions and discussion 4.3.3.

1.4.3 Other functions of the Neurofascins.

The Nfasc155–Caspr–Contactin complex promotes oligodendrocyte process migration.

In the CNS, before myelin formation, oligodendrocytes extend processes along axons; and the process of each oligodendrocyte migrates to eventually form nodes of Ranvier. Oligodendrocyte process migration is an early critical step for myelination. In teased spinal cords where oligodendrocytes do not express Nfasc155, there is a delay in process migration, which is restored to be similar to WT when Nfasc155 is re-expressed on a Neurofascin-null background (Zonta et al., 2008). This indicates that Nfasc155 and the adhesion complex promotes the migration of oligodendrocyte processes in the CNS.

Regulation of Neurite outgrowth

Neurites are undifferentiated axons or dendrites extended by cultured neurons and neurite outgrowth is likely to be a key process during neuronal migration and differentiation. *In vitro*, a Neurofascin-Fc chimera protein increases the neurite outgrowth of cultured tectal neurons from chick (Volkmer et al., 1996). An experiment on mouse reaggregated cerebellar cells showed that Nfasc186-Fc depresses neurite outgrowth but Nfasc155-Fc promotes neurite outgrowth (Koticha et al., 2005). In another chick Dorsal Root Ganglion (DRG) culture study, Nfasc166, which is an early isoform in chick, is required for neurite outgrowth and Nfasc186 depresses the outgrowth (Pruss et al., 2006). Further *in vitro* study has shown that Nfasc166 can interact with fibroblast growth factor receptor 1 (FGFR1) through both extra- and intracellular domains. But only the intracellular domains are necessary and sufficient to active the FGFR1 domain, which promotes neurite outgrowth (Kirschbaum et al., 2009). Neural CAM (NCAM), a cell surface glycoprotein whose extracellular portion contains five Ig-like domains and two FNIII (fibronectin type III)

repeats functionally interacts with FGFR (Hinsby et al., 2004). Although Nfasc166 and NCAM have very similar extracellular domain compositions, the intracellular domain of Nfasc166 which interacts with FGFR1 is different from NCAM. There is no study on Nfasc166 mediated FGFR-dependent biochemical events, so it is unclear whether Nfasc166 can regulate FGFR with the same mechanism as NCAM.

Nfasc186 is essential for AIS stabilization

The axon initial segment (AIS) is the unmyelinated proximal part of an axon close to the cell body. Recent experiments suggest that the composition and topographical organization of the initial segment is dynamically and precisely organized (Colbert et al., 2002, Kole et al., 2008, Hu et al., 2009, Fleidervish et al., 2010, Grubb et al., 2010, Kuba et al., 2010). Like nodes of Ranvier, the AIS has a high concentration of Na_v channels which are believed to be the cause of the low threshold for initiation of action potentials at the AIS. AnkyrinG promotes clustering of Na_v channels at the AIS (Hedstrom et al., 2008, Zhou et al., 1998). Other proteins also found at the node include K_v channels (Clark et al., 2009), the scaffolding protein βIV-Spectrin and the cell-adhesion molecules Nfasc186 and neuron-glia related cell-adhesion molecule (NrCAM) (Rasband et al., 2010). Through a FIGQY motif in its cytoplasmic domain, Nfasc186 is able to bind to AnkyrinG and localize at the AIS (Davis et al., 1994, Dzhashiashvili et al., 2007, Lemaillet et al., 2003).

Different from nodes of Ranvier, the clustering of Na_v channels at the AIS seems to be independent of Neurofascins. An *in vitro* study showed, after shRNA knockdown of Nfasc186 in cultured hippocampal neurons, only NrCAM and Brevican were affected, all other components including Na_v channels were still targeted to the AIS (Hedstrom et al., 2007). Meanwhile, in Neurofascin knockout mice, when Nfasc186 is not expressed, NrCAM is mislocalized but other AIS proteins can target to the AIS without Neurofascins (Zonta et al., 2011). These results suggested that Nfasc186 is not involved in the targeting of sodium channels to the AIS.

However, although it is not required for AIS assembly, Nfasc186 is essential for AIS protein maintenance (Zonta et al., 2011). Conditional deletion of Nfasc186 in adult

mice leads to the loss of key components of AIS including Na_v channels. Purkinje cells with a disrupted AIS, but intact nodes of Ranvier, are no longer able to fire spontaneous action potentials. Interestingly, following stimulation those Purkinje cells are still able to generate evoked action potentials but with significantly altered characteristics (Zonta et al., 2011). These mutants had an altered gait, and testing their motor coordination and balance using a rotarod revealed significant deficits in mutant animals compared to controls. And in the paper they stated the phenotype could not be attributed solely to disruption of Purkinje cell AIS function since many other neuronal cell types including spinal motor neurons were affected as well.

1.4.4 Neurofascins in neurological diseases.

Since Neurofascins are key components of nodes of Ranvier and AIS in the nervous system, the role of Neurofascins in neurological diseases has been explored in several studies recently.

Autoantibodies of Neurofascins in diseases

Assays to detect antibodies against human Nfasc155 and Nfasc186, and showed that autoantibodies to Neurofascins are found in 4% of patients with chronic inflammatory demyelinating polyneuropathy (CIDP) and acute inflammatory demyelinating polyneuropathy (AIDP) (Ng et al., 2012). In this study only 4% of patients had antibodies against Neurofascins; the large number of patients who did not have them suggest that the Neurofascins are unlikely to be important primary target autoantigens (Hughes et al., 2012).

However, those studies only detected the antibodies at one time point, there were no follow-up studies to explain the antibodies' appearance during the development of the disease and disappearance with treatment or recovery, so there is no way to determine if Neurofascin antibodies are a cause or effect of the diseases (Hughes et al., 2012).

The serum reactivities observed were against only one of the two isoforms of Neurofascin, even though the extracellular domain structures of Nfasc155 and

Nfasc186 are very similar, with the difference being only in the 2 domains closest to the transmembrane region (Sherman et al,. 2005, Hughes et al., 2012). By expressing truncated variants of Nfasc155 and Nfasc186, the FnIIIC (which were referred to as fibronectin type III repeats 3-4 in the original paper) domain was identified as the target for Nfasc155-specific reactivity and Mucin and FnIIIE domains for Nfasc186 specificity (Hughes et al., 2012).

Hence, the role in pathogenicity of these antibodies is still unclear. In previous observations the presence of antibodies to Nfasc186 in the presence of complement disrupted nerve conduction and antibodies to Nfasc155 inhibit myelination by blocking the formation of the Caspr/Contactin/Nfasc155 complex (Mathey et al., 2007, Charles et al., 2002), they suggested similar phenomena could occur in human patients (Hughes et al., 2012). But no experiment was conducted to examine their theories.

Neurofascins in MS

Multiple sclerosis is characterized by perivascular inflammation, myelin and oligodendrocyte damage, axonal loss and astrocytic scarring. Nfasc186 and Nfasc155 are closely associated with the integrity of myelin and axons since they have important roles in the assembly of nodal and paranodal domains during myelination and node of Ranvier maintenance (Sherman et al., 2005, Zonta et al., 2008). However, little is known concerning how areas of inflammation, demyelination or remyelination in the multiple sclerosis brain could influence the composition and integrity of the nodal components.

One of the studies has focused on the expression pattern of Nfasc155 and Nfasc186 to determine the changes that occur at the node of Ranvier during the formation and repair of multiple sclerosis lesions (Howell et al., 2006). In that study it was shown that in sections of MS post-mortem brains, significant changes in Nfasc186 and Nfasc155 expression and localization were found in the demyelinated areas of lesions. The changes include highly elongated Nfasc186 staining and also elongated or disrupted Nfasc155 staining. Smi32 antibody can be used to detect neurofilament

dephosphorylation associated with demyelination and this is known to be present to a large extent in active multiple sclerosis lesions (Trapp et al., 1998). Co-staining with anti-Nfasc155 showed that disruption of Nfasc155 expression is associated with early axonal pathology; also changes in Nfasc186 staining associated with axon pathology (Howell et al., 2006). Interestingly they found that Nfasc155 is disrupted in areas of inflammation around the lesions and Nfasc155 disruption precedes the changes at the node of Ranvier and Nfasc186 expression, which suggested Nfasc155 changes start from the early phase of MS disease before demyelination and remyelination (Howell et al., 2006). Also they found that the disruption of Nfasc155 in remyelination plaques is less extensive compared with the demyelinated lesions (Howell et al., 2006) indicating that Nfasc155 is involved in remyelination of the lesions in MS.

Knowing that Nfasc155 is disrupted in areas of inflammation in MS, some studies have focused on the relationship between autoantibodies in MS patients and Neurofascins. Western blots using patient sera to probe Neurofascins in enriched brain lysates, it was reported that, out of 22 multiple sclerosis (MS) patients, ~20% percent of their sera had a prominent response to bands around 150-180 kD (band sizes varies between patients) (Fig. 6), which is approximate the size range of Nfasc186 and Nfasc155. Then by using two-dimensional gel electrophoresis and purified IgG from patients, they found Nfasc155 extracellular domains can be recognized by the autoantibodies from MS patients. They then showed those autoantibodies also recognize Nfasc186 (Mathey et al., 2007). By using an MS disease animal model, Mathey et al (2007) also explored the pathomechanisms related to Neurofascin autoantibodies. They found that transfer of Neurofascin antibodies exacerbated the clinical phenotype of Experimental Allergic Encephalomyelitis (EAE); also transfer of antibody only resulted in acute axonal damage in the absence of demyelination or increased inflammation in the CNS (Mathey et al., 2007). This suggested that the node of Ranvier is in a protected environment, the nodal protein components like Neurofascins do not encounter antibodies in normal situations. Furthermore, *in vitro* and *vivo*, Neurofascin antibodies inhibit neurotransmission (Mathey et al., 2007). Here only 22 patients

were studied by Mathey et al, more patients are needed for a proper statistical study to understand whether autoantibodies of Neurofascin are pathogenetically significant. However, from animal models in their study, it suggested an initial breaking down of the myelin sheath is needed for the autoantibodies to cause damage. Hence, the effects of the autoantibodies of Neruofascin on human patients, if any, is likely to be caused by the demyelination in MS, instead of the trigger of MS.

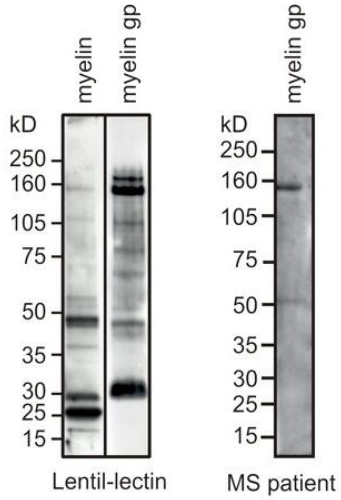

Figure 6. Antibodies to Neurofascins were identified in patients with MS (Mathey et al., 2007).
Human myelin and the myelin glycoprotein (gp) fraction were separated by SDS-PAGE and blotted, and glycoproteins were detected using biotinylated lentil-lectin (left). Using this myelin glycoprotein fraction to screen patient sera identified antibody responses to a variety of components, including Nfasc155 (right) (Mathey et al., 2007).

However in human MS patients, axonal loss is responsible for the development of chronic neurological deficits (when Neurofascin antibodies are at the highest levels), but the pathomechanisms that initiate or exacerbate axonal injury in this inflammatory demyelinating disease remain obscure (Mathey et al., 2007).

Neurofascin 155 low (Nfasc155-L) in MS

In early studies (Schafer et al., 2004, Sherman et al., 2005), a single band representing Nfasc155 was revealed by western blot with standard electrophoretic separation of spinal cord homogenates from wild-type mice. However, two bands, Nfasc155 high (Nfasc155-H) and Nfasc155 low (Nfasc155-L), are revealed after

extended electrophoresis of mice brain lysates (Pomicter et al., 2010). By using the brain lysate from a glial conditional Neurofascin knockout mouse CNP promoter-regulated Cre expression (CNP-Cre/Nfasc^{flox}) (Pillai et al., 2009), they found both Nfasc155-H and Nfasc155-L are expressed in glial cells. Interestingly, in two out of eight MS brain samples of donors, the expression level of Nfasc155-L was up regulated (Fig. 7) (Pomicter et al., 2010). It was suggested that Neurofascins are involved in some neuronal pathological changes, and also indicates new isoforms of Neurofascins also have possible active roles in neurological diseases.

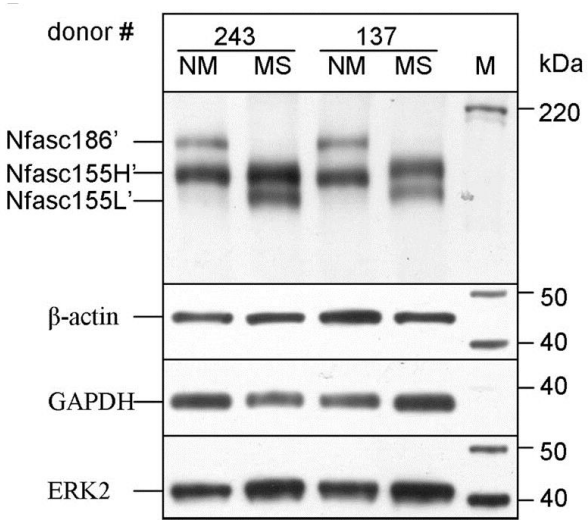

Figure 7. The pattern of Neurofascin 155H and Neurofascin 155L is altered in multiple sclerosis plaques (Picture from Pomicter et al., 2010)
Normal-appearing white matter-multiple sclerosis (NM) and multiple sclerosis plaque (MS) samples from the same donors were run side by side on a Western blot. Results showing Neurofascin 155L is present only in the plaque samples (Pomicter et al., 2010).

Neurofascin protein localization is altered in cerebral hypoperfusion.

Cerebral hypoperfusion is suggested to contribute to the development of white matter changes in the aging brain (Fernando et al., 2006). A mouse model of chronic cerebral hypoperfusion, which mimics the modest, sustained reductions in blood flow of the aging brain, was used to analyze the integrity of Neurofascins and other key proteins at the paranodal and nodal regions in response to hypoperfusion. Immunolabeling showed that the number of Nfasc155 positive nodes is significantly reduced in the hypoperfusion model (Shibata et al., 2004, Reimer et al., 2011). From

3 days to 1 month after hypoperfusion, the loss of Nfasc155 became more pronounced (Reimer et al., 2011). In addition, EM images showed the number of septate-like junctions of paranodal loops in hypoperfused samples was highly reduced (Reimer et al., 2011). These authors also found in the corpus callosum and internal capsule the length of Na_v channel staining at nodes was significantly increased after 3 days hypoperfusion. This seems likely to be the consequence of the loss of the diffusion barrier formed by Nfasc155-Caspr-Contactin complex. More interestingly, the observation of an intact length of Nfasc186 and AnkyrinG when the distribution of the Na_v channels is extended was contrary to the view that Nfasc186 might indirectly interact with Na_v channels through AnkyrinG and ßIV spectrin. Further, it suggested that Na_v channels can interact with other proteins rather than Nfasc186 and AnkyrinG.

In all the above studies, it is still difficult to conclude that the Neurofascins have a key involvement in causing the major clinical phenotype of human disease; however, these studies do suggest that the Neurofascins and their autoantibodies may have roles in the pathological changes which happened during the process of disease.

1.4.5 Neurofascin in kidney

Neurofascins were thought to be only expressed in the nervous system, however, a recent study has shown that Neurofascins are expressed in kidneys and could have a role there (Sistani et al., 2013). By both RT-PCR and western blot, an isoform of Neurofascin was detected in the glomerular fraction of kidney, and based on its size on western blot it is Nfasc186. Immunofluorescence showed that the Neurofascin signal is very strong in the glomerulus, whereas no immunoreactivity was observed outside of glomeruli (Sistani et al., 2013). In the glomerulus, Nfasc186 was detected at the urinary side of nephrin staining and it seems to localize to the major processes marked with vimentin (Sistani et al., 2013). When different development stages of kidney were studied, Neurofascin was first observed at the capillary-stage glomerulus, where the staining colocalized with vimentin; then Neurofascin was detected both on the basal aspects and at the apical membrane of developing podocytes, again, colocalizing with vimentin (Sistani et al., 2013). Through kidney

maturation Neurofascin is colocalized with the podocytes, which supports the idea that Nfasc186 associates with processes extended by podocytes (Sistani et al., 2013).

1.5 Proteins that interact with Neurofascins

1.5.1 Paranodal Nfasc155-Caspr-Contactin complex.

Nfasc155 colocalized with Caspr and Contactin at the paranodal region and forms the Nfasc155-Caspr-Contactin complex and this complex forms the septate-like paranodal junctions that flank the node of Ranvier (Charles et al., 2002, Sherman et al., 2005).

Nfasc155 is likely to have a pioneer role at the paranodes, because its targeting to the paranodes does not depend on the expression of Caspr and Contactin and it is required for the localization of the Caspr-Contactin complex (Charles et al., 2002). In conditional Nfasc155 knockout mice, like Contactin and Caspr knockouts, the organization of the paranodal loops was preserved; however, the characteristic transverse bands were absent. In addition, the spacing between the paranodal loops and the axolemma was often wider (Pillai et al., 2009). In summary, Nfasc155 appears to initialize the assembly of the Nfasc155-Caspr-Contactin complex, but this complex needs all three proteins together to be functional and maintain the integrity of the paranodes (Fig. 8).

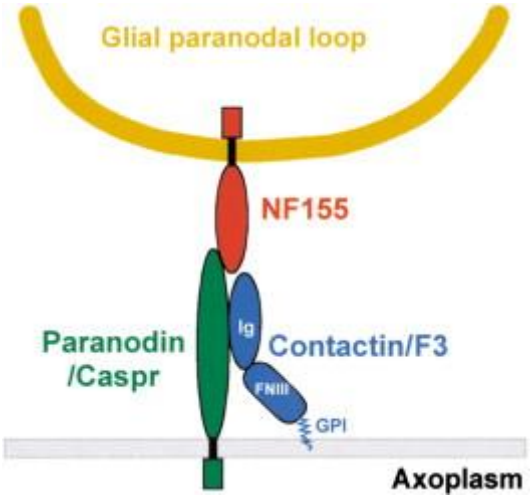

Figure 8. Schematic representation of the molecular organization of the paranodal complex (Charles et al., 2002).
The interaction of Nfasc155 (NF155 in picture) expressed in glial cells with Caspr and Contactin expressed in axons, forms the Nfasc155-Caspr-Contactin complex at the paranodes.

Contactin

Contactin is a neural glycosyl-phosphatidylinositol (GPI)-anchored IgSF cell adhesion molecule (Ranscht et al., 1998, Brümmendorf et al., 1989, Gennarini et al., 1989, Berglund et al., 1994). Through *cis* and *trans* interactions Contactin interacts with multiple proteins, including Caspr and Nfasc155 (Peles et al., 1997, Volkmer et al., 1998). Contactin is expressed on axons and dendrites of diverse neuron populations. *In vitro* assays have revealed functions for Contactin in neurite extension Gennarini et al., 1991, Durbec et al., 1992, Peles et al.,1995), fasciculation (Chang et al., 1987, Rathjen et al., 1987), and repulsion (Pesheva et al., 1993).

In Contactin knockout mice it was clearly shown that the paranodal junction is disrupted. The electron microscope (EM) images of the nodes of Ranvier in PNS showed the ultrastructure of paranodal junctions is abnormal (Boyle et al., 2001). The paranodal gap between the axolemma and the apposing myelin loops is significantly widened and also electron dense transverse bands that are thought to represent sites of direct adhesive contact between the terminal myelin loops and the axolemma are missing in Contactin knockout mice (Fig. 9). Moreover, immunolabeling also showed Caspr is missing from the paranodal region in the

mutants. Interestingly, Nfasc155 is still targeted to the paranodal region (Fig. 9) (Boyle et al., 2001).

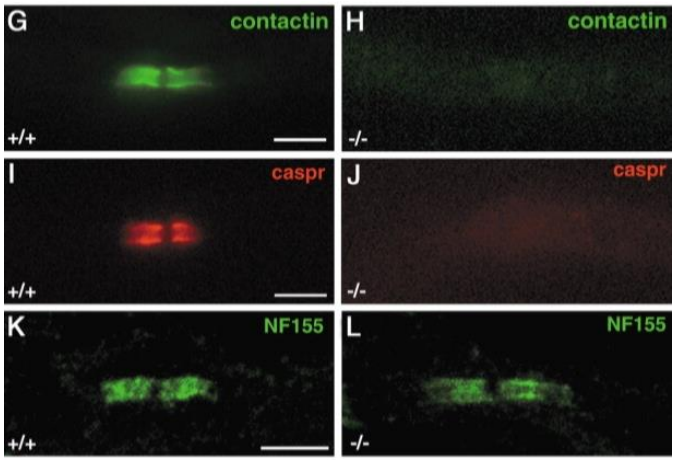

Figure 9. Immunofluorescence showing Nfasc155 is targeted to paranodes without Contactin and Caspr (Boyle et al., 2001).
Immunolabeling showed that compared with controls (G,I,K) when Contactin is deleted (H) the Caspr is mislocalized (J), but Nfasc155 is still targeted to the paranodes (L). Scale bar, 5 µm.

Caspr

The adhesion molecule Caspr (Contactin associated protein, also named Paranodin) forms a complex with Contactin on axons that is concentrated at the paranodal junctions (Fig. 8) (Einheber et al., 1997, Menegoz et al., 1997, Peles et al., 1997, Rios et al., 2000). Caspr and Contactin are integral junctional components because mice deficient in these proteins exhibit severe disruptions of normal paranodal interactions (Bhat et al., 2001, Boyle et al., 2001, Rios et al., 2003). Similar to Contactin knockout mice, the Caspr mutant also has compact myelin sheaths in both CNS and PNS, whereas various abnormalities of the paranodal region were observed by EM on longitudinal sections. The abnormalities include the absence of the regular array of transverse bands between paranodal loops and the paranodal loops are severely disorganized in the paranodal region. Also immunolabeling shows the lack of Contactin but the presence of Nfasc155 at paranodes of Caspr in knockout mice (Bhat et al., 2001, Rios et al., 2003).

1.5.2 Major nodal proteins

Studies have identified many nodal proteins in both PNS and CNS; among them AnkyrinG, NrCAM Gliomedin and Brevican are shown/suggested to have direct interaction with Nfasc186 (Fig. 10).

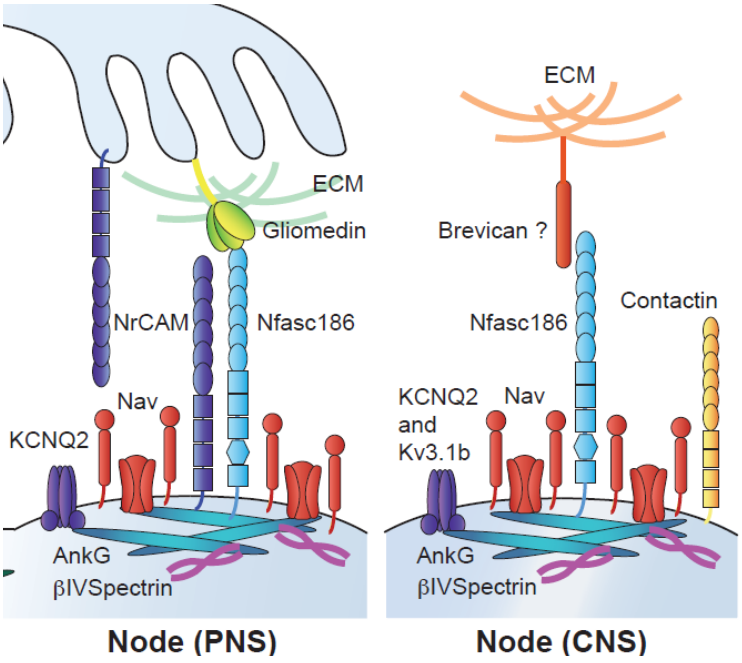

Figure 10. Schematic representation of the molecular organization of the nodal complex in both CNS and PNS (modified from Desmazieres et al., 2012). The major nodal proteins which have been identified at the nodes of Ranvier in both PNS and CNS. In the PNS, Gliomedin, NrCAM and AnkyrinG (AnkG) have been shown to directly interact with Nfasc186. Other proteins interact with Nfasc186 through AnkyrinG. In the CNS, Brevican is suggested to interact with Nfasc186 but this has not been confirmed yet. In the CNS, the other protein interactions are shown to be similar to PNS.

AnkyrinG

Ankyrins consist of three major domains: a membrane-binding domain with a common folding structure and 24 consecutive repeats (the MB domain), a spectrin-binding domain (the S domain), and a death domain with the C-terminus (the DC domain) (Bennett et al., 2001). Biochemical studies suggest that ankyrins are multivalent molecules and can form lateral homophilic and heterophilic complexes between integral membrane proteins (Michaely et al., 1995). Of the three ankyrin isoforms, AkyrinG is concentrated at the axon initial segment and nodes in

myelinated axons and directly interacts with axonal Na_v channels (Bennett et al., 2001, Kordeli et al., 1995). In Neurofascin knockout mice, AnkyrinG fails to target to the nodes of Ranvier (Sherman et al., 2005), which supported the view that the intracellular domain of Neurofascin serves as part of the docking site for AnkyrinG (Davis et al., 1993). In conditional AnkyrinG knockout mice, Na_v channels are absent from axon initial segments, and the neurons show severe deficits in action potential firing (Jenkins et al., 2001, Zhou et al., 1998). This indicates AnkyrinG has a very important role in clustering Na_v channels to the AIS. However, the interaction between Neurofascin and AnkyrinG is not important for the formation of AIS (Zonta et al., 2011). Thus, the role of AnkyrinG in clustering of Na_v channels to nodes of Ranvier remains unclear so far.

NrCAM

NrCAM is a neural cell adhesion molecule (CAM), like Nfasc186, that is enriched at PNS nodes (Davis et al., 1996, Lambert et al., 1997) and has been implicated in the assembly of nodes of Ranvier (Custer et al., 2003, Sherman et al., 2005 and Zonta et al., 2008). The observation that the binding of NrCAM-Fc fusion protein to Chinese Hamster Ovary (CHO) cells was dependent on Neurofascin expression (Lustig et al., 2001) and a study in the chick that NrCAM acted as a cell surface receptor for Neurofascin (Volkmer et al., 1996) both suggest there is a direct interaction between NrCAM and Nfasc186. The fact that expression of NrCAM-Fc protein inhibits AnkyrinG and Na_v channel clustering in Schwann cell-neuron co-cultures provided the first functional evidence for a role of CAMs in the development of the node of Ranvier (Lustig et al., 2001). Also Neurofascins and NrCAM can interact with AnkyrinG via their cytoplasmic domains (Bennett et al., 1999) and may thereby recruit Na_v channels to the nodes through their interaction with AnkyrinG. NrCAM localization precedes Na_v channel clustering at Schwann cell edges and also genetic deletion of NrCAM results in a delay in both Na_v channel and AnkyrinG clustering but not in myelination. Nevertheless, nodes ultimately form properly in the absence of NrCAM. This suggests that NrCAM is involved in node development, but it is not essential for the formation of nodes of Ranvier.

Gliomedin

Gliomedin is an *N*-glycosylated trimeric molecule secreted by Schwann cells (SCs) and incorporated into the extracellular matrix (Eshed et al., 2005, Eshed et al., 2007, Maertens et al., 2007). Autoantibodies to Gliomedin as well as Neurofascins have been identified in experimental allergic neuritis, a model of Guillain-Barré syndrome (Lonigro et al., 2009). Soluble Neurofascins (Nfasc186 and Nfasc155) and NrCAM specifically bind to Gliomedin-expressing COS7 cells (Eshed et al., 2005). Also soluble Gliomedin can bind to Neurofascins and NrCAM expressing cells (Eshed et al., 2005). In another experiment, the FnIII domains of Nfasc186 were implicated in interaction with Gliomedin (Labasque et al., 2011). All this suggested there are interactions between Gliomedin and Neurofascin. The exact function of Gliomedin is still unclear, but in the absence of Gliomedin Na_v channels cannot target to the heminodes during myelination (Feinberg et al., 2011). Hence, it has been proposed that after glial NrCAM tethering Gliomedin to Schwann cell microvilli, the NrCAM/Gliomedin complex serves as a Schwann cell signal for Na_v channel clustering at heminodes by binding to axonal Nfasc186 (Feinberg et al., 2011).

Brevican

Brevican is one of the most important neural proteoglycans in the mature brain. It constitutes a key component of perineuronal nets (PNN) and ECM, and the ECM is thought to be able to stabilize synapses in neural networks and inhibit neurite outgrowth (Yamaguch et al., 2000, Hockfield et al., 1990). When adding soluble GFP-Brevican, punctate GFP-Brevican binds to Nfasc186-transfected cells, but not to untransfected or NrCAM-transfected cells, which suggested that Brevican interacts with Nfasc186 (Hedstrom et al., 2007). *In vivo* investigation of Brevican shows that Brevican is not ubiquitously present at the nodes of all myelinated axons and is predominantly found at the nodes of large diameter axons in CNS (Bekku et al., 2009). Moreover, TN-R and phosphacan are only found at the nodes of Ranvier which express Brevican (Bekku et al., 2009). This suggests a crucial role of Brevican in creating a specialized matrix in such large diameter axonal nodes. Meanwhile, Brevican is only one component of the perineuronal net that surrounds most CNS

neurons during postnatal development, suggesting that they are structures integral to mature neurons. Brevican is also enriched at mature and developing nodes, suggesting that it may contribute to node formation and/or maintenance. However, the primary role of Brevican regarding to the nodes of Ranvier is still unclear.

1.5.3 AIS proteins

The molecular organization of the AIS has many features in common with nodes of Ranvier and juxtaparanodes (Fig. 11). The AIS is comprised of ion channels ($Na_v1.x$, KCNQ2–KCNQ3 and $K_v1.x$), cell adhesion molecules (NrCAM, Nfasc186 a disintegrin and metalloproteinase domain-containing protein 22 (ADAM22), transient axonal glycoprotein 1 (TAG1, also known as contactin 2) and CASPR2), extracellular matrix molecules (brevican and versican), cytoskeletal scaffolds (AnkG, βIV spectrin and postsynaptic density protein 93 (PSD93)) and other signalling proteins(casein kinase II (CK2), phosphorylated nuclear factor-κB (pNFκB) and phosphorylated inhibitor of κBα (pIκBα)) (Rasband et al., 2010). Nfasc186 is dispensable for the assembly of AIS but in adult animals the Nfasc186 has a key role in maintaining the integrity of AIS (Zonta et al., 2011) (Fig. 11).

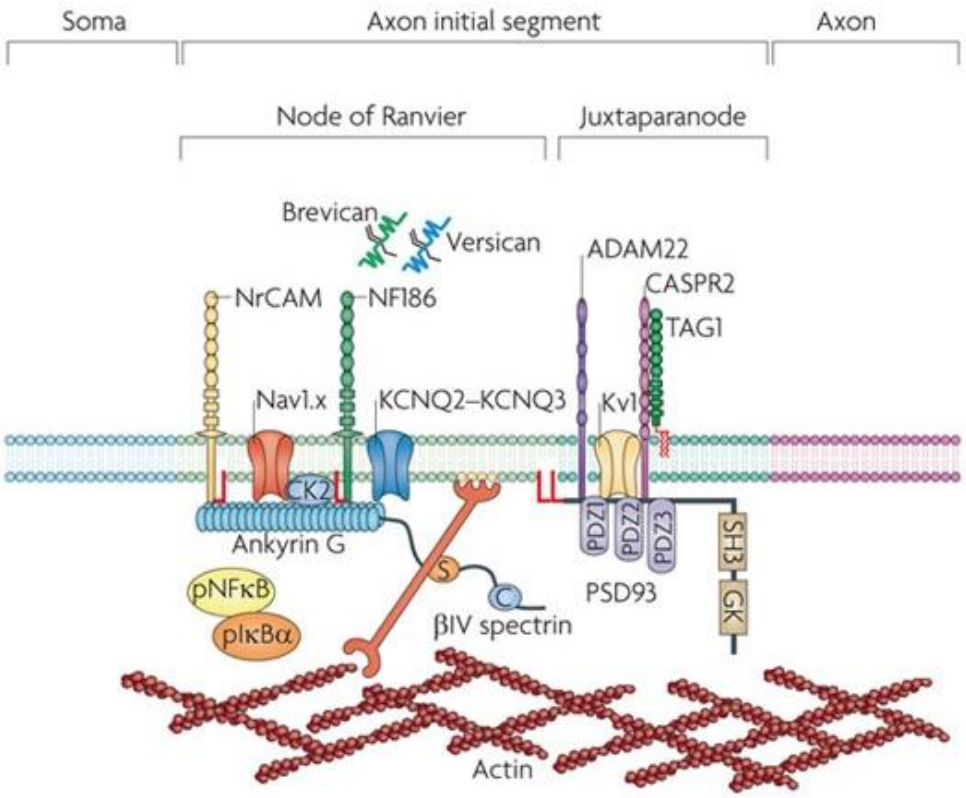

Figure 11. The protein composition of the AIS (Rasband et al., 2010).
Diagram showing the major AIS proteins many of which have also been identified at the nodes of Ranvier in both PNS and CNS.

Doublecortin

When cultured hippocampal neurons are stained for Doublecortin (DCX) and Neurofascins, surface Neurofascins and DCX were not strikingly colocalized; however, there was a readily detectable intracellular pool of Neurofascins, which partially colocalized with DCX. This intracellular pool of Neurofascins was widely dispersed throughout the whole cell and did not cluster underneath the AIS (Yap et al., 2012). This suggested there is no direct interaction between Neurofascin and DCX. Interestingly, reducing DCX levels decreases the relative AIS enrichment of HA tagged Neurofascins; also endocytosis of HA tagged Neurofascin is stimulated when co-expressing DCX in PC12 cells. Endocytosis of endogenous Neurofascins is also diminished in neurons that do not express DCX (Yap et al., 2012). These observations indicate that though DCX and Neurofascins may not directly interact, DCX may have a role in the enrichment of Neurofascins at the AIS.

1.6 Post translational modifications of Neurofascins.

Besides differential splicing of the *Neurofascin* gene resulting in different isoforms of Neurofascins, Neurofascins can also undergo post translational modifications.

1.6.1 Nfasc 155 is N-Glycosylated

Glycosylation is a prime regulator of protein function such as protease activity (Steen et al., 2001), intracellular trafficking (Yan et al., 2008), protein binding (Milev et al., 1995, Zhou et al., 2008) and stability (Buck et al., 2004, Gao et al., 2007, Li et al., 2007). Peptide-*N*-Glycosidase F (PNGase F) is an amidase that cleaves complex oligosaccharides from *N*-linked glycoproteins. Electrophoresis of untreated and PNGase F treated Neurofascins side-by-side showed shifts on western blots induced by deglycosylation (Pomicter et al., 2010). In the same experiment they showed Nfasc155-H and Nfasc155-L both shifted but still retained 2 different sizes, which indicates that, although Neurofascins are glycosylated, the difference between Nfasc155-H and Nfasc155-L is not simply differential *N*-linked glycosylation (Pomicter et al., 2010). They also claimed that Nfasc155-H and Nfasc155-L may have distinct functions related to their different states of glycosylation (Pomicter et al., 2010).

1.6.2 Neurofascin 186 is O-mannosylated

Protein O-mannosylation is an important modification in mammals, and deficiencies of *O*-mannosylation have recently been associated with diseases like Walker–Warburg syndrome and different forms of muscular dystrophies such as Muscle–Eye–Brain disease and Fukuyama congenital muscular dystrophy (Kobayashi et al., 1998, Bernab éet al., 2002, Shenoy et al., 2010). Although, it has already been shown that the amount of O-mannosyl glycans in brain is very high, only very few specific proteins have been identified as O-mannosylated (Pacharra et al., 2012). Electrospray ionization mass spectrometric analysis of peptides from endogenous Neurofascins was performed on an LTQ Orbitrap Discovery system (Thermo) equipped with a

Proxeon nano ESI-source and coupled to a Proxeon Easy nLC II system. Endogenous Nfasc186 from mouse brain was purified and analyzed. Several O-mannosylated peptides were identified, which are located all over the protein and not stringently within the Mucin domain as in α-dystroglycan, showing that O-mannosylation in mammals is independent of its Mucin domain (Pacharra et al., 2012). However, the possible function of O-mannosylation of Neurofascins is still not clear.

1.6.3 Nfasc186 is phosphorylated

Phosphorylation of proteins is an important regulatory mechanism, and many enzymes and receptors are activated or inhibited by phosphorylation and dephosphorylation. Reversible phosphorylation often results in a conformational change in the structure in many enzymes and receptors, causing them to become activated or deactivated. Neurofascins can be phosphorylated. Using an anti-phosphotyrosine antibody, Neurofascins, especially Nfasc186, are tyrosine phosphorylated *in vivo* in a time-dependent fashion, with the maximal level of phosphotyrosine immunoreactivity present during the embryonic period (Garver et al., 1997). The same group also identified the highly conserved FIGQY tyrosine in the cytoplasmic domain as the principal site of phosphorylation (Garver et al., 1997). Meanwhile, by showing activation of tyrosine kinases or inactivation of tyrosine phosphatases completely eliminate the ability of Nfasc186 to coimmunoprecipitate ankyrins, they showed that phosphorylation of Neurofascins regulates the interaction between Nfasc186 and AnkryinG (Garver et al., 1997).

N-Glycosylation, O-mannosylation and phosphorylation are the 3 identified post translational modifications of Neurofascins demonstrated in three different studies (Garver et al., 1997, Pomicter et al., 2010, Pacharra et al., 2012). However, the functions of those post translational modifications *in vivo* are still poorly understood.

1.7 Domain functions of Neurofascins.

The *Neurofascin* gene encodes six immunoglobulin domains, five fibronectin type III repeats, a Mucin domain, a single transmembrane region and a cytoplasmic domain.

Those domains have different functions some of which have been revealed in recent studies.

1.7.1 IgG domains

A function of the IgG domains has been revealed by an *in vivo* study, in which Nfasc155 IgG5-6 domains were specifically deleted from glial cells in a transgenic mouse (Thaxton et al., 2010). In these mice after the deletion of IgG5-6, Nfasc155 was still targeted to some of the paranodes. However, the Caspr fluorescence labelling showed a diffused and disrupted pattern; also, the K_v channels were redistributed into the paranodal space (Thaxton et al., 2010). Hence, the loss of Nfasc155 IgG5-6 alone in mice resembles the phenotypes of *Nfasc155* conditional knockout mice, including paranodal disorganization and loss of paranodal septae junction (Pillai et al., 2009). This indicates that the IgG5-6 domains are important for the interaction between Nfasc155 and the Caspr-Contactin complex.

Furthermore, in the same paper (Thaxton et al., 2010) the author used another animal model, in which the IgG5-6 of both Nfasc186 and Nfasc155 were deleted. But they found the nodal components were still targeted to the nodes normally, which included Na_v channels and AnkyrinG. This suggested that the IgG5-6 domain is dispensible for the function of Nfasc186 at the formation and maintenance of the nodes of Ranvier.

Nfasc186 lacking IgG5-6 and all FnIII domains was transfected into mouse neuroblastoma (N2a) cells, the NrCAM-Fc protein could still bind to the cells. However, after transfection with Nfasc186 lacking IgG1-6 domains, NrCAM-Fc failed to bind to the cells (Labasque et al., 2011). This suggests that there is a binding site at the IgG1-4 domains of Nfasc186 which interacts with NrCAM. It had been shown previously that the interaction between NrCAM and Neurofascin influences AnkyrinG and Na_v clustering at the node of Ranvier (Lustig et al., 2001). Hence, IgG1-4 domains could be important for the formation of nodes of Ranvier.

1.7.2 FnIII Domains

Pull-down assays have been performed by incubating extracts from HEK293 cells transfected with different truncated forms of Nfasc186 with Gliomedin-Fc covalently immobilized onto activated agarose beads. These showed that the deletion of either the IgG1-6 domains only or FnIIIA-D domainsonly of Nfasc186 did not affect interaction with Gliomedin. But the deletion of all these domains led to the abolition of interaction with Gliomedin (Labasque et al., 2011). Also, in the same paper (Labasque et al., 2011), the authors claimed that the Mucin domain is not implicated in Gliomedin binding based on previous observations (Koticha et al., 2006). Hence, it has been suggested that both IgG and FnIII domains have Gliomedin binding sites (Labasque et al., 2011).

Without a Mucin domain Nfasc186 can bind with relatively high affinity to Schwann cells, which suggested that Nfasc186 without the Mucin domain can still bind to Gliomedin (Koticha et al., 2006). Furthermore, an Fc fusion protein containing only three FnIII domains of Nasc186 bound to Gliomedin expressing cells (Labasque et al., 2011). This supported the view of the importance of the FnIII domains of Nfasc186 in Gliomedin interaction.

1.7.3 Mucin and FnIIIE domains of Nfasc186

Mucin and FnIIIE domains are the domains specific to Nfasc186. It has been shown that the Mucin domain is O-mannosylated (Pacharra et al., 2012). No interaction between Mucin/FnIIIE domains and other nodal components at the nodes of Ranvier have been found thus far; but there is an indication that the Mucin and FnIIIE domains are involved in the regulation of cell adhesion and neurite out growth.

An *in vitro* study using reaggregated cerebellar neurons has shown that when Nfasc186-Fc was expressed in L1-Fc expressing cells, cell adhesion was inhibited, although Nfasc155-Fc did not inhibit cell adhesion (Koticha et al., 2005). Subsequent domain analysis showed that the Mucin and FnIIIE domains together are sufficient to inhibit cell adhesion in culture (Koticha et al., 2005). Those results indicate that

regulatory activity of Nfasc186-Fc on cell adhesion is associated with the Mucin and FnIIIE domains of Nfasc186.

An *in vivo* study in chick compared the expression pattern of different isoforms of Neurofascins and their neurite outgrowth promoting activities (Pruss et al., 2009). The authors found the form of Neurofascin, Nfasc185 in chick, which is equivalent to Nfasc186 in mammals, inhibits neurite outgrowth in chick embryos. After showing Neurofascins and axonin-1 colocalized at E9, they found that the FnIIIE (fifth FnIII-like) domain is associated with a reduced binding capacity of Neurofascin to axonin-1. Because axonin-1 can strongly promote neurite outgrowth from chicken embryonic dorsal root ganglia neurons (Kuhn et al., 1991), the FnIIIE domain of Nfasc186 may also inhibit neurite outgrowth by reducing Nfasc186 binding ability to axonin-1.

1.7.4 Cytoplasmic domain

FGFR1 (fibroblast growth factor receptor 1) belongs to the four known fibroblast growth factor receptors (FGFRs) families, which represent a highly diverse signalling system important for migration, proliferation, differentiation, and survival of many different cell types (Ornitz et al., 2001). Because endogenous Neurofascin co-precipitates with FGFR1, one study suggested Nfasc166 (an embryonic form of Neurofascin in chick) can promoter neurite outgrowth thorough FGFR1. However, only Nfasc166 but not Nfasc186 can co-precipitate with FGFR1. Interestingly, although both the Nfasc166 cytoplasmic/intracellular and extracellular domains could co-precipitate with FGFR1, only the intracellular domain of Neurofascins was both necessary and sufficient to promote neurite outgrowth (Kriebel et al., 2012).

As mentioned earlier, the intracellular domain of Neurofascins may be modified by tyrosine phosphorylation at the FIGQY-motif (KDSLVDpYGEGGEGQFNEDG SFIGQpYTVRKD) (Kriebel et al., 2012). Interestingly, the phosphorylated FIGQY motif favours interaction with Doublecortin while it is accessible to AnkyrinG binding in the dephosphorylated state (Kriebel et al., 2012). Based on their tyrosine phosphorylation study, Garver suggested that the phosphorylation of FIGQY-motif might represent an important regulatory element in the localization of Neurofascins

during development (Garver et al., 1997, Kriebel et al., 2012). However, no evidence has been shown to support this idea.

In summary, the IgG1-4 domains of Nfasc186 could be important for the formation of nodes of Ranvier through the interaction with NrCAM. The IgG5-6 domains of Nfasc155 are important for the interaction between Nfasc155 and the Caspr-Contactin complex. IgG and FnIII domains have binding sites for Gliomedin. Mucin and FnIIIE domains of Nfasc186 can inhibit cell adhesion; and FnIIIE domain of Nfasc186 may also inhibit neurite outgrowth by reducing Nfasc186 binding ability to axonin-1. Cytoplasmic domain of Neurofascins was both necessary and sufficient to promote neurite outgrowth. And FIGQY-motif derived from the cytoplasmic domain of Neurofascin may regulate the localization of Neurofascins during development.

1.8 Cerebellar developmental

During embryogenesis, the developing cerebellum undergoes a series of sequential, morphological events such as neurogenesis, cell migration, axon pathfinding, dendritogenesis and synaptogenesis (Sotelo et al., 2004). During mid-gestation (E13.5) Purkinje cells (Fig. 12 orange) are produced in the cerebellar plate and move from the ventricular zone (VZ) of the cerebellar plate neuroepithelium (CPN) toward the rhombic lip migratory stream (RLS) and nuclear transitory zone (NTZ). At the same time, most or all Reelin-producing cells (Pax6 positive cells) (Fig. 12 green) are produced in the upper rhombic lip (URL) and migrate into the nuclear transitory zone (NTZ), which later on develops into deep cerebellar nuclei projection neurons and granule cells (Robert F. Hevner 2008, pp 141-158). In section 3.1.6 I asked if the third isoform of Neurofascin affects the cell migration of cerebellar development.

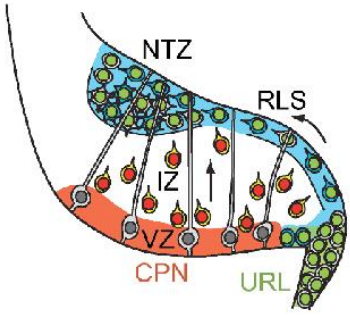

Figure 12. Diagram explaining cellular migrations during cerebellar development (adapted from Robert F. Hevner 2008, pp 141-158).
Within the developing cerebellum (E13.5) Purkinje cells (orange) migrate from the ventricular zone along radial glial cells (gray) through the intermediate zone (IZ) into RLS or NTZ. Reelin-producing cells (green) also migrate from the URL along the RLS into NTZ. The directions of migration are indicated with arrows.

1.9 Purpose of this project

This project comprised two parts, both related to the roles of the Neurofascins in the developing nervous system. The overarching hypothesis is that Neurofascins are important for the formation and maintenance of node of Ranvier, especially the clustering of Na_v.

1.9.1 Identify and characterize a third isoform of Neurofascin in mouse.

A Western blot study showed three different isoforms of Neurofascins. However, only two major isoforms of Neurofascins have been well studied in mouse, Nfasc155 and Nfasc186. These two isoforms have different domain compositions, they are expressed in different cells and have different functions in organizing nodes and paranodes during myelination. Knowing so much about the other two Neurofascins, questions about the third isoform, Nfasc140, start to emerge. This begs a number of questions:

- What is the domain structure of Nfasc140?
- When and where is Nfasc140 expressed?
- Is Nfasc140 necessary and sufficient for formation of a functional node of Ranvier?

In order to address these questions, this work aims to gain insight into Nfasc140 in the following ways:

- Using western blot and RT-PCR analysis to establish the domain composition of Nfasc140.
- Using western blot and immunofluorescence to study the expression of Nfasc140 in different animal tissues from different ages, and to establish where and when the protein is expressed
- Using different transgenic animals to determine the cell type that expresses Nfasc140
- Using transgenic approach to express Nfasc140 on a Neurofascin knockout background to study whether Nfasc140 can cluster Nav to the node of Ranvier.

1.9.2 The relationship between intact paranodal axoglial junctions and Na_v channels clustering.

Different studies have shown conflicting observations and conclusions about whether paranodal axoglial junctions can promote the clustering of Na_v channels at the nodes. Previous study in our lab has shown Nfasc155–Caspr–Contactin complex is sufficient to cluster Na_v at the nodes using a transgenic animal line (Zonta et al., 2008). But it has been suggested that our transgenic line may have epitopic expression of Nfasc155 in neurons (Thaxton et al, 2011). My question here is:

- Can I find a different approach to exam the function of Nfasc155–Caspr–Contactin complex in Na_v clustering?

In order to address the questions, this work aims to gain a better understanding of the role of paranodal axoglial junctions in clustering Na_v channels in the following ways:

- Generating a cre line in which cre is active in neurons only.
- Using the cre line to delete all neuronal Neurofascins at early age but keep the glial Neurofascin expression under its endogeous promoter.
- Studying the Nav clustering in this mouse line in which nodes are disrupted after the deletion of neuronal Neurofascins and Nfasc155–Caspr–Contactin complex is presented under endogeouse promoters.

2. Materials and Methods

All mouse lines used in this work were of congenic C57Bl6 background. C57Bl6 strain was chosen due to its robustness, easy breeding and availability of knowledge in its physiology and genetics. Most importantly, many neurobiological mutations have been generated and studied in this strain.

All animal work conformed to UK legislation (Scientific Procedures) Act 1986 and the Edinburgh University Ethical Review policy.

2.1 RT-PCR

2.1.1 Full length *Nfasc140* RT-PCR

TRIzol® Reagent (Life Technologies) was used to extract mRNA from fresh tissues. After sacrificing animals, the whole brains or hindbrains from wild-type animals were taken immediately. Brain tissues were weighed and TRIzol® Reagent (1 mL TRIzol per 50–100 mg brain tissue) was added. After homogenization by hand in 1.5ml tubes using plastic pestles RNA was purified according to the manufacturer's instructions and the air dried RNA was dissolved in 30 µl water.

To eliminate any DNA contamination, a DNase treatment was applied to the RNA solution. DNA-free™ Kit (Ambion) was used. Then a spectrophotometer (GeneQuant1300, GE healthcare) was used to measure the concentration of mRNA. An A260 reading of 1.0 is equivalent to ~40 µg/ml single-stranded RNA. The A260/A280 ratio is used to assess RNA purity. An A260/A280 ratio of 1.8 2.1 is indicative of highly purified RNA.

Moloney Murine Leukemia Virus Reverse Transcriptase (M-MLV RT, Promega) was used to synthesize the first-strand of cDNA from mRNA. 2 µg of RNA was mixed with 0.5µg random primers in a total volume of 14 µl. This was heated to 70℃ for 5min and then cooled on ice immediately. The following were then added: 5 µl M-MLV 5x Reaction Buffer, 1.25 µl 10mM dNTP, 1 µl M-MLV RT and 2.75 µl

water (25 µl in final volume). After mixing well the reactions were incubated for 60 min at 37 ℃ and 15 min at 42 ℃. The control group had water instead of M-MLV RT.

After first-strand cDNA synthesis, cDNA was diluted 10 times and used as the template for the following full length Neurofascin PCR. 5 units of Phusion DNA polymerase (NEB) was used, the PCR primers were: M186EcoSalF1 (5'-ATGGCCAGGCAGCAG GCGCCAC-3') M186 Not stop R1 (5'-CCATCTATTCCCTTGCCTGA-3'). PCR program was : 1 cycle of 98 ° C denaturation for 5 min, 53.5 ℃ annealing for 30 s, and 72 ℃ extension for 130 s. 2 cycle of 98 ℃ denaturation for 1min, 53.5 ℃ annealing for 30 s, and 72 ℃ extension for 2min and 10 s. 37 cycle of 98 ℃ denaturation for 30 s, 53.5 ℃ annealing for 30 s, and 72 ° C extension for 130 s. The final extension was at 72 ℃ extension for 5min. After running on a 1% agarose gel a single band was detected and sequencing showed it was the 140 kDa isoform of Neurofascin first described by the group of Vann Bennett in 1996.

Primers used for sequencing the whole cDNA sequence were:
T7 (5'-TAATACGACTCACTATAGGG-3')
IG6R1 (5'-CCGAGGACCAGGTGGCCAAG -3')
mFn3BR1 (5'-CGCCACTTGACAATGTAGCG -3')
3DR1 (5'- AAGCGGTAACGCGACACTGG-3')
Sp6 (5'-TATTTAGGTGACACTATAG -3')

2.2 Construct preparation for transgenesis

2.2.1 *Thy-1-Nfasc140 (T140)* strategy:

To drive the expression of Nfasc140 with a Flag tag at its C-terminus under the control of the Thy-1 (thymus cell antigen 1) promoter, a vector with the full length *Nfasc140* cDNA with a Flag tag sequence was generated. As the 5'-end (exon3-exon19,sixIgG domains) of *Nfasc186* and *Nfasc140* are similar, hence, the 5'-end segment was released from a *Thy-1-Nfasc186* construct (Zonta *et al.,* 2011) using

EcoRI and BamHI and ligated into the MP32 vector to introduce a SalI site at the 5'-end of the sequence.

mRNA was extract from P1 mouse brain and the first strand cDNA was synthesised using the same protocols above. Using Primers: Ig6186F1 (5'-GGCCACTC CAACTAACCGTTTG-3') and m186NotstopR1 (5'-CCATCTATTCCCTTGCCTGA-3'), *Nfasc140* 3'-end segment (exon19 - exon33) was amplified from the first strand cDNA.

A single step "patch" PCR (Squinto *et al.,* 1990) using three oligonucleotide primers was used to add a Flag tag at the C-terminus of the *Nfasc140* 3'-end segment, upstream of the termination codon (TGA), as follow: the forward primer was Ig6186F1 (5'-GGCCACTCCAACTAACCGTTTG-3'). The first reverse primer (Flag1) added half the Flag sequence and it also included a Gly-Gly sequence to bridge the Nfasc140 and the Flag tag (5'-TTGTCATCGTCATCCTTGTAGTCACCTCCGGCAAGGGAATAGA TGGCA-3'). The second reverse primer (Flag2) had the rest of the Flag tag, followed by a stop codon and a unique HindIII restriction site (5'-GGCCCAAGCTTTCACTT GTCATCGTCATCCTT-3').

Optimized primer ratios were used. Approximately 20 ng of cDNA template were used in a total 50 µl PCR reaction containing Pfu polymerase buffer, 0.2 mM dNTPs, 0.2 µM forward primer, 0.002 µM reverse primer FLAG1, 0.2 µM reverse primer FLAG2 and Pfu polymerase (1U, NEB). The PCR program is: 1 cycle of 98℃ denaturation for 1 min, 5 cycles of 98℃ denaturation for 30 s, 55℃ annealing for 30 s, and 72℃ extension for 4 min. The first part of the PCR reaction favoured the amplification using the 5' and FLAG1 primers, after which conditions were modified to allow the 5' and FLAG2 primer pair to amplify the product generated from the first amplification. The second part of PCR included 25 cycles of 98℃ denaturing for 30 s, 60℃ annealing for 30 s and 72℃ for 4 min. The last cycle was 72℃ extension for 4 min.

The PCR product was purified using the QIAquick PCR purification kit (QIAGEN). The PCR product of the *Nfasc140* 3'-end segment with Flag tag was digested by BamHI and HindIII and consequentially the 5'-end Nfasc140 segment with SalI site was released from the MP32 vector. Two segments were ligated at BamHI sites and the whole Nfasc140-Flag was then inserted into the NotI and HindIII sites of pSP72 vector (Promega). The ligation was performed using 1 U of T4 DNA Ligase, Quick Ligase Buffer (New England BioLabs) at room temperature for 10 min. Competent XL1-blue cells were transformed (Sanbrook and Russell, 2001) and plated on Luria-Bertani medium (LB) agar (Melford) containing 0.1 mg/ml Carbenicillin.

In order to introduce another SalI site at the 3'-end, *Nfasc140-Flag* was cut with NotI and HindIII and inserted into vector pBlueScript SK. Then the Nfasc140-Flag was released from two SalI sites and dephosphorylated with alkaline phosphatase (NEB). pTSC21K vector (Lüthi *et al.*, 1996) was digested with XhoI successively. Nfasc140-flag was then inserted into pTSC21K vector using the ligation method described above. Nfasc140-flag positive clones were grown overnight in 5 ml LB with 1mg/ml Carbenicillin and purified by SDS/alkaline lysis using a plasmid DNA purification kit (Nucleospin, Macherey-Nagel). Plasmids were then sent for sequencing to check for errors (DNA Sequencing Service, Dundee University). Sequencing primers:

Fn3DF1 5'- CAGGCGGTTCAGAGTCCGAC - 3'
ThyR2 5' - GCTAGTGGTATGCATGGAGGGAG - 3'
ThyF2 5'- GGCAAAGGACCTTAGGCAGTGT -3'

The mouse *Nfasc140*-Flag was cloned into the XhoI site of the pTSC21k vector and was released using Not I (Fig. 13).

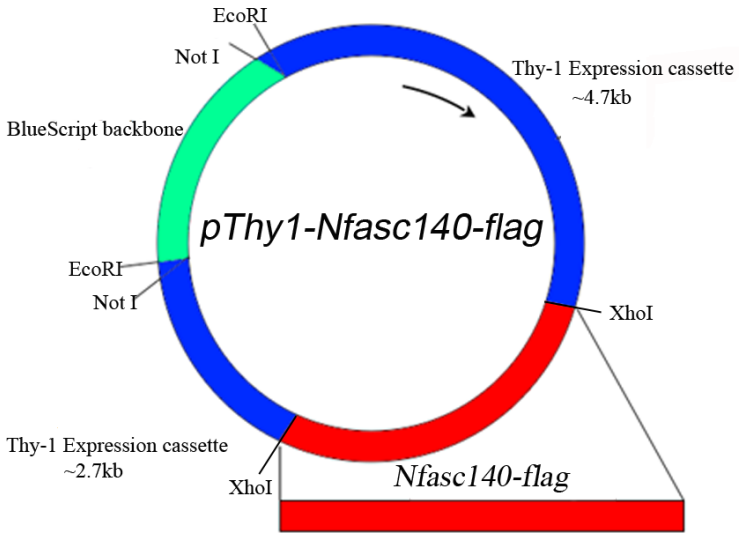

Figure 13. Schematic representation of the *Thy1-Nfasc140-flag* vector.
Red portion of the vector represents the *Nfasc140-flag* cDNA which was inserted into the XhoI site of the vector. The blue and segments show the backbone of the Blue Script and Thy-1 Expression cassette.

2.2.2 *Thy-1-Cre* strategy:

The pCreERT2 vector (Feil *et al.*, 1997 and Imai *et al.*, 2001) was used as the template to amplify the *Cre* sequence. A primer pair was designed to introduce 2 XhoI sites on each side of the DNA and a Kozak sequence just before the *Cre* sequence. The forward primer is CRE FW: (5'-GCGCTCGAGACCATGTCCAATTTACTGACC GTAC-3'); the reverse primer is Cre RV: (5'-CGCCTCGAGCTAATCGCCAT CTTCCAGCAG-3').

Approximately 20 ng of cDNA template were used in a total 50 µl PCR reaction containing Pfu polymerase buffer, 0.2 mM dNTPs, 0.2 µM forward primer, 0.002 µM reverse primer FLAG1, 0.2 µM reverse primer FLAG2 and Pfu polymerase (1U, NEB) The PCR program is: 1 cycle of 98 ℃ denaturation for 30 s, 55 ℃ annealing for 30 s, and 72 ℃ extension for 40 s. 10 cycle of 98 ℃ denaturation for 10 s, 55 ℃ annealing for 30 s, and 72 ℃ extension for 40 s. 25 cycle of 98 ℃ denaturation for 10 s, 65 ℃ annealing for 30 s, and 72 ℃ extension for 40 s. 1 cycle of 98 ℃ denaturation for 100 s and 72 ℃ extension for 4 min.

15 µl PCR product was digested with 20 units of XhoI in 37 ℃ for 2 h, and then heated to 65 ℃ for 15 s to inactivate XhoI. De-phosphorylation was performed on the PCR product. 4 µl buffer 10x, 1 µl alkaline phosphatase (NEB.) 5 µl H_2O, 30 µl digested DNA were mixed and put into 50 ℃ for a 30min reaction.

Using the ligation method mentioned before, the *Cre* was cloned into the XhoI site of the pTSC21k vector (Lüthi *et al*., 1997) and was released using NotI (Fig. 14).

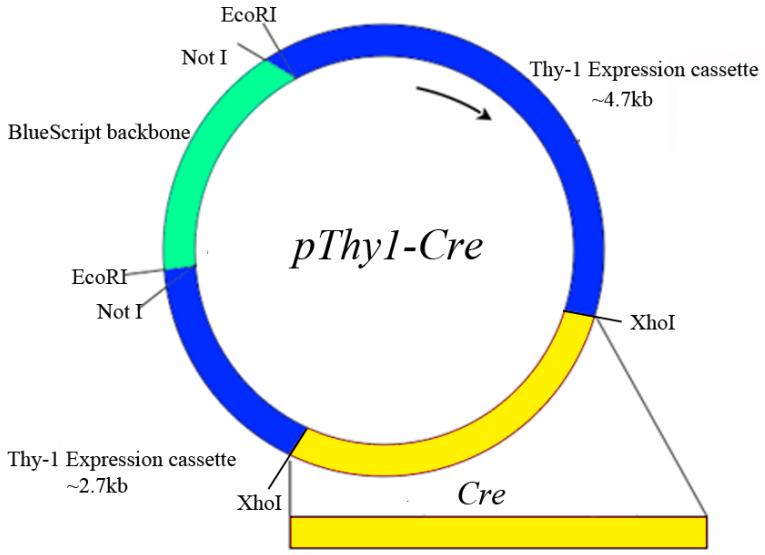

Figure 14. Schematic representation of the *Thy1-Cre* vector.
The yellow portion of the vector represents the *Cre gene* which was inserted into the XhoI site of the vector. The blue and green segments show the backbone of the Blue Script and Thy-1 Expression cassette.

2.2.3 DNA purification for injection

Dr Barbara Zonta purified the DNA for microinjection. Briefly, prokaryotic sequences were removed by NotI digestion of 50 µg of plasmid, followed by purification of the insert on 0.8% low melting point agarose gel electrophoresis. The transgene was excised and the agarose was digested with Gelase (Epicentre Biotechnologies) according to the manufacturer's instructions. The DNA was then purified on an Elutip-D column (Whatman), followed by ethanol precipitation and resuspension in injection buffer (0.1 mM EDTA, pH 8.0, 10 mM Tris HCl, pH 7.5). The DNA was dialysed against injection buffer and the concentration measured.

Finally, the purified DNA was diluted with injection buffer to obtain a final concentration of 2.5 μg/ml.

2.2.4 Pronuclear microinjections of DNA

Pronuclear microinjections of the transgene and embryo transfers (Hogan *et al.,* 1994) were performed by Heather Anderson. Briefly, fertilized oocytes were obtained from super ovulated C57BL6/CBA F1 hybrid female mice mated with F1 hybrid males. After injection, fertilized eggs at the one or two-cell division stage were transferred into pseudo-pregnant MF1 foster mothers. Genotyping using ear biopsies was done at approximately P21.

2.3 Animals and genotype screening

All animal procedures reported in this work were performed according to Home Office regulations, Animals (Scientific Procedures) Act 1986.

2.3.1 *Nfasc*$^{-/-}$ mice

Nfasc$^{-/-}$ mice were generated by homologous recombination in ES cells as previously described (Sherman *et al.,* 2005). Briefly, the targeting construct was designed to generate S129 ES cells clones with a deletion of exon 5 (3 kb), which introduces a frame shift resulting in a stop codon in exon 6. One clone with the desired modification (2D7) was then injected into C57Bl/6-derived blastocysts, transferred into pseudo-pregnant mothers to generate chimeras. *Nfasc*$^{+/-}$ mice were backcrossed to a C57BL/6 background for at least six generations before experimental analysis.
Since *Nfasc*$^{-/-}$ mice die by postnatal day (P) 7, litters were harvested at P6 and identified by genotyping using biopsy.

2.3.2 *Nfasc*^{flox} mice

Nfasc^{flox} mice were generated in our lab as previously described (Zonta *et al.,* 2011). Using the same strategy as the one used for *Nfasc*$^{+/-}$ mice, but with an alternative excision where only the PGK*neo*-HSV*tk* cassette was removed and where the preserved exon 4 was flanked by two *loxP* sites.

2.3.3 Transgenic mice T140

The vector with Flag tagged Nfasc140 driven by the Thy-1 promoter was digested with Not I to release the transgene. The DNA purification and injection was conducted as described before (2.2.3 DNA purification for injection and 2.24 Pronuclear microinjections of DNA). Transgenic founders were identified by PCR (see details below), back-crossed to a C57BL6 background and interbred with *Nfasc*$^{+/-}$ to generate *Nfasc*$^{-/-}$*/Nfasc140* mice.

2.3.4 Transgenic mice *T186*

The T186 transgenic mouse line was generated by Dr Barbara Zonta and Dr Anne Desmazieres (Zonta *et al.,* 2011). The full length *Nfasc186* cDNA with a flag tag was inserted in to the pTSC21k vector (Lüthi *et al.,* 1997) and was released using NotI. And the transgenic mice were generated as for *T140* mice.

2.3.5 Generating *Nfasc*$^{-/-}$*/T140* and *Nfasc*$^{-/-}$*/T186* mice

Since *Nfasc*$^{-/-}$ die at p7, *Nfasc*$^{+/-}$ was crossed with *T140* to generate *Nfasc*$^{+/-}$*/T140* mice; then *Nfasc*$^{+/-}$*/T140* was interbred with *Nfasc*$^{+/-}$ again to generate *Nfasc*$^{-/-}$*/T140*. *Nfasc*$^{-/-}$*/T186* was generated using the same breeding strategy. The genotyping PCR procedures for all those animals will be described later.

2.3.6 Ear and tail biopsies

Ear biopsies were digested overnight at 55 ℃ in 50 µl lysis buffer (150 µl for 5 mm tail clips). 50 µl lysis buffer contained 50 mM TRIS, 50 mM pH 8.0 EDTA, 0.25% SDS and 1.3 µl Proteinase K (1mg/ml, Roche). After digestion, unpurified lysate was vortexed, spun briefly and the supernatant was diluted 1:10 in double distilled (MilliQ) water. For PCRs, 2 µl of the ear or tail diluted digests were added to the PCR reaction as DNA templates.

2.3.7 PCR for colony and animal biopsies

For animal tissues, the PCR reactions were performed in a total 25 µl consisting of 1 X Go Taq Buffer, 1.5 mM MgCl2, 0.2 mM dNTPs, 0.5 µM of primers and 1 U of Go Taq polymerase (Promega) in MilliQ water. Positive and negative controls were always included alongside the test samples.

For colony PCR, colonies which were grown on agar plates and single colonies were randomly picked and resuspended in 5 µl LB. And 2 µl of them were added to the PCR reaction as DNA templates.

The PCR conditions for Go Taq polymerase (Promega) were: 1 cycle 94℃ denaturing for 2 min, 57℃ annealing for 30 s and 72℃ extension for either 1 min or 30 s according to the size of the product. This was followed by 30 cycles of 94℃ for 40 s, 57℃ for 30 s and 72℃ for either 1 min or 30 s. The final step consisted of 94℃ for 40 s, 57℃ for 30 s and 72℃ for 2 min. (according to different PCR program the annealing temperature and extension time vary.)

According to the size of the PCR products, they were resolved on 0.8-2% agarose gel in TAE buffer containing 0.5 µg/ml ethidium bromide and visualised by UV transillumination (Uvitec, Cambridge).

2.3.8 Various genotyping

Nfasc$^{-/+}$ and *Nfasc*$^{-/-}$ PCR

To identify the Neurofascin heterozygous (Nfasc$^{-/+}$) or Neurofascin knock out (Nfasc$^{-/-}$) mice, the primers were designed to flank exon 4. The forward primer NFFW1 (5'-GTGCTGATCCAGCCTAAAGC-3') and the reverse primer NFRV1 (5'-TCAGCTGTTTTGAGCCACAC-3') generated approximately a 1.1 kb and a 700 bp products in wild type and null mice respectively (Fig. 15). The PCR conditions were: 1 cycle of 94℃ denaturation for 1.5 min, 55℃ annealing for 30 s, and 72℃ extension for 3.5 min. This was followed by 38 cycles of 94℃ for 30 s, 55℃ for 30 s,

and 72 ℃ extension for 1 min 10 s. Finally, the last cycle consisted of 94 ℃ for 40 s, 55 ℃ for 30 s and 72 ℃ for 6 min.

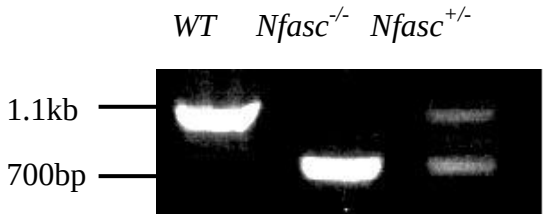

Figure 15. PCR diagram showing the genotyping result of Wild-type, *Neuorfascin* knock-out and heterozygous mice.
PCR of DNA from a WT mouse generated a product with the size of around 1.1kb. The *Nfasc*$^{-/-}$ generated a band at around 700bp. And PCR of the *Nfasc*$^{+/-}$ generated two bands at both 1.1kb and 700bp.

T140 PCR

To identify the flag tagged full length *Nfasc140* PCR was performed by using a forward primer En3DF1: (5'-CAGGCGGTTCAGATCCGAC-3') located at the Fibronectin IIID domain and a reverse primer 186flag2: (5'-GGCCCAAGCTTTCACTTGTCAT CGTCATCCTT-3') located at the FLAG tag sequence. The transgene generated a PCR product of approximately 500 bp (Fig. 16). The PCR conditions consisted of 1 cycle of 94 ℃ denaturation for 2 min, 58 ℃ annealing for 30 s, 72 ℃ extension for 40 s, followed by 33 cycles of 94 ℃ for 40 s, 58 ℃ for 30 s, and 72 ℃ for 40 s. The final cycle consisted of 94 ℃ for 40 sec, 58 ℃ for 30 sec, and 72 ℃ for 5 min.

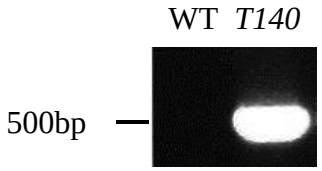

Figure 16. PCR diagram showing the genotyping result of *T140* transgenic mice.
Genomic DNA from *T140* transgenic mouse generated a PCR product of around 500 bp.

T186 PCR

To identify the flag tagged full length *Nfasc18*6, a PCR was performed by using a forward primer En3EF1: (5'-GTGGTTGAGTACATCGACAG-3') located at the

Fibronectin IIIE domain specific for *Nfasc186* and a reverse primer 186flag2: (5'-GGCCCAAGCTTTCACTTGTCATCGTCATCCTT-3') located at the FLAG tag sequence. The transgene generated a PCR product of approximately 600 bp (Fig. 17). The PCR conditions consisted of 1 cycle of 94℃ denaturation for 2 min, 56℃ annealing for 30 s, 72℃ extension for 40 s, followed by 33 cycles of 94℃ for 40 s, 56℃ for 30 s, and 72℃ for 40 s. The final cycle consisted of 94℃ for 40 sec, 56℃ for 30 sec, and 72℃ for 5 min.

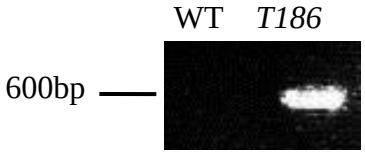

Figure 17. PCR diagram showing the genotyping result of *T186* transgenic mice.
Genomic DNA from *Thy1-Nfasc186Flag* transgenic mice generated a PCR product of 600 bp.

Thy-1-Cre PCR

To identify the mouse carry *Thy-1-Cre*, PCR was performed by using a forward primer F6: (5'-CCAATTTACTGACCGTACACC-3') and a reverse primer R4: (5'-AGCGTTTTCGTTCTGCCAAT-3') both of them located at the *Cre* sequence. The transgene generated a PCR product of approximately 600 bp (Fig. 18). The PCR conditions consisted of 1 cycle of 94℃ denaturation for 2 min, 56℃ annealing for 30 s, 72℃ extension for 40 s, followed by 33 cycles of 94℃ for 40 s, 56℃ for 30 s, and 72℃ for 40 s. The final cycle consisted of 94℃ for 40 sec, 56℃ for 30 sec, and 72℃ for 1 min.

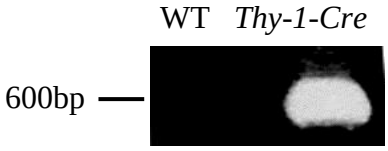

Figure 18. PCR diagram showing the genotyping result of *Thy-1-Cre* transgenic mice.
Genomic DNA from *Thy1-Cre* mice generated a PCR product of 600 bp.

Nfasc$^{flox/+}$ and *Nfasc*$^{flox/flox}$ PCR

To identify the mouse carry *loxP* flanked Neurofascin allele/alleles, PCR was performed by use of a forward primer NFFW1: (5'-GTGCTGATCCAGCCTAAAGC-3') and 2 reverse primers NFLS1R: (5'-TGCGAAGTTATGGGCCCCAG-3') and NFLS2R: (5'-CCTCTCCAAGCAGAGTACTC-3'), they located at the both sides of the exon4 of *Neurofascin* sequence. The WT generated a PCR product of 917 bp and the transgene generated a PCR product of 414 bp (Fig. 19). The PCR conditions consisted of 1 cycle of 94 ℃ denaturation for 2 min, 60 ℃ annealing for 30 s, 72 ℃ extension for 1 min 10 s, followed by 36 cycles of 94 ℃ for 40 s, 60 ℃ for 30 s, and 72 ℃ for 1 min 10 s. The final cycle consisted of 94 ℃ for 40 sec, 60 ℃ for 1min, and 72 ℃ for 1 min.

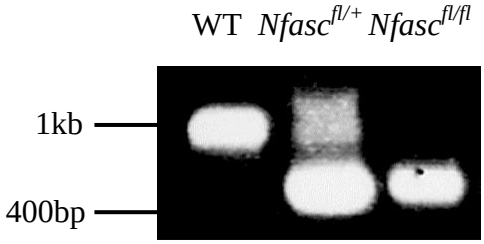

Figure 19. PCR diagram showing the genotyping result of *LoxP* flanked *Neuorfascin* mice.
PCR of WT mouse generated a product of around 1kb. The $Nfasc^{fl/fl}$ had a band at around 400bp. And PCR of the $Nfasc^{fl/+}$ generated bands at both 1kb and 400bp.

2.4 Indirect Immunofluorescence

2.4.1 Tissue fixation and preparation for immunostaining

Mice at different ages, from adult to P6, were anesthetised with an intraperitoneal injection of euthatal (50-60 µl per adult and p6 animal). To perfuse the animal, 4% paraformaldehyde in 0.1 M phosphate buffer (PB) was injected through the left ventricle, pH 7.4. 20 ml paraformaldehyde PB solution was used per adult mouse and 10 ml paraformaldehyde PB solution was used per P6 mouse during perfusion. After perfusion, whole brains and cervical spinal cords (C2-C7) were dissected out and post-fixed in the same fixative for 5 min; quadriceps nerve and sciatic nerves were

harvested and post-fixed for 15 min at room temperature; brains from young and adult mice were post-fixed for 3 h.

2.4.2 Frozen-sections

The preparation for immunostaining: specimens were washed 3 X 10 min in 0.1 M PB and cryoprotected in 5% sucrose in PB for 2 h, 15% sucrose in PB for 2 h and then in 25% sucrose in PB at 4℃ overnight. Tissue samples were oriented appropriately in O.C.T. embedding matrix compound (CellPath Ltd) and frozen with dry ice cooled isopentane. The blocks were then stored at -80℃ until use. Consecutive 10-14 μm parasaggital brain sections and transverse sections of cervical spinal cords were cut using a Leica CM 3050 S cryostat and collected on 3-aminopropyltriethoxysilane (TESPA)-coated glass slides. Sections were dried and stored at -20℃ until use.

2.4.3 Teased fibre preparation

After fixation, quadriceps and sciatic nerves and cervical spinal cords were washed in PBS 3 X 10 min each and placed in a 35 mm Petri dish. The perineurium of quadriceps and sciatic nerves was removed and fibre bundles were separated using a pair of acupuncture needles, in PBS on TESPA-coated slides.

Cervical spinal cords were placed in the Petri dish with the ventral side facing up and the ventral funiculus *or* columns were carefully peeled from either side, very close to the central gulf (the median fissure), with fine forceps. Small fragments of tissue were then placed in a drop of PBS on TESPA-coated slides. Using acupuncture needles, by gently pushing or dragging the small tissue on slides the single fibres were separated from the bulk of the tissue. Teased fibres slides were air dried for immunohistochemistry or stored at -20℃ for future use.

2.4.4 Immunostaining and photo acquisition

Teased fibres and fixed tissue sections on glass slices were first treated with blocking buffer (5% fish gelatin, 0.1% TritonX100 for teased fibres or 0.15% TritonX100 for tissue sections in PBS) for 1 h at room temperature in humidified chambers. Primary

antibodies were diluted accordingly in the same blocking buffer and applied on slices overnight at room temperature. The slices were washed with PBS for 5 times, each time for 5 min and fluorescent-conjugated secondary antibodies were applied in blocking buffer for 1 h and 15 min at room temperature. After blocking, the slices were washed with 0.1% Tween20 in PBS 5 times, 5 min for each wash. The slices were then mounted with Vectashield (Vector Laboratories.)

The primary and secondary antibody dilutions are included in the section 2.8 Antibodies used for immunolabelling.

To acquire images for morphological analysis, an Olympus BX60 microscope equipped with a Hamatsu ORCA-ER digital camera and OpenLab software (version 5.0) was used. All high magnification immunofluorescent photos were acquired using a Leica TCL-SL confocal microscope and proprietary software (Leica confocal softer ware version 2.6.1). FITC, TRITC and Alexa Fluor-647 fluorophores were excited with an Argon (488 nm) and HeNe (543 nm) laser respectively. For each photo, 4 (6 for AIS pictures) images at different points along the Z-axis were scanned and the maximum projection of the Z series were used. Photos were rendered using Photoshop CS6 (Adobe).

2.5 Western Blot

2.5.1 Protein extraction

Animals were sacrificed by treatment with CO_2 or by cervical spinal cord dislocation. Animal tissues such as brain, spinal cord and peripheral nerves were frozen in dry ice or liquid nitrogen immediately. Frozen tissues were store in -80 ℃. Phosphate buffer saline (PBS) with 1x Complete protease inhibitor cocktail (Roche) and 1 mM PMSF was cooled on ice to be used as the homogenization buffer.

For CNS tissues, brain and spinal cord, 200 µl of homogenization buffer with 1% sodium dodecyl sulfate (SDS) were added to 0.04 g tissue (for P30 and older animals, 150 µl was used per 0.04 g tissue). Homogenization was conducted in a 1.5 ml tube

and a plastic pestle was attached to a drill (Black&Deker, 450W) to homogenise the tissues. The lowest drill spin speed was used to homogenise tissue for 30-60 s, and the tissue lysates were on ice and cool all the time. After homogenization, a 13,000 rpm centrifugation was applied to the lysate for 1 min and the supernatant was carefully moved to another tube. Protein concentration was estimated using the BCA (Bicinchoninic acid) assay (Pierce). And an appropriate amount of sodium dodecyl sulfate (SDS), dithiothreitol (DTT) and 4X sample buffer (20% glycerol, 130 mM Tris pH 6.8, bromophenol blue) were added into the lysate so that the lysate should have a final concentration of 4% SDS, 100 mM DTT and 1X sample buffer. The lysate was then mixed quickly and boiled for 10min.

For PNS tissues, nerves nerves were homogenized in 50 µl of RIPA buffer (50 mM Tris pH 7.5, 150 mM NaCl, 1% NP-40, 0.1% SDS, 0.5% sodium deoxycholate, 1 mM EDTA) containing phosphatase and proteinase inhibitors on ice for 25 min. After centrifugation at 13000 rpm at 4^{o}C for 20 min, the supernatant was recovered. Protein concentration was determined and proteins were prepared as described above.

2.5.2 Immunoblotting

SDS-Page gels were poured in a casting frame (Bio Rad). Each running gel contained 5-15% acrylamide, 0.375 M pH8.8 Tris, 0.1%SDS, 0.1%APS, 0.1-0.05% TEMED. The stacking gel was 5% acrylamide, 0.12 M pH 6.8 Tris, 0.1%SDS, 0.1%APS, 0.1-% TEMED. After loading samples into the wells, the gel was run with running buffer (25 mM Tris, 192 mM glycine, 0.1% SDS, pH8.3) at 180V, until the blue dye reached the bottom of the gel.

The gel was transferred to nitrocellulose membrane (Whatman, Protran) in buffer containing 25 mM Tris HCl pH 8.3, 250 mM glycine and 20% methanol for 2 h at 400 mA inside a transfer tank (Hoefer). The membrane was blocked overnight at 4 ℃ in 5% skimmed milk, 0.1% Tween 20 in PBS.

To detect specific proteins, the membrane was incubated with primary antibodies, diluted as specified in Table 1 and 2 (section 2.8 Antibodies used for

immunolabelling) with blocking buffer containing 0.2% gelatine, 0.1% Tween20 in PBS for 1 h at room temperature. After 6 times 5 min washes in blocking buffer, the membrane was incubated with species-specific HRP-labelled secondary antibodies for 45 min at room temperature. The excess of secondary antibody was removed by 6 times 5 min washes in PBS and detected using the enhanced chemiluminescence (ECL) method (Santa Cruz Biotechnology).

2.6 Quantitative analysis

2.6.1 Quantification of nodes with Nfasc186 and Na_v channel immunoreactivity

To compare the percentage of nodes displaying Na_v channel immunoreactivity among P6 *Nfasc*$^{fl/fl}$ and *Tcre-Nfasc*$^{fl/fl}$ (3 animals each), teased fibres from both CNS (ventral columns of cervical spinal) and PNS (quadriceps nerves) were labelled with various antibodies. Teased fibres were triple-labelled with NFC-2, MNF-2 and Na_v channel. NFC-2 was used as a marker of both nodal protein Nfasc186 and paranodal protein Nfasc155. MNF-2 was used to detect Nfasc186 only at the nodes.

Confocal images of 40 nodes per animal under the same condition were randomly chosen from different axons and captured. Two animals were used in each condition. Only the nodes which had been flanked by two paranodes were chosen and used for statistical analysis. Means of percentage of Nfasc186 and/or Na_v channel positive nodes and were calculated using Excel.

2.6.2 Protein level measurement on western blots.

Western blot was scanned with Epson scanner (3200). The relative density for proteins samples were measured using softer ware ImageJ 1.47t (National Institutes of Health) according to the method from http://lukemiller.org. Basically, it measures the size and intensity of the protein band on western blot and comparing two bands it gives the relative density between 2 bands. And also by comparing the loading control the density can be adjusted accordingly.

2.7 Physiology and behaviour analysis

2.7.1 Nerve Conduction Velocity

Femoral nerves and their quadriceps branch were carefully dissected from WT, T140 and T186 mice at the age of 2 months (n=6), and maintained in oxygenated mammalian HEPES physiological solution which contains 137 mM NaCl, 5 mM KCl, 2 mM CaCl2¬, 1 mM MgCl2¬, 5.5 mM D-glucose and 5 mM HEPES, pH 7.2-7.4. For periods of no longer than 15 min, nerves were transferred and placed on an array of silver electrodes (Fig. 21 A) with 1 mm intervals in a chamber and surrounded by 37oC liquid paraffin to isolate nerves from other electrical interference. Compound action potentials (CAP) were recorded from the distal end of the quadriceps branch by stimulating the proximal end of the femoral or quadriceps nerve with a square wave (0.15 ms, 0.8-2.5 V, mostly around 1 V). Depending on the length of the nerves, a few recordings were required at different conduction distances. The conduction distance was altered from 5 mm to max. 11 mm by connecting the stimulating electrode to different silver electrodes array successively at a decreasing distance from the recording electrodes. According to the wave shapes of CAP signals, the voltage of stimulus was adjusted to make the wave shapes and wave amplitude between nerves are similar in order to ensure the stimulation of a similar sub-group of nerve fibres (Fig. 20B). Signals of CAP were converted to digitized signals using Scope software (PowerLab/Scope data acquisition system from AD instrument and a Mac computer). Latencies of the onset of CAP were measured, which is the time gap between the starting of stimulation and the appearance of the peak of the CAP for all conduction distances(Fig. 20B). The conduction velocity was calculated from the slope of the regression line by plotting conduction distances against the corresponding latencies. Recordings were repeated 2-3 times for each nerve. The conduction velocity per animal was determined by averaging the mean conduction velocity recordings from both nerves.

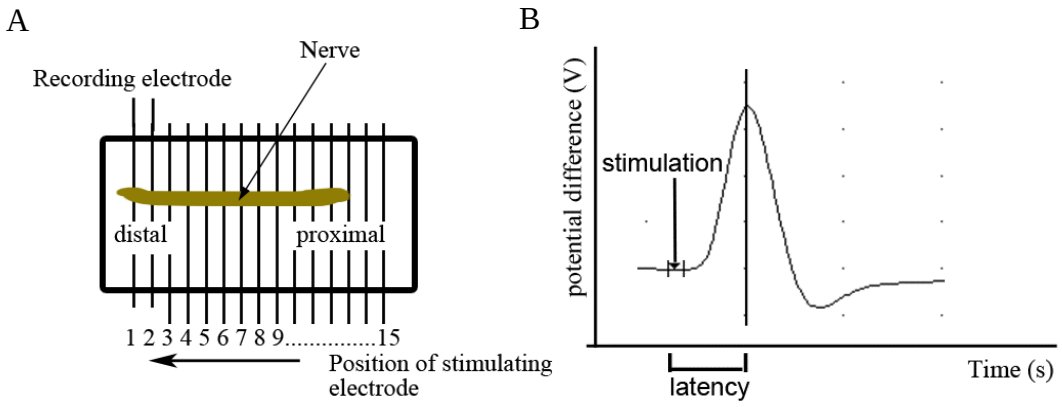

Figure. 20 Diagram of recoding a compound action.

A. The schematic picture showing a never on an array of electrodes. And the electrode was connect to the stimulate from silver electrodes no.15 towards no.1 when stimulating the nerves.
B. The wave shape of a CAP signal was demonstrated there. The latency of one CAP was the time between stimulation and the wave reaching highest amplitude.

2.7.2 RotaRod

2-month-old WT, *T140/Nfasc*$^{-/-}$ and *T186/Nfasc*$^{-/-}$ mice (4 per group) were trained on a 5-lane mouse RotaRod (Ugo Basile) for two consecutive days before the test on day 3. Animals were placed on a rotating RotaRod (3-cm diameter) sequentially at 24 rpm and 32 rpm for a maximum of 60 s, four times at each speed. Each trial run was separated by a 10 min rest period. During the 60 s, mice were removed from the RotaRod either when they fell off the rod or they hold the rod rotating with rod for 2 cycles. The mean latency of each mouse to fall or rotate with rod, which measures the length of time each animal was able to stay on the rod, was determined by the mean latency from the four trials for each rotating speed obtained on day 3.

2.8 Statistics

All statistical analysis was performed and graphs were produced using GraphPad Prism (version 5.0c). All values are expressed as mean ± SEM. Unpaired, two-tailed Student's t- test was used to determine statistical significance between 2 groups of samples. One-way analysis of variance (ANOVA) followed by Tukey HSD multi-

comparison post-test was used to assess *p* values between multiple samples (3 or more unpaired groups).

2.9 Antibodies used for immunolabelling

The following tables show the antibodies used for indirect immunofluorescence (IF) and Western blotting (WB), also their working dilutions is shown here.

Table 1. Primary antibodies

Antibody name	Species	Source	Dilution
Anti β Actin (2-15)	Rabbit	P.J. Brophy	1:10000 (WB)
Anti βIII Tubulin	Mouse, monoclonal IgG_{2b}	Sigma	1:500 (WB)
Anti βIV Spectrin	Rabbit	P.J. Brophy	1:200 (IF)
Anti Ankyrin G	Mouse, monoclonal IgG_1	Calbiochem	1:50 (IF)
Anti Ankyrin G	rabbit	V. Bennett	1:1000 (IF)
Anti Calbindin D-28K	Mouse, monoclonal IgG_1	Sigma	1:1000 (IF)
Anti Calbindin D-28K	Rabbit	Swant	1:5000 (IF)
Anti CASPR	Mouse, monoclonal IgM	M. Rasband	1:50 (IF-WB)
Anti CASPR	Rabbit	D.Colman	1:5000 (IF)
Anti FLAG M2	Mouse, monoclonal IgG_1	Sigma	1:400 (IF)
Anti GFAP (GA5)	Mouse, monoclonal IgG_1	Boehringer	1:100 (IF)
Anti L-MAG	Rabbit	P.J. Brophy	1:2000 (IF) 1:4000 (WB)
Anti-MBP	Chicken, IgY	Chemicon	1:25 (IF)
Anti MBP (peptide 7)	Rabbit	P.J. Brophy	1:2000 (IF) 1:5000 (WB)
Anti MNF-2(Nfasc186)	Rabbit	P.J. Brophy	1:400 (IF) 1:2000 (WB)
Anti NFC1 (Pan Neurofascin)	Rabbit	P.J. Brophy	1:1000 (IF) 1:2000 (WB)
Anti NFC3 (Pan Neurofascin)	Sheep	P.J. Brophy	1:1000 (IF) 1:2000 (WB)

Anti NFF3 (Nfasc155)	Rabbit	P.J. Brophy	1:1000 (IF) 1:2000 (WB)
Anti NF-H 200kD	Mouse, monoclonal IgG_1	Sigma	1:200 (IF)
Anti NrCAM (1)	Rabbit	P.J. Brophy	1:200 (IF)
Anti OSP/Claudin 11	Mouse, monoclonal IgG2a	A. Gow	1:100
Anti OSP/Claudin 11	Rabbit	Zymed	1:50(IF) 1:500 (WB)
Anti Pan Na_v channels	Mouse, monoclonal IgG_1	Sigma	1:100

Table 2. Secondary antibodies

Antibody name	Species	Source	Dilution
Alexa Fluor-568-conjugated anti mouse IgG2b	Goat	Molecular Probes	1: 1000
Alexa Fluor-647-conjugated anti mouse IgG1	Goat	Molecular Probes	1:200
Alexa Fluor-647-conjugated anti rabbit IgG	Donkey	Molecular Probes	1:300
FITC-conjugated anti chicken IgY	Donkey	Jakson	1:50
FITC-conjugated anti mouse IgM	Goat	Southern Biotec	1;100
FITC-conjugated anti rabbit IgG	Goat	Cappel	1:200
FITC-conjugated anti-goat IgG	Donkey	Jackson	1:100
FITC-conjugated anti rabbit IgG	Donkey	Jackson	1:100
HRP-conjugated anti mouse IgG	Goat	Jackson	1:2000
HRP-conjugated anti rabbit IgG	Goat	Jackson	1:50,000
HRP-conjugated anti sheep IgG	Donkey	SAPU	1:2,500
TRITC-conjugated anti mouse IgG1	Goat	Jackson	1:50,000
TRITC-conjugated anti mouse IgG2a	Goat	Jackson	1:100
TRITC-conjugated anti guinea pig IgG	Donkey	Jackson	1:150
TRITC-conjugated anti rabbit IgG	Donkey	Jackson	1:100

3. Results

3.1 The study of Nfasc140

3.1.1 Identifying the transcript of the third isoform of Neurofascin

The *Neurofascin* (*Nfasc*) gene comprises 34 exons, with the ATG start site residing within exon 3. Previous studies have shown that *Nfasc* is transcribed to produce several isoforms generated by alternative pre-mRNA splicing (Volkmer et al., 1992, Volkmer et al., 1996, Hassel et al., 1997). 3 different isoforms of Neurofascin proteins were identified by western blot (David et al., 1996). However little is known about the third isoform of Neurofascin, named Nfasc140 based on its mobility on a SDS-gel (Davis et al., 1996). To determine the domains composition of Nfasc140, RT-PCR was conducted using mRNA extracted from WT (wild type) animals at different ages in order to first isolate the Nfasc140 cDNA. In previous studies Neurofascin transcripts were amplified in small segments, a strategy which has the potential to generate as yet unidentified potential Neurofascin isoforms consisting of different combinations of exons (Volkmer et al., 1996; Hassel et al., 1997). In order to reveal the sequence of Nfasc140 directly, I chose to clone all the possible Neurofascins transcripts from the known first coding exon to the last one by PCR.

Two primers were used to clone the entire coding region of the Neurofascins (described in Materials and methods 2.1.1). Since the primer pair selected was not specific for a particular isoform of Neurofascin, multiple bands were anticipated. Interestingly, only single bands were generated from the RT-PCR reaction of WT mouse cDNA at E15.5, P17 and P30 (Fig. 21A). The reason that only a single band, instead of multiple bands, was observed in each RT-PCR could be that the concentration of mRNA of Neurofascins at different ages varies. Therefore only the predominate isoform of Neurofascins would be amplified by the RT-PCR reaction. Isolation of the resulting bands from the agarose gel and subsequent sequencing revealed a Neurofascin transcript present in E15.5 cDNA that encoded neither

Nfasc186 or Nfasc155. Furthermore, the only Neurofascin transcript present in both P17 and P30 cDNA encoded Nfasc155. Sequence analysis and comparison by MacVector of the two major isoforms of Neurofascins (Nfasc186 and Nfasc155) with the newly identified transcript revealed that it lacked exons 5, 10, 24, 25 and 29-31(Fig. 21B). Since this new transcript is smaller in size than the other two major isoforms and had a different exon combination, I speculated that it was the transcript for Nfasc140.

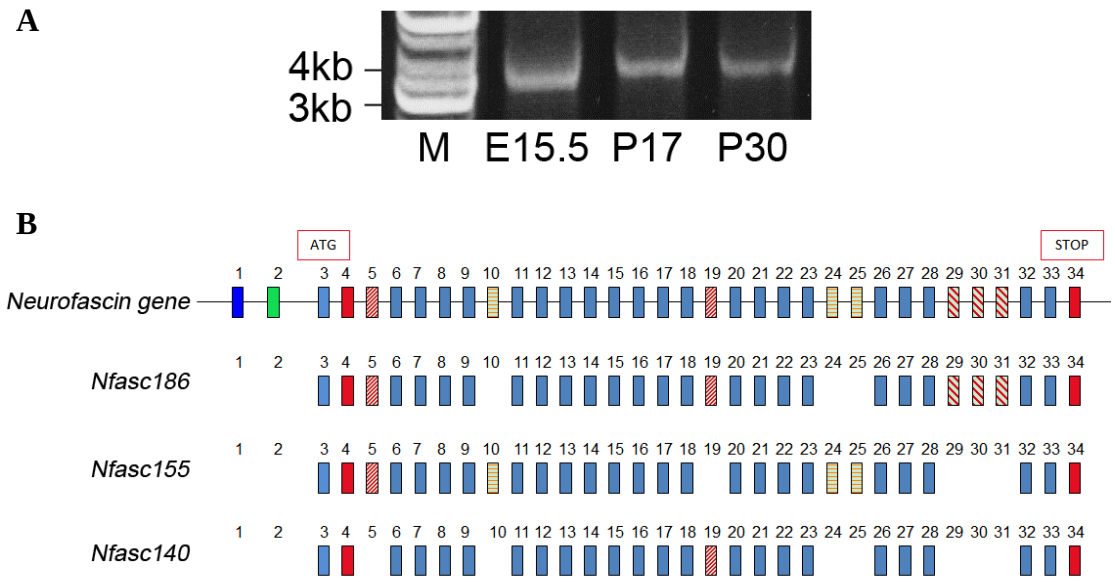

Figure 21. Nfasc140 cDNA isolated by full length RT-PCR
A. Full length RT-PCRs were performed on cDNA from E15.5, P17 and P30 hindbrain tissues from WT mice. At E15.5, a new Neurofascin isoform was detected which was smaller in size compared to RT-PCR bands from *Nfasc155* in lane P17 and P30.
B. Schematic representation of the *Nfasc* gene which contains 34 exons. Exon 3 to exon 34 are the coding exons. The *Nfasc140* sequencing result showed that it lacks the 5, 10, 24, 25 and 29-31 exons.

3.1.2 Domain structure of Nfasc140

After establishing the sequence of the *Nfasc140* transcript, the domain structure of Nfasc140 was predicted based on the sequence and domain structures of Nfasc186 and Nfasc155 (Fig. 22). Nfasc140 is predicted to have six IgG domains, the fibronectin type III domains (FnIIIA, FnIIIB, FnIIID), a transmembrane region and a

cytoplasmic domain. Nfasc140 lacks the FnIIIC and Mucin domains, specific for Nfasc155 and Nfasc186 respectively.

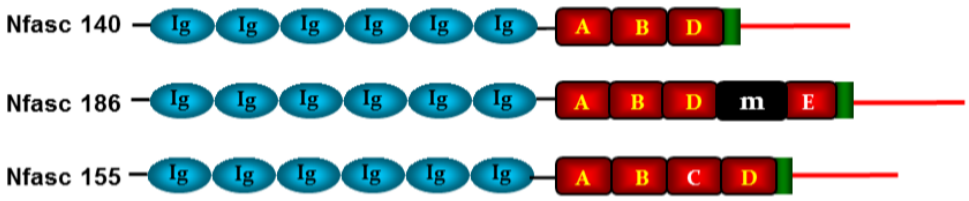

Figure 22. The domain structure of Nfasc140, Nfasc186 and Nfasc155
The domain structure of Nfasc140 was predicted based on the transcript sequence. Note that it does not have any unique domains when compared with Nfasc155 and Nfasc186 structure.

To further confirm the domain structure of Nfasc140, three different Neurofascin peptide-specific antibodies were used to probe WT mouse brain lysates by Western blot. Since Nfasc140 has a high expression level at E15.5 (Fig. 24), comparison of WT brain homogenates at E15.5 and P60 would show whether Nfasc140 was also present in adult animals. Using an antibody raised to the cytoplasmic domain of all known Neurofascins, NFC1, specific bands corresponding to Nfasc186, Nfasc155 and Nfasc140 were present (Fig. 23A). In contrast, the MNF2 antibody which is specific for the Mucin-like domain detected Nfasc186 at both E15.5 and P60 but did not detect Nfasc140 (Fig. 23B). Another antibody, NFF3, which recognizes the Nfasc155-specific FnIIIC domain, only detected Nfasc155 in WT brain homogenates at P60 and could not detect Nfasc140 (Fig. 23B). These data are consistent with the sequence data suggesting that Nfasc140 lacks the FnIIIC domain of Nfasc155 and the Mucin-like and FnIIIE domains of Nfasc186.

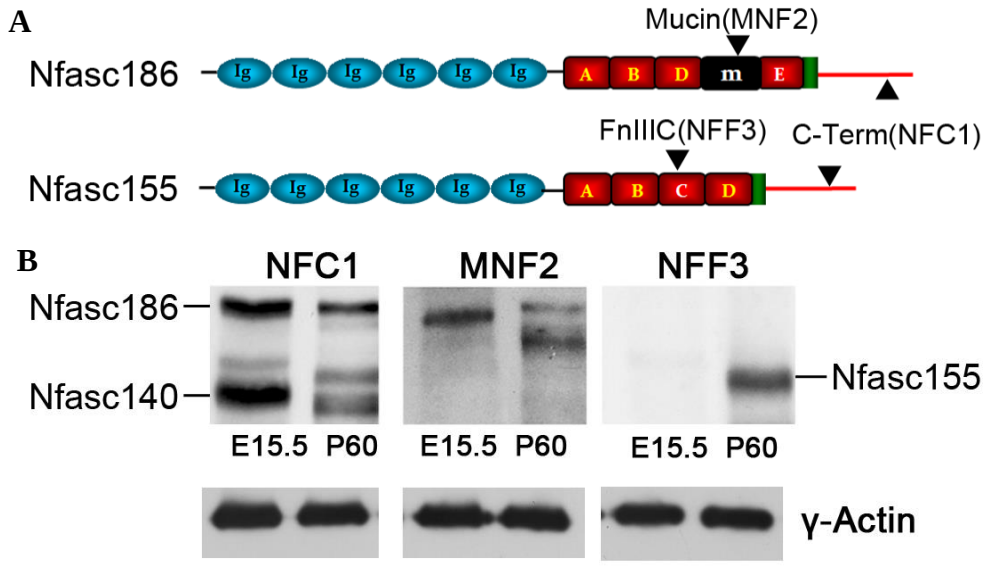

Figure 23. Domain composition of Nfasc140 is confirmed by Western blot.

A. Schematic picture showing regions of antibody specificity. MNF2 antibody recognizes the Mucin-like domain of Nfasc186, NFF-3 antibody recognizes the FnIIIC domain of Nfasc155 and NFC1 recognizes the C-terminus of all Neurofascins.

B. Hindbrain tissue isolated from E15.5 and P60 animals were probed with different Neurofascin antibodies. NFC1 antibody recognized two strong bands at E15.5, the upper one is Nfasc186, and the bottom one is Nfasc140, the faint band in the middle is likely to be a non-specific band because it does not appear in postnatal tissues. At P60, NFC1 recognized Nfasc186 at the top, Nfasc155 in the middle and Nfasc140 at the bottom. MNF-2 antibody recognized Nfasc186 only at E15.5 but an extra band appeared below Nfasc186 at P60, I think the extra band could be a degradation of Nfasc186 or non-specific band. NFF3 antibody did not detect anything from E15.5 lysate, because myelination is not started at this age; at P60 a single band Nfasc155 was detected by NFF3. Hence, MNF2 and NFF3 did not recognize Nfasc140. Only NFC1 can recognize Nfasc140. Here, all E15.5 lanes loaded the same amount of protein from the same animal. And so did the P60 lanes.

3.1.3 Nfasc140 is differentially expressed during CNS development

Studies in the chick have shown that Nfasc166, which has a similar domain structure to Nfasc140, is only expressed at the embryonic stage in development (Hassel et al., 1997, Burkarth et al., 2007, Kirschbaum et al., 2009). However, I have demonstrated

that mouse Nfasc140 can also be detected in adult CNS lysates. To provide a better understanding of this age-related change in level, the expression pattern of Nfasc140 was analyzed during mouse development. CNS lysates from wild type mice at different ages (E13, E15, P1, P4, P8, P12 and P45) were isolated and analyzed by Western blots using the NFC1 antibody. The results showed that the level of expression of Nfasc140 is high in the embryo but that it is down regulated at birth but expression then increases again after P8 (Fig. 24).

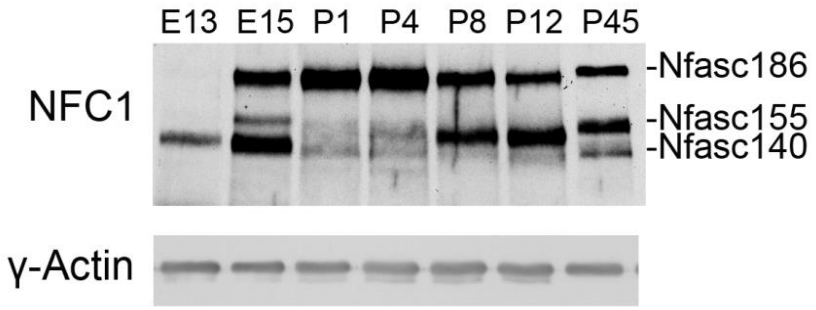

Figure 24. Western blot results showing the expression pattern of Nfasc140 in CNS

Whole head lysate at E13.5 and hindbrain lysates at all other ages were probed with NFC1 antibody. At E13 the predominant isoform is Nfasc140. And Nfasc140 expressing is high at E15. The level of expression of Nfasc140 was very low, barely detectable, from P1 to P8. From P8 Nfasc140 protein increased and reached a high level again at/before P45. Two whole mouse heads were used in the E13 lysate, two mouse hindbrains were used in E15 and one mouse hindbrain were used in the lysates of other ages. For each age, three animals (six animals at E13 and E15) were taken from different litters. And all three experiments showed the same expression pattern. Normalized with γ-Actin.

Interestingly, Western blot using antibodies against myelin basic protein (MBP), a major component of mature myelin, showed that both Nfasc140 and MBP expression levels increase around P10, suggesting that Nfasc140 might be involved in early myelination (Fig. 25).

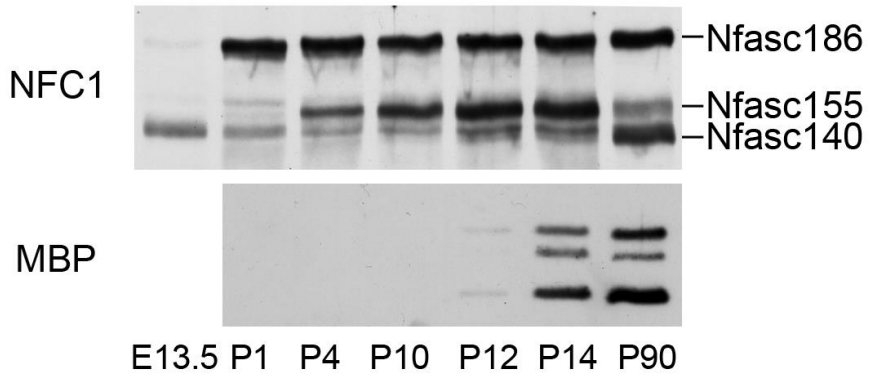

Figure 25. Nfasc140 and MBP expression levels increase at similar ages.
Western blots using whole head lysate at E13.5 and hindbrain lysate at other ages. NFC1 antibody was used to show expression levels of Nfasc140 compared to Nfasc186 and Nfasc155 at different ages. Anti-MBP was used to indicate the onset of myelination. Two whole mouse heads were used in E13 lysate and one mouse hindbrain were used in the lysates of other ages. For each age, two animals (four animals at E13) were taken from different litters. And two experiments showed the same expression pattern. Nfasc186 is used as loading control except lane E13.5, at which age the Nfasc186 level is too low.

3.1.4 Nfasc140 is differentially glycosylated

Western blot analysis of WT adult hindbrain lysate using the NFC1 antibody revealed that the strong band, which runs at a similar mobility to Nfasc140, is a doublet (Fig. 26). Previous work (Volkmer et al., 1992, Davis et al., 1993, Maier et al., 2005 and Pomicter et al., 2010) has shown that Neurofascins are glycosylated. Since the hindbrain is made up of distinct structures, with differing roles, it is possible that post-translational modifications of Nfasc140 may be different according to the brain region. To examine this possibility, tissue lysates were collected from adult wild type pons and cerebellum. Interestingly, after separating hindbrain into cerebellum and pons, western blot analysis showed that the upper band of the doublet was enriched in the lysate of pons and the lower one was concentrated in the cerebellum lysate (Fig. 26A). To check whether the mobility difference was caused by differential glycosylation, tissues were deglycosylated by treating WT adult brain homogenates with PNGaseF. After deglycosylation, the tissue lysates of pons and cerebellum were run on western blot and probed with NFC1 antibody. Results showed the bands present in pons or cerebellum lysates shifted to the same level after

deglycosylation (Fig. 26B). This strongly suggests that the doublet corresponds to differentially glycosylated Nfasc140 in different parts of the adult hindbrain.

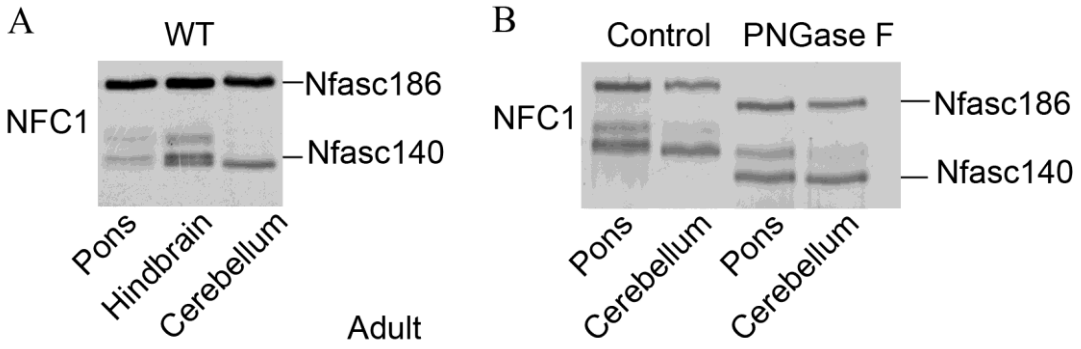

Figure 26. Nfasc140 in different tissues is differentially glycosylated

A. Western blotting revealed that Nfasc140 in adult pons and cerebellum have different mobilities which accounted for the doublet in hindbrain lysate of adult mice.
B. The Western blot showed that after PNGaseF treatment Nfasc140 in pons and cerebellum shifts to the same level.

The two band pattern of Nfasc140 in adult is caused by differential glycosylation of Nfasc140 in different tissues. At the same time I wondered whether the mobility differences of Nfasc140 between E15.5 and P60 tissues were also caused by differential glycosylation. To explore the reason for difference, PNGaseF deglycosylation was repeated using brain lysates from E13 and P60 (Fig. 27). However the result did not resolve the question. After deglycosylation, unlike the P60 lysates, lysates from E13 showed a much wider and fuzzy band which ran slightly higher than Nfasc140 from adult on Western blot (Fig. 27). This fuzzy band could be caused by phosphorylation (Kizhatil et al., 2002) or any other post-translational modifications of Nfasc140. Because the mobility of those bands in different ages were so similar, it was very unlikely there would be any domain difference between the bands of E13 tissues and adult tissues. I therefore hypothesized that the bands from E13 and P60 represented the same Nfasc140 protein which had different post-translational modifications at different development stages.

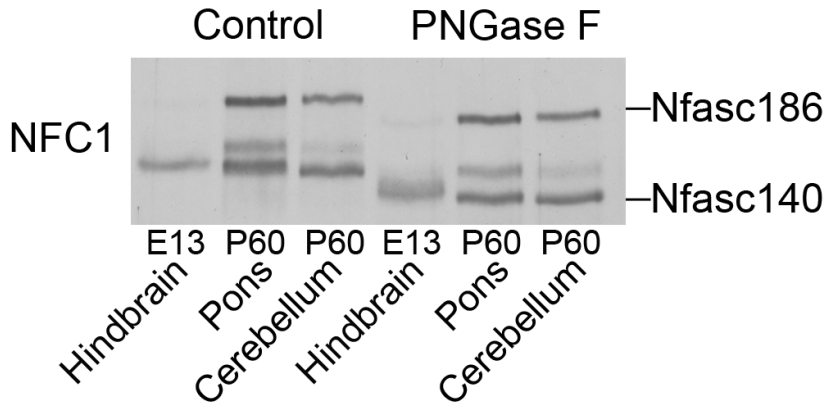

Figure 27. Deglycosylation on tissues from E13 and P60
Before deglycosylation (control), Nfasc140 from E13 and P60 pons had the same size. After deglycosylation (PNGase F), Nfasc140 from E13 shifted down and became fuzzy, and it appeared to be bigger in size than Nfasc140 from P60. Experiment repeated three times with different digestion time and enzyme concentration, the same results were observed in all repeats.

3.1.5 Nfasc140 is a neuronal protein

My results so far have shown that Nfasc140 is an isoform of Neurofascin with a domain structure that differs from both neuronal Nfasc186 and glial Nfasc155. Next, I asked in which cell types Nfasc140 is expressed. Three different Cre mouse lines were used here to conditionally delete Neurofascins in different cells.

First, to determine whether Nfasc140 is expressed by glial cells or neurons, a mouse line where Cre recombinase is driven by the 2´, 3´-cyclic nucleotide 3´-phosphodiesterase (CNP) promoter (Lappe-Siefke et al., 2003) was crossed with mice carrying *Nfasc* floxed alleles to generate mice in which Nfasc155 was specifically inactivated in glial cells (*CNP-Cre/Nfasc*$^{fl/fl}$). These mice die around P17. Western blots using hindbrain lysates from these mice showed that at P4, a time when Nfasc155 is normally detected, Nfasc155 was no longer present, whereas Nfasc140 could still be detected (Fig. 28 left). These data support the hypothesis that Nfasc140 is a neuronal isoform. To exclude the possibility that Nfasc140 might have a lower turnover rate compared to Nfasc155, a tamoxifen inducible glial conditional knockout line was used. Mice carrying one *Nfasc* floxed allele and one null allele (*Nfasc*$^{fl/-}$) were crossed with mice expressing Cre fused to the estrogen receptor (CreERT2) which is driven by the myelin-forming-glia-specific proteolipid protein

(PLP) promoter (*PLP-Cre ERT2*). At P90, one month after tamoxifen treatment, Nfasc186 and Nfasc140 were still detectable by Western blotting whereas deletion of Nfasc155 was almost complete (Fig. 28).

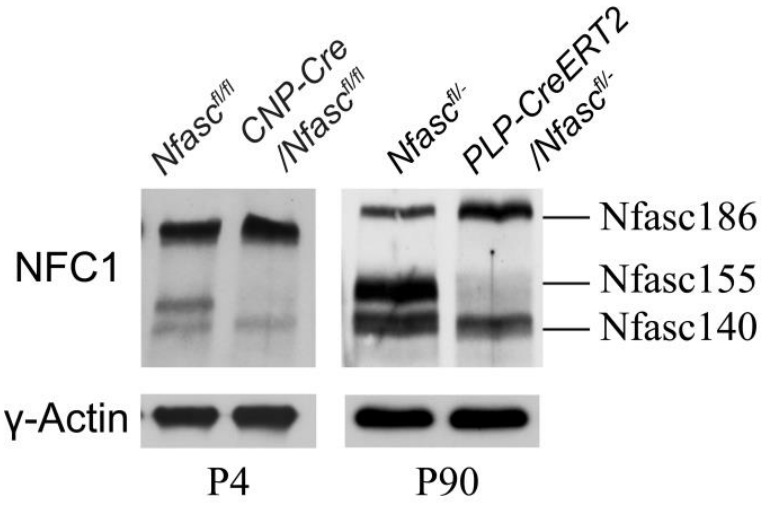

Figure 28. Nfasc140 is not expressed by glial cells.
Western blot using NFC1 antibody showed only Nfasc155 was deleted in *CNP-Cre/Nfasc$^{fl/fl}$* mouse at P4, whereas Nfasc186 and Nfasc140 are present (left). Nfasc155 was also undetectable in the inducible conditional *PLP-CreERT2/Nfasc$^{fl/-}$* mice but Nfasc140 was still present (right). Two animals from different litters were used here for each experiment. Loading was normalized with γ-actin.

These results indicated that Nfasc140 is not an oligodendroglial protein. To confirm that Nfasc140 is neuronal, mice expressing a tamoxifen inducible Cre driven by the neuronal Thy-1 promoter (*Thy1-CreERT2*) were crossed with mice carrying one *Nfasc* flox allele and one null allele (*Nfasc$^{fl/-}$*) to inactivate Nfasc186 in neurons (*Thy1-CreERT2/ Nfasc$^{fl/-}$*). Spinal cord lysates of control (*Nfasc$^{fl/-}$*) and conditional *Thy1-CreERT2/ Nfasc$^{fl/-}$* mice 4.5 months post tamoxifen treatment were probed with the NFC1 antibody (Fig. 29). The major neuronal isoform, Nfasc186 was absent from tamoxifen treated conditional mutant mice and Nfasc140 was highly reduced, suggesting that Nfasc140 is present in neurons (Fig. 29). This also suggested that Nfasc140 appeared to be more stable than Nfasc186.

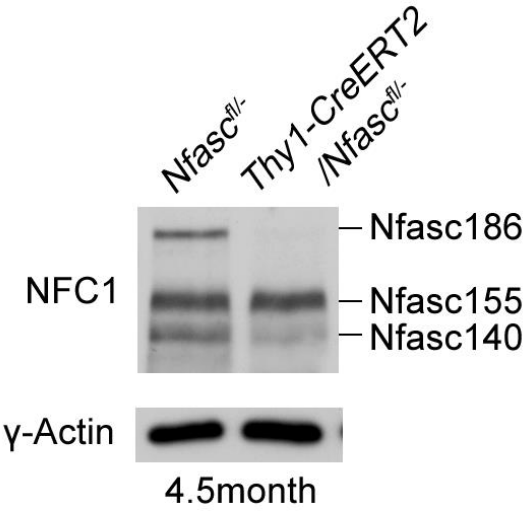

Figure 29. Nfasc140 is present in neurons.
Western blot analysis using the NFC1 antibody showed that both Nfasc186 and Nfasc140 were highly reduced in adult *Thy1-CreERT2/Nfasc*$^{fl/fl}$ mouse lysate at 4.5 months after tamoxifen injection. Three animals from different litters were used. Normalization was using γ-Actin. Level of Nfasc140 in mutants was only 0.39±0.11 times of Nfasc140 in WT. Relative density of protein samples was measured with ImageJ and adjusted according to the γ-Actin band density. (means ± SEM; n = 3 for each)

3.1.6 Nfasc140 is highly concentrated in the developing cerebellum

Since cellular migration is still occurring in the cerebellum at E13.5 and Western blots have shown that Nfasc140 is the predominate isoform of Neurofascins at this embryonic stage (Fig. 23), I examined the cellular location of Nfasc140 by immunofluorescence. NFC1 immunofluorescence staining is concentrated along the cerebral cortex and also inside the cerebellum at E13.5 (Fig. 30). By E15.5, very strong immunofluorescence staining of deep cerebellar nuclei in wild type animals was observed. Western blots of E15.5 hindbrain indicated that Nfasc186 is also present along with Nfasc140 at this stage of embryogenesis (Fig. 21). To determine which isoform is expressed at this stage in the developing cerebellum, I performed double staining using NFC1 and Nfasc186 specific antibodies. No immunofluorescent staining was present in the cerebellum of WT animals at E15.5 using the Nfasc186-specific antibody alone (Fig. 21). This suggests that Nfasc140 is the isoform of Neurofascin which is concentrated in developing cortex and

cerebellum, and indicates that Nfasc140 might have important function(s) during cerebellar development.

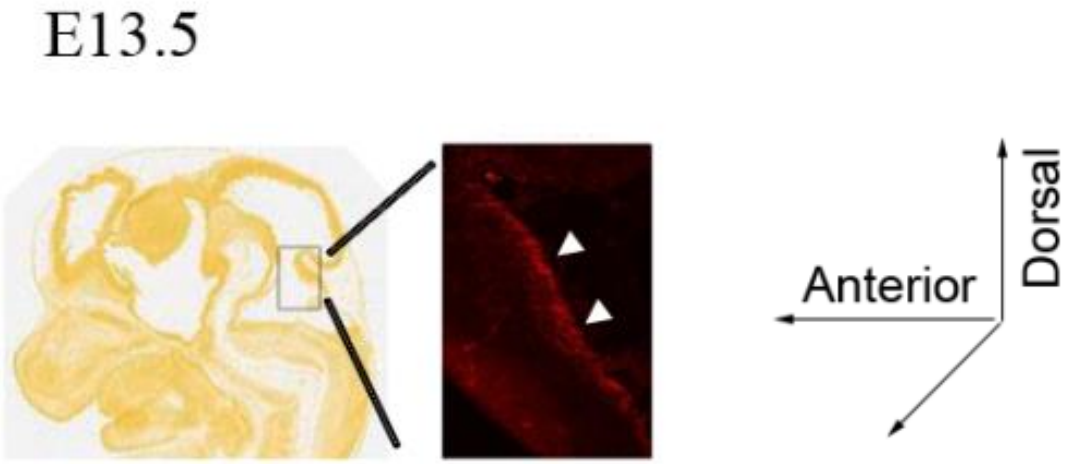

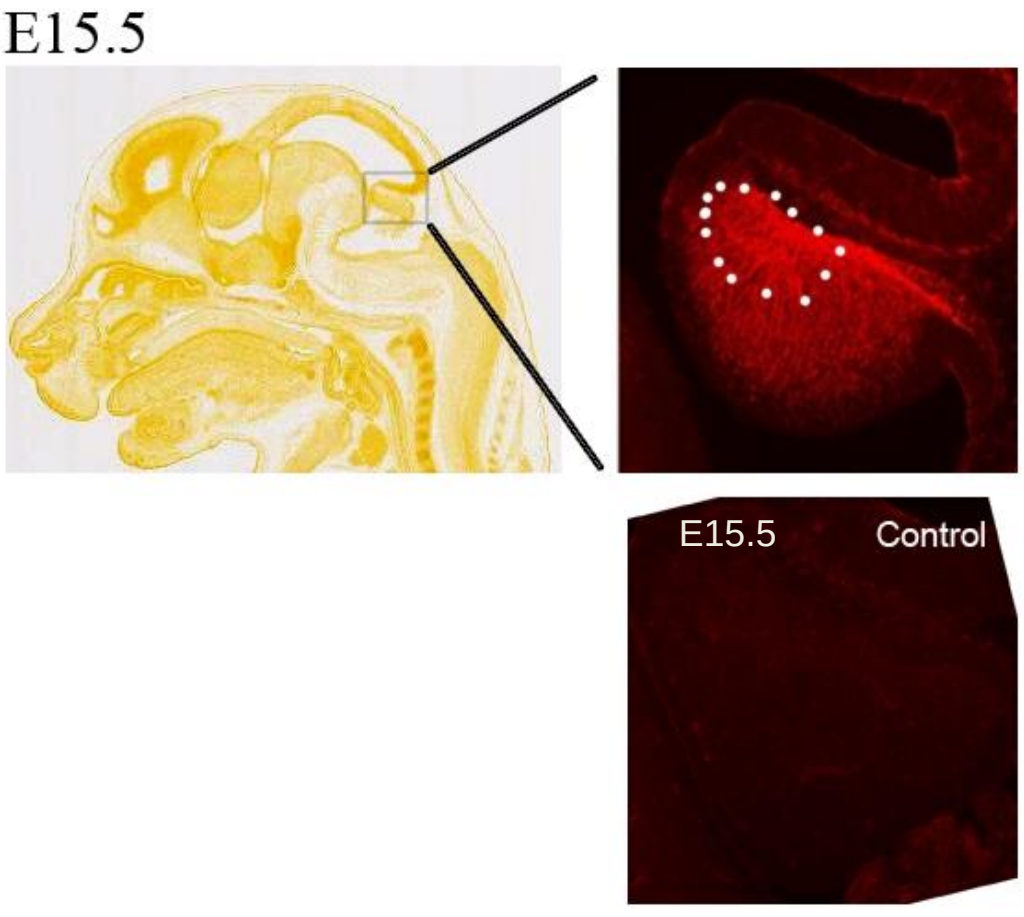

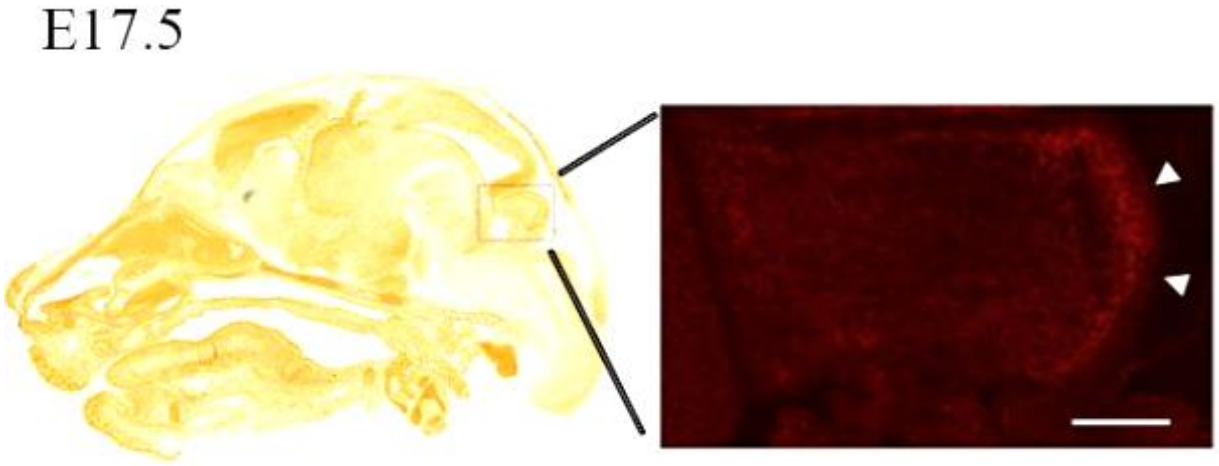

Figure 30. Confocal imagines showing Neurofascin localization during embryogenesis.
Fluorescent microscope images of sagittal sections of WT mouse embryos at the indicated ages were adapted from the *Allen Brain Atlas (http://mouse.brain-map.org)* to indicate the histological localization of the immunofluorescence. NFC1 antibody in red was used here to stain Neurofascin in the cerebellum and WT animals.
At E13.5 Nfasc140 immunoflourescence was concentrated at the rhombic lip migratory stream (RLS) and nuclear transitory zone (NTZ) (white arrows).
At E15.5 Neurofascins were concentrated in the developing deep cerebellar nuclei (white circle) and also almost the whole cerebellum has strong Neurofascin staining. Cerebellum from Neurofascin knockout animal at E15.5 was used as a negative control.
At E17.5 the Neurofascin signal decreased substantially and was concentrated at the external granular layer (white arrows). Scale bar 250 µm. (Negative control of NFC1 staining of Neruofascin knockout animal tissues at E17.5 is in Fig.32.)

Neurofascin knockout mice (*Nfasc*$^{-/-}$) do not express any of the isoforms of Neurofascin and die in the early postnatal period (P7) (Sherman et al., 2005). To investigate potential function(s) of Nfasc140, Nfasc$^{-/-}$ and WT brain slices were collected and stained with various antibodies to analyse possible differences between mutant and WT mice.

Nfasc140 appears to be concentrated at the nuclear transitory zone at E13.5 (Fig. 30), which eventually develops into the deep cerebellar nuclei at older age (E17.5). Previous studies have shown that Purkinje cell migration is not affected in Nfasc$^{-/-}$ mice at P6 (Zonta 2011). So, instead of Purkinje cells, the rhombic lip-derived cells which express the transcription factor Pax6 (Andrew et al., 2006) were studied. Pax6-positive cells are derived in the URL and migrate through RLS to NTZ (Fig. 12). Immunofluorescent co-staining using antibodies against NFC1 and Pax6 showed clear Pax6-positive cells migrating from the URL, RLS and NTZ in both WT and Nfasc$^{-/-}$mice at E15.5 (Fig. 31). Since there were no obvious differences in the number of Pax6-positive cells between *Nfasc*$^{-/-}$ and WT mice at E15.5, cell migration did not appear to be affected in *Nfasc* null mice.

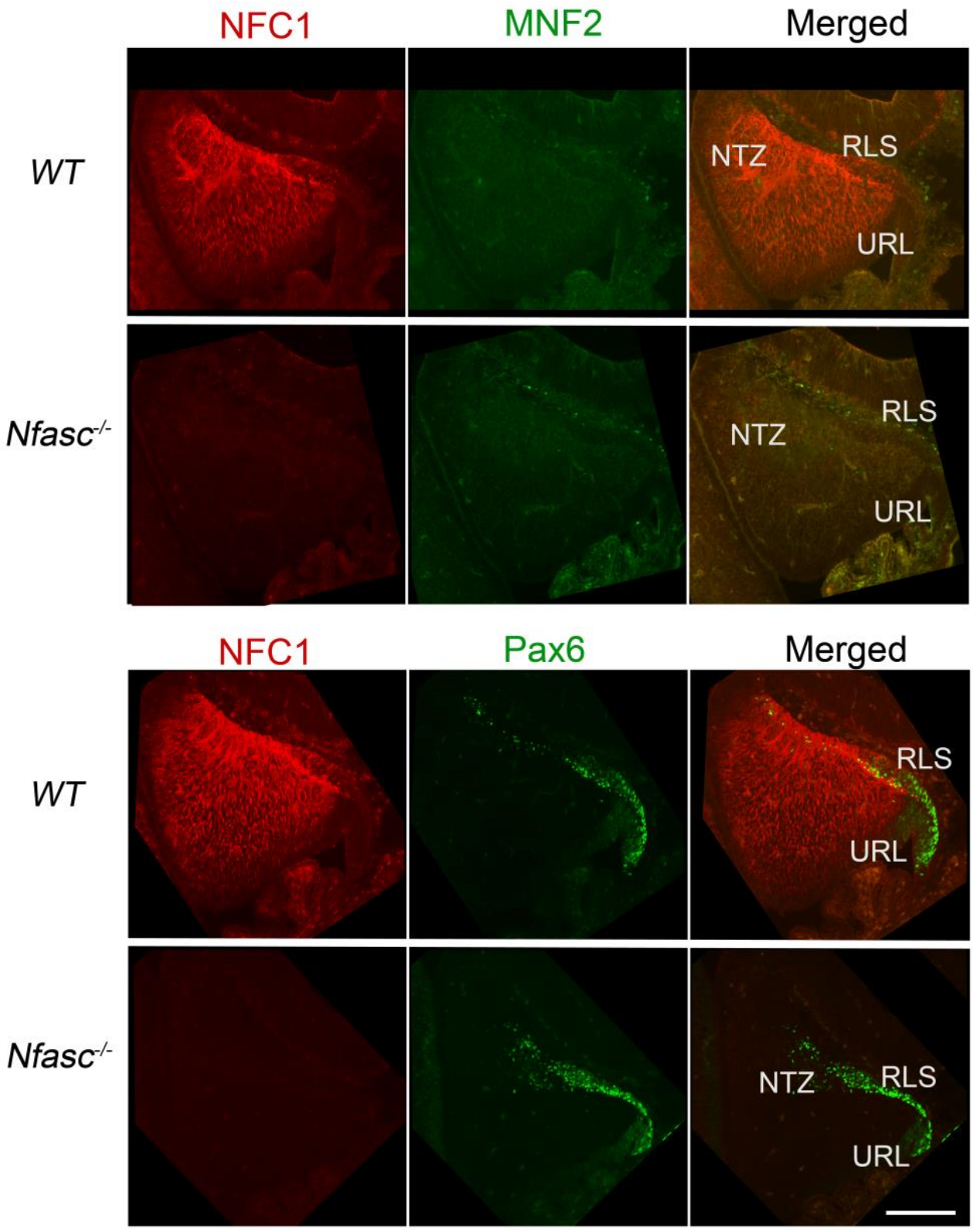
NFC1
MNF2
Merged
WT
NTZ
RLS
URL
Nfasc-/-
NTZ
RLS
URL
NFC1
Pax6
Merged
WT
RLS
URL
Nfasc-/-
NTZ
RLS
URL

Figure 31. Migration of rhombic lip-derived cells is unaffected in Neurofascin null embryos

Confocal images of Sagittal sections of WT E15.5 cerebellum stained with NFC1, MNF2 and Pax6 antibodies. NFC1 antibody showed strong signal at the NTZ in WT animals; however no MNF2 (Nfasc186 specific Ab) co-staining was detected. These two observations suggest that Nfasc140, not Nfasc186, is present in the NTZ of the cerebellum. NFC1 and Pax6 co-staining showed clear Pax6 positive cells migrating from URL, RLS and NTZ in both WT and Nfasc$^{-/-}$ mice indicating that the migration was not affected in Nfasc null mice. Scale bar 200 µm.

To confirm cells were migrating normally during later cerebellar development, brain slices from mutant and WT mice were collected at E17.5 and stained with Pax6 and NFC1 antibodies. Results were similar to those obtained at E13.5, with no difference in the distribution of Pax6-positive cells observed between *Nfasc*$^{-/-}$ and WT mice (Fig. 32), providing further support that cell migration is not altered when Neurofascin is absent.

Therefore the functions of Nfasc140 at early development stages are still not clear. However, Neurofascins do not appear to be important for cell migration in the developing cerebellum.

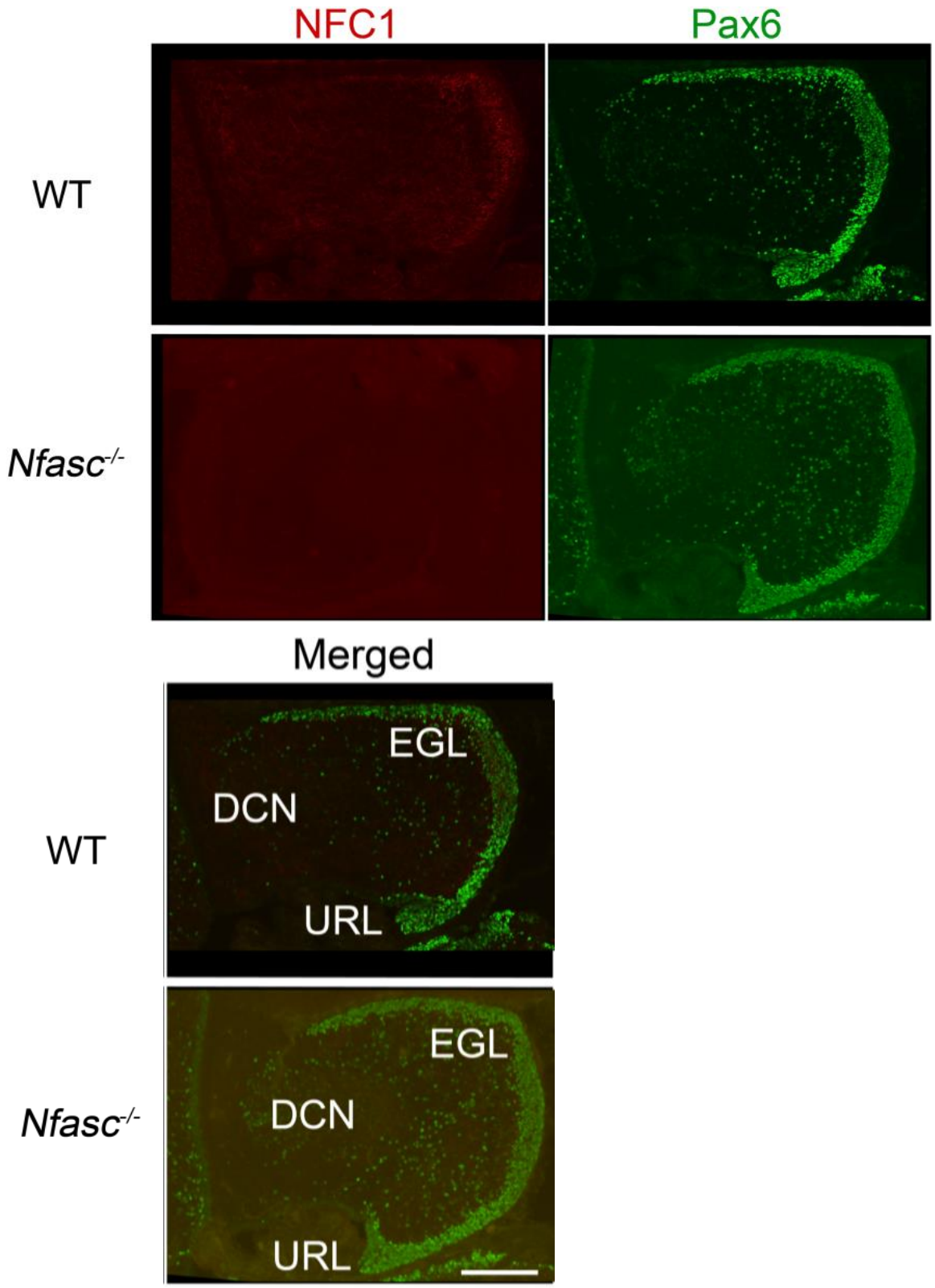

Figure 32. Pax6 positive cell migration is unaffected in *Nfasc*$^{-/-}$ mouse.
Confocal images showed at E17.5 Neurofascin staining (NFC1) was faint and concentrated at the external granular layer (EGL which derived from RLS at E15.5). Pax6-positive cells were observed in the deep cerebellar nuclei (DCN),

which is derived from NTZ , the EGL and URL in both WT and *Nfasc*$^{-/-}$ mice. Scale bar 250 µm.

3.1.7 Generation of a transgenic mouse line expressing Nfasc140-flag *in vivo*

Since there are no unique domains to which it is possible to raise Nfasc140-specific antibodies, I decided to use transgenic mice to study the function of Nfasc140. A transgenic line (*T140*) was generated expressing full-length Nfasc140 with a FLAG tag at its C-terminus (Nfasc140-flag) under the control of the neuronal *Thy-1* promoter (Fig. 13). Western blot of *T140* hindbrain lysates using two Neurofascin antibodies and Flag antibodies (anti-Flag) showed that Nfasc140-flag is expressed in vivo and the corresponding band has an electrophoretic mobility between endogenous Nfasc140 and Nfasc155 (Fig. 33).

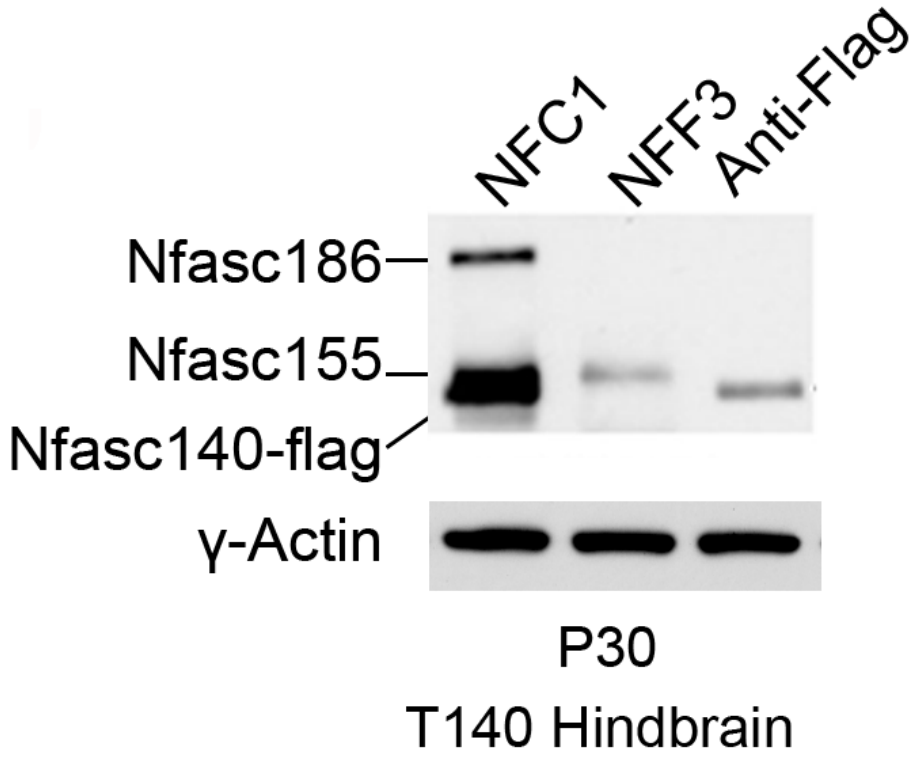

Figure 33. Western blot showing the expression of flag-tagged Nfasc140 in transgenic mouse brain.
Western blot was performed on hindbrain lysates from T140 transgenics on a WT background at P30. NFC1 detects Nfasc186, Nfasc155 and a strong 140 kD band which corresponds to transgenic Nfasc140. NFF3, the Nfasc155-specific antibody, detected Nfasc155 only and anti-Flag detected he Nfasc140-flag band which ran lower than Nfasc155. Normalized with γ-Actin.

3.1.8 Nfasc140-flag is concentrated at nodes in both CNS and PNS

Within the CNS and PNS, Nfasc186 is targeted to the nodes of Ranvier and Nfasc155 is targeted to the paranodal regions (Tait et al., 2000, Sherman et al., 2005, Zonta et al,. 2008 Zonta et al., 2011). I have established that, like Nfasc186, Nfasc140 is expressed in neurons (Fig. 28) but unlike Nfasc186, Nfasc140 lacks the Mucin and FNIII E domains (Fig. 21). The role of these domains in transportation and targeting of Neurofascins is still unclear, therefore I examined where transgenic Nfasc140 is targeted.

Transgenic mouse tissues from the CNS and PNS at P30 were isolated, fixed and their fibres teased out. Immunofluorescence of teased fibres from sciatic nerves (PNS) and the ventral funiculus of the spinal cord (CNS) showed that Nfasc140-flag was targeted to nodes in both the PNS and CNS (Fig. 34). This indicates that the Mucin and FNIII E domains are not required for the transportation and targeting of Neurofascins. It was already known that transgenic Nfasc186 is targeted to nodes of Ranvier so transgenic Nfasc186 mice were used in my study as a comparison.

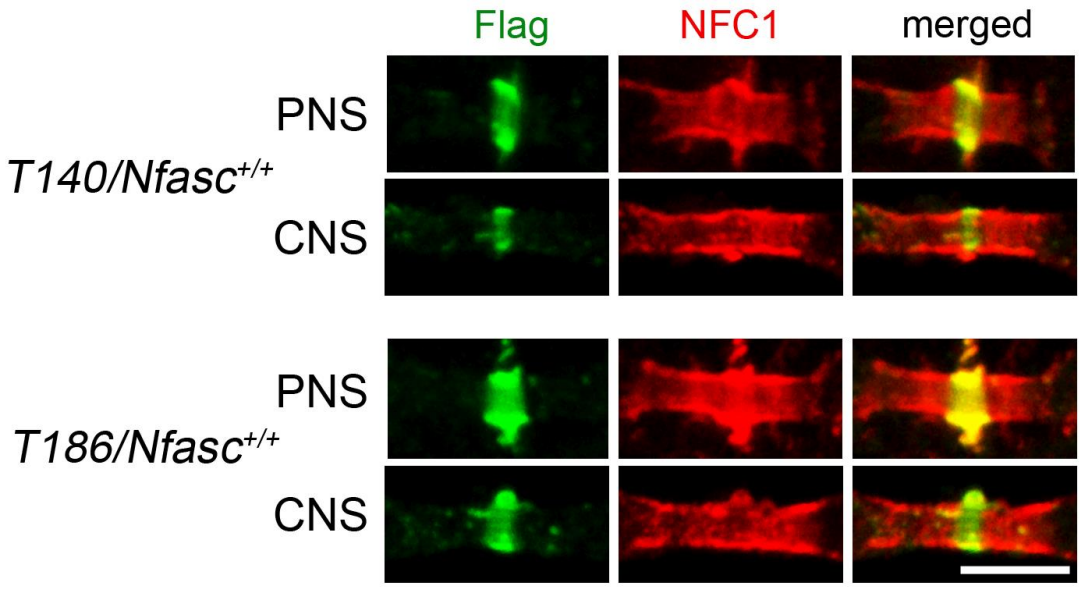

Figure 34. Immunofluorescence showing Nfasc140-flag is targeted to the nodes of Ranvier.
Confocal images of teased sciatic nerves (PNS) and ventral funiculus (CNS) were stained with antibodies against anti-Flag (Green) and Neurofascin (NFC1, red). Nfasc140-flag and Nfasc-186 are targeted at the nodes of Ranvier in both CNS and PNS. Scale bar, 5 µm.

3.1.9 Nfasc140-flag can be targeted to the AIS

Previous studies showed that Nfasc186 is targeted to the axonal initial segment (AIS) (Hedstrom et al,. 2007, Zonta *et al.*, 2011). Because Nfasc140 is neuronal and targeted to nodes, like Nfasc186, the ability of Nfasc140 to target to the AIS was studied. After generating mice expressing Nfasc140-flag or Nfasc186-flag on a *Nfasc*$^{-/-}$ background (*T140/Nfasc*$^{-/-}$ and *T186/Nfasc*$^{-/-}$), cerebellar slices from *T140/Nfasc*$^{-/-}$ and *T186/Nfasc*$^{-/-}$ were stained with NFC1 and Flag antibodies. Immunofluorescent results showed that both transgenic animals have NFC1 and Flag staining at the AIS (Fig. 35). Since the transgenic animals were on an Nfasc-null background, the results indicated both Nfasc140-flag and Nfasc186-flag can be targeted to the AIS. Also the Nfasc140 and Nfasc186 are also targeted to the plasma membrane of Purkinje cells near the AIS.

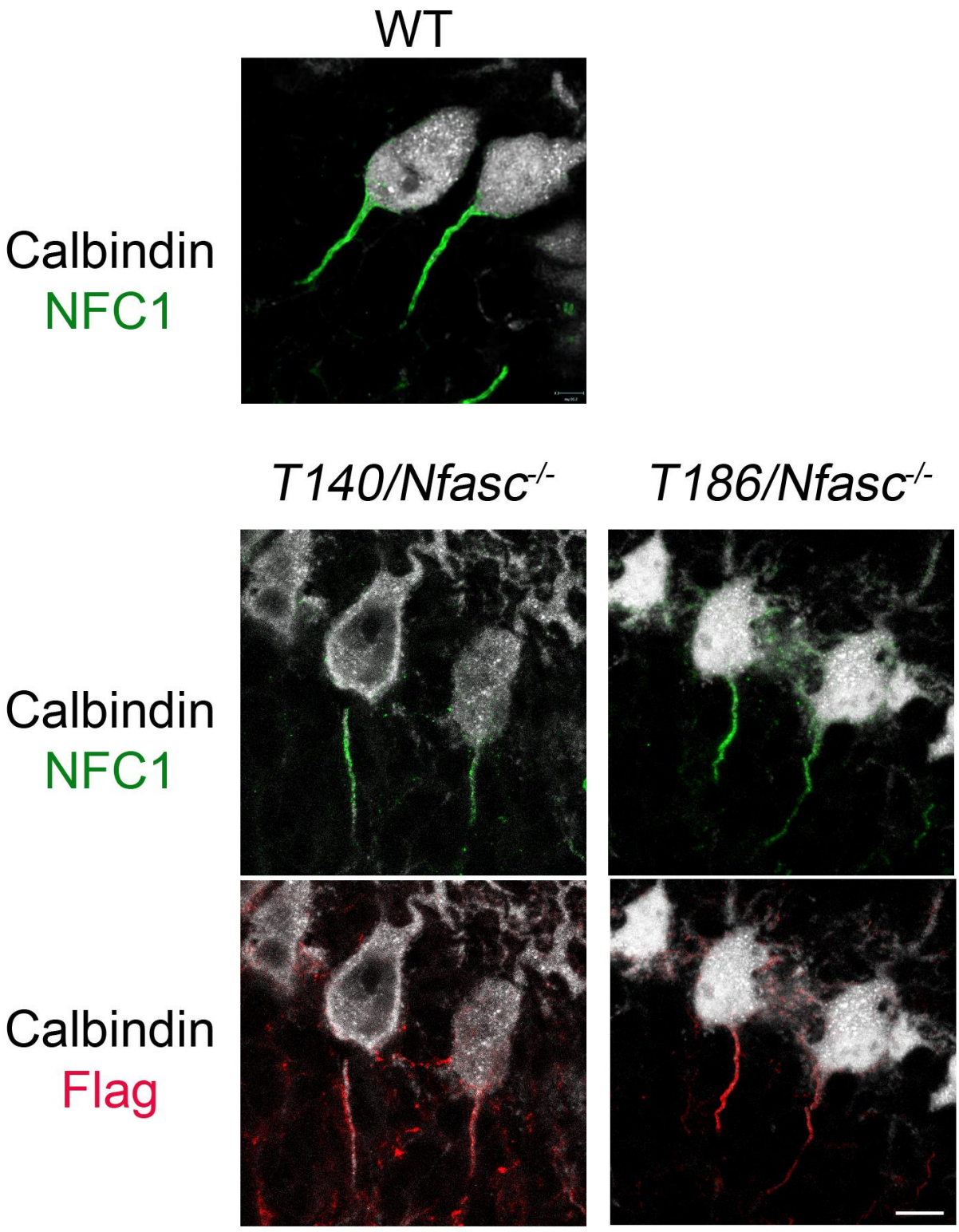

Figure 35. Immunofluorescence showing Nfasc140-flag and Nfasc186-flag are targeted to the AIS.

Calbindin antibodies stained the cerebellar Purkinje cells and the AIS. Both

NFC1 and Flag antibodies stained the Nfasc140-flag at AIS in *T140/Nfasc*$^{-/-}$ mice and Nfasc186-flag in *T186/Nfasc*$^{-/-}$ animals at the age of P8. Scale bar, 10 µm.

It has recently been shown that Nfasc186 plays an important role in maintaining the integrity of the AIS in adult animals (Zonta *et al.,* 2011). To determine whether Nfasc140 or Nfasc186 alone persist at the AIS and maintain the protein structure of the AIS, older mice (P60) were sacrificed, their cerebella isolated and immunofluorescent staining conducted. Both Nfasc140-flag and Nfasc186-flag were still targeted at the AIS, suggesting that the flag tag does not interfere with targeting and maintenance of the 2 isoforms of Neurofascins. Furthermore, these data also suggest that the Mucin and FNIII E domains of Nfasc186 are not involved in the targeting of Neurofascins to the AIS, as Nfasc140-flag is still targeted to the AIS (Fig. 35).

3.1.10 The level of expression of Nfasc140-flag and Nfasc186-flag are higher than the level of endogenous Neurofascins.

The function of Nfasc186 has been studied (Zonta *et al,.* 2008; Zonta *et al.*, 2011). Nfasc140 was been shown to have many similar characteristics compared to Nfasc186, since they are both expressed in neurons and are both targeted to the nodes and AIS (Fig 27, 28, 33 and 34). Because the transgenic Nfasc140-flag and Nfasc186-flag have a very different promoter from the endogenous Nfasc140 and Nfasc186, to further understand Nfasc140-flag and Nfasc186-flag, the levels of expression of Neurofascins were examined and compared with the endogenous ones. Western blots showed that both transgenic proteins were over-expressed under the control of Thy-1 promoter (Fig. 36).

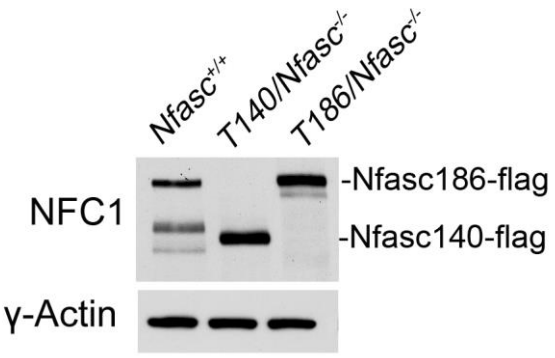

Figure 36. Western blot showed Nfasc140-flag and Nfasc186 are both over expressed comparing with WT
Hindbrain lysates from WT, *T140/Nfasc*$^{-/-}$ and *T186/Nfasc*$^{-/-}$ mice were blotted with NFC1 antibody. The Nfasc140-flag band and Nfasc186-flag band had stronger signal intensities than the endogenous protein indicating they were over expressed in transgenic animals. The flag tagged Nfasc140 and Nfasc186 are larger than the endogenous proteins, due to the addition of the flag tag.

The results showing the level of expression of Nfasc140-flag was 2.25 ± 0.3 times more than endogenous Nfasc186. And Nfasc186-flag was 1.77±0.2 times more than endogenous Nfasc140. And Nfasc186-flag is 1.03 ± 0.2 times of Nfasc140-flag. Relative density of samples were measured with ImageJ and adjusted according to the γ-Actin band density. (means ± SEM; n = 3 for each) Normalized with γ-Actin.

3.1.11 Nfasc140-flag can rescue the nodal complex in both CNS and PNS

Both Nfasc186 and Nfasc155 have important roles regarding the nodal and paranodal protein organization at the nodes of Ranvier. In Neurofascin knockout mice the nodal components are missing from the nodal area in both PNS and CNS (Fig. 37) (Sherman et al., 2005, Zonta et al., 2008). Expression of Nfasc186 in neurons can rescue the nodal complex in both PNS and CNS on an Nfasc$^{-/-}$ background. And the expression of Nfasc155 rescues the CNS nodal complex (Zonta et al., 2008). Meanwhile, we have found that the Nfasc140-flag was able to target to the nodes. For the above reasons, the ability of Nfasc140 to organize the nodal complex is explored here.

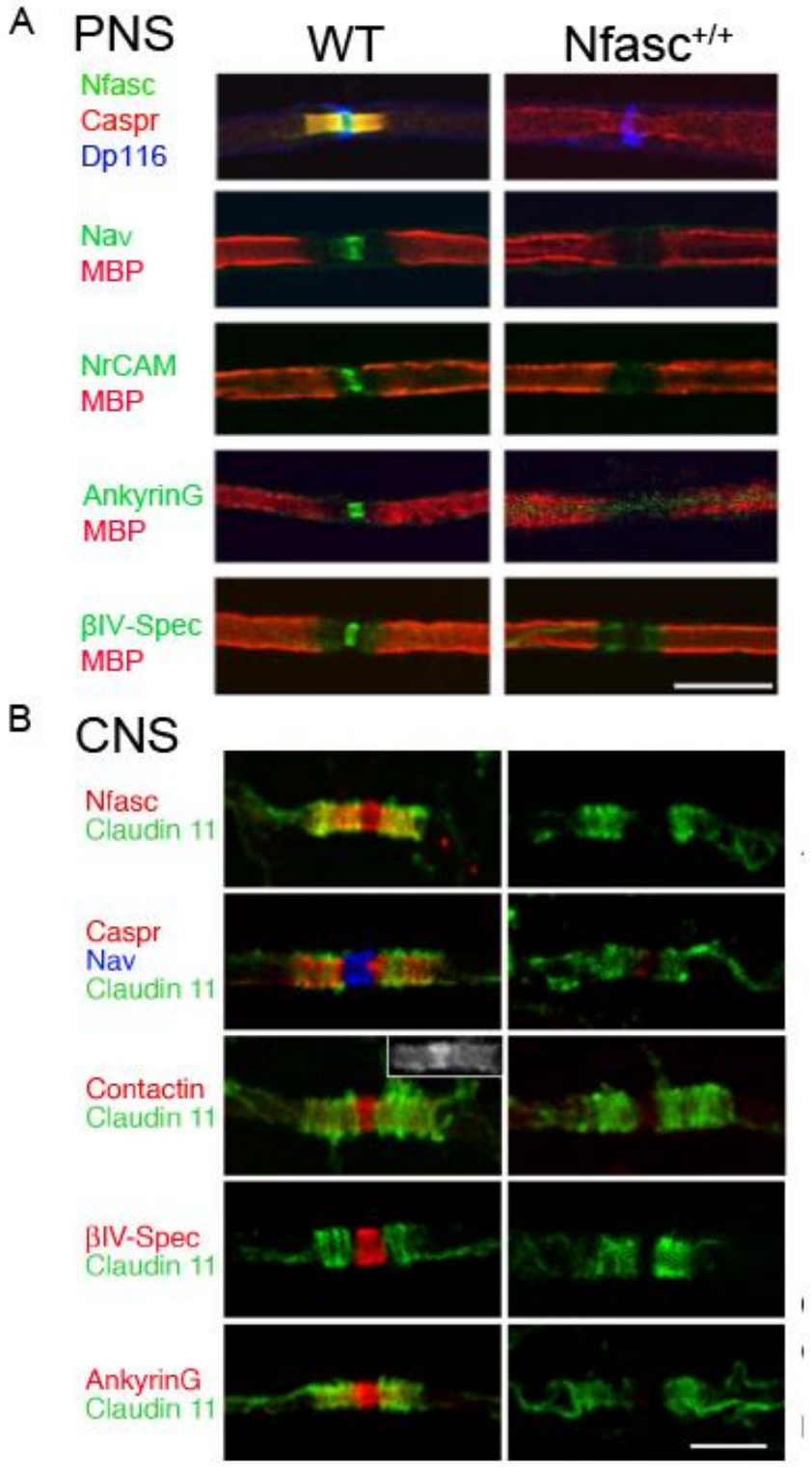

Figure 37. Nodal components were mislocalized in Nfasc$^{-/-}$ mouse (Sherman et al., 2005, Zonta et al., 2008)

Confocal images showed in Nfasc$^{-/-}$ animals Na_v, NrCam, AnkyrinG and βIV-Spectrin, are mislocalized from the nodes in PNS (A). The nodal components, Na_v, NrCam, AnkyrinG and βIV-Spectrin, were mislocalized in CNS (B). Scale bar, 5 μm.

After expressing the Nfasc140-flag on an *Nfasc*$^{-/-}$ background (*T140/Nfasc*$^{-/-}$), teased fibres from both PNS and CNS were stained with various antibodies. Meanwhile, animals with Nfasc186-flag on an *Nfasc*$^{-/-}$ background (*T186/Nfasc*$^{-/-}$) were also used as a comparison in order to further understand any differences between Nfasc140 and Nfas186 in their ability to cluster nodal components.

Immunofluorescence showed that Nfasc140-flag and Nfasc186-flag were both capable of reconstituting the nodal complex (Fig. 38). When either Nfasc140-flag or Nfasc186-flag were present at the nodes, Na_v channels were targeted to the nodes. Hence, Nfasc140-flag and Nfasc186-flag have the same ability to organise the nodes of Ranvier. Moreover, that fact that Nfasc140, lacking the Mucin and FNIIIE domains, could also recruit βIV-Spectrin, AnkyrinG, NrCam (PNS), Gliomedin (PNS) and Brevican (CNS) to the node, indicated that those two domains are dispensable for the interactions between neuronal Neurofascins and other nodal proteins.

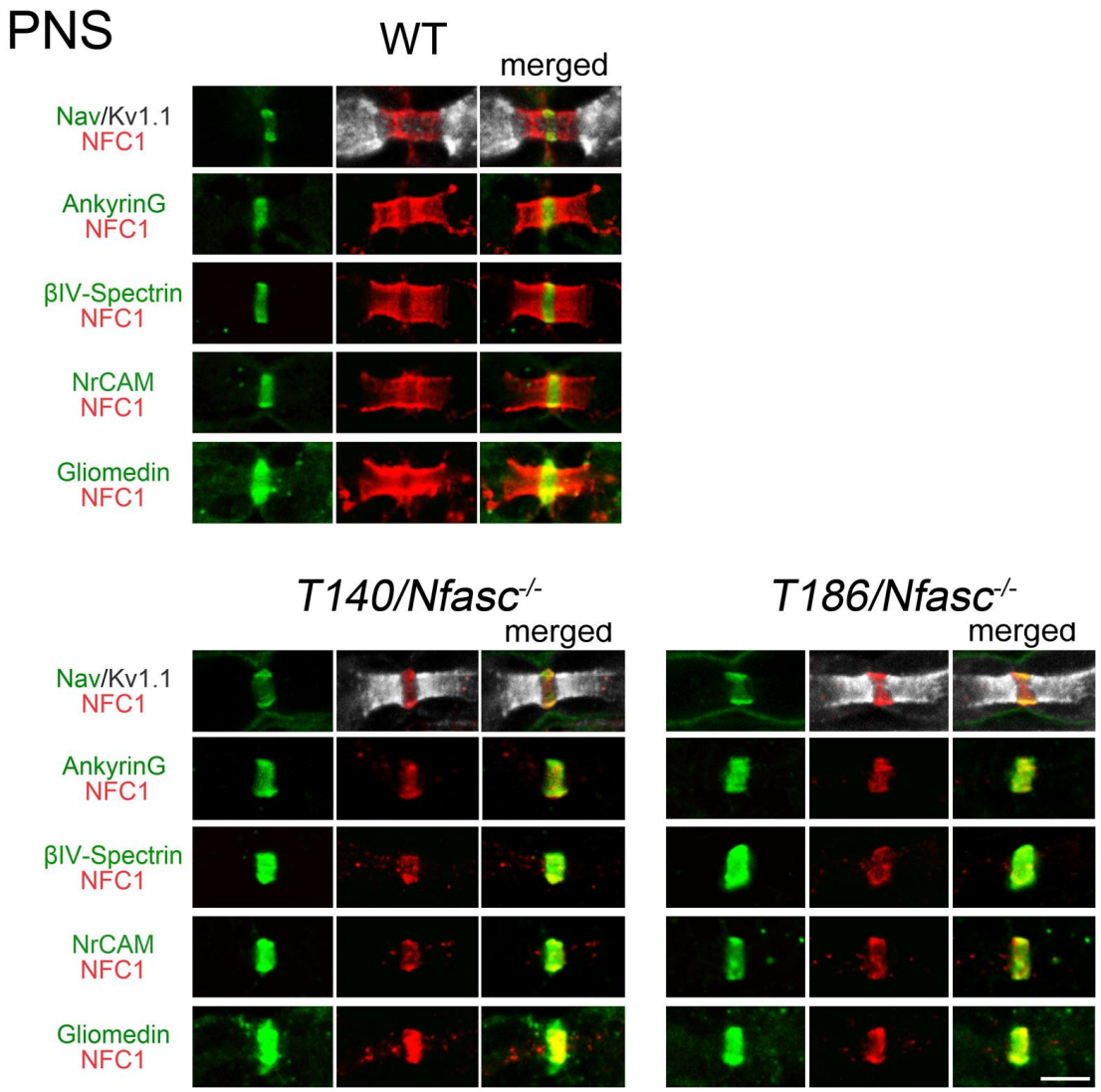
PNS
WT
merged
Nav/Kv1.1
NFC1
AnkyrinG
NFC1
βIV-Spectrin
NFC1
NrCAM
NFC1
Gliomedin
NFC1
T140/Nfasc-/-
merged
T186/Nfasc-/-
merged
Nav/Kv1.1
NFC1
AnkyrinG
NFC1
βIV-Spectrin
NFC1
NrCAM
NFC1
Gliomedin
NFC1

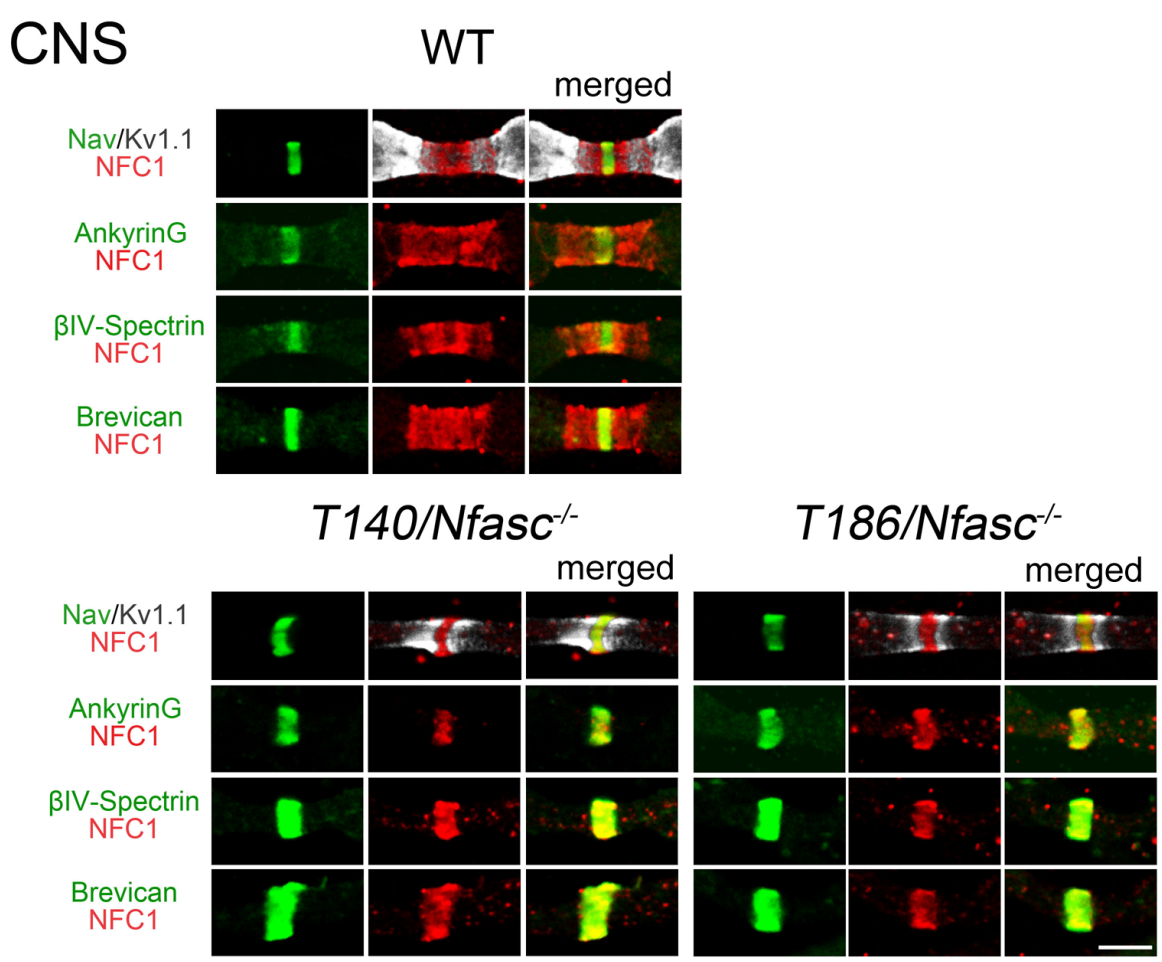

Figure 38. Nodal components of the PNS and CNS are rescued by Nfasc140-flag and Nfasc186-flag.

Immunostaining of teased quadriceps fibres (PNS) at P60 shows that when either FLAG-tagged Nfasc140 or Nfasc186 are expressed on a Nfasc$^{-/-}$ background they can bring back the nodal components, Na_v, ankyrinG, βIVspectrin, NrCAM and gliomedin. Meanwhile, in the Na_v/K_v1.1/NFC1 triple staining panel, because the transgenic does not have Nfasc155, the Na_v (green) relocalized next to the K_v1.1 (gray) without NFC1 (red) in the middle. This suggested the rescue of the node was not accompanied by reformation of the axoglial junction and, as a consequence, juxtaparanodal K_v1.1 channels were mislocalized when compared to WT.

Similarly, Immunostaining of spinal cord ventral funiculus fibers (CNS) at P60 shows that both FLAG-tagged Nfasc140 and Nfasc186 can rescue the nodal components, Na_v, AnkyrinG, βIVspectrin and Brevican when expressed on a Neurofascin-null background. As for the PNS, juxtaparanodal K_v1.1 were relocalized next to Na_v. All scale bars, 5 µm.

3.1.12 Expression of Nfasc140-flag or Nfasc186-flag partially restores nerve function

Nfasc155 is an indispensable component of the Nfasc155-Caspr-Contactin adhesion complex at the paranode. Here two different transgenic animals were shown which lacked Nfasc155 and the paranodal adhesion complex. From the triple staining of Na_v channel, K_v channel and NFC1, it was clear that the absence of Nfasc155 resulted in a missing barrier between Na_v channels and K_v channels. This presumably contributes to the reduction of the nerve conduction velocity shown below (Fig. 39).

These transgenic animals started to show signs of neurological defects from P20, including tremors, weak hindlimbs and hindlimb clasping. Even though the hindlimbs were obviously abnormal, however, in the lab environment both of the transgenic animal can survive for at least one year (*T140/Nfasc*$^{-/-}$ and *T140/Nfasc*$^{-/-}$, 2 of each were kept in animal units feeding for one year and then sacrificed.).

Some ectopic expression of both Nfasc140-flag and Nfasc186-flag can be seen along the axons, which was not observed in WT animals (see Fig. 38 above). This might be caused by the over expression of both transgenic proteins under the control of Thy-1 promoter. It is unclear whether this ectopic protein expression would affect nerve function. However, Caspr-null mice have very similar reductions in nerve conduction velocity, suggesting that the decreased rates observed in the transgenics are due to disrupted paranodal axo-glial junctions (Diane Sherman, personal communication).

Furthermore, studies on contactin knockout mouse (Boyle et al., 2001) showed that when contactin was deleted, Caspr ,but not Nfasc155, was mislocalized, which led to a shift of K_v channels from juxtaparanodal region towards the paranodal region of the septate-like junctions at the paranodes of PNS fibres, and nerve conduction velocity was reduced compared to wild type animals.

A

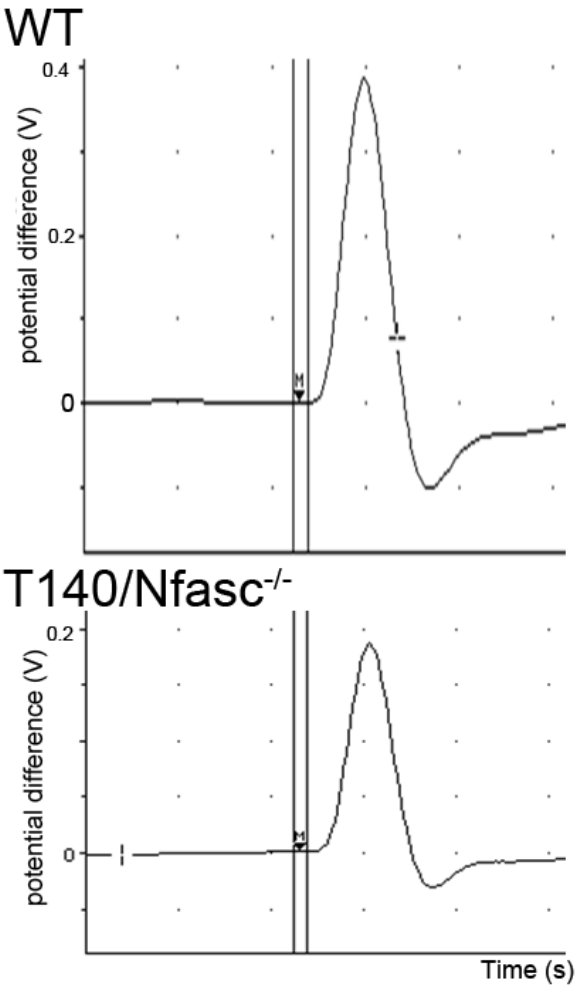
WT
0.4
0.2
0
potential difference (V)
T140/Nfasc-/-
0.2
0
potential difference (V)
Time (s)

B

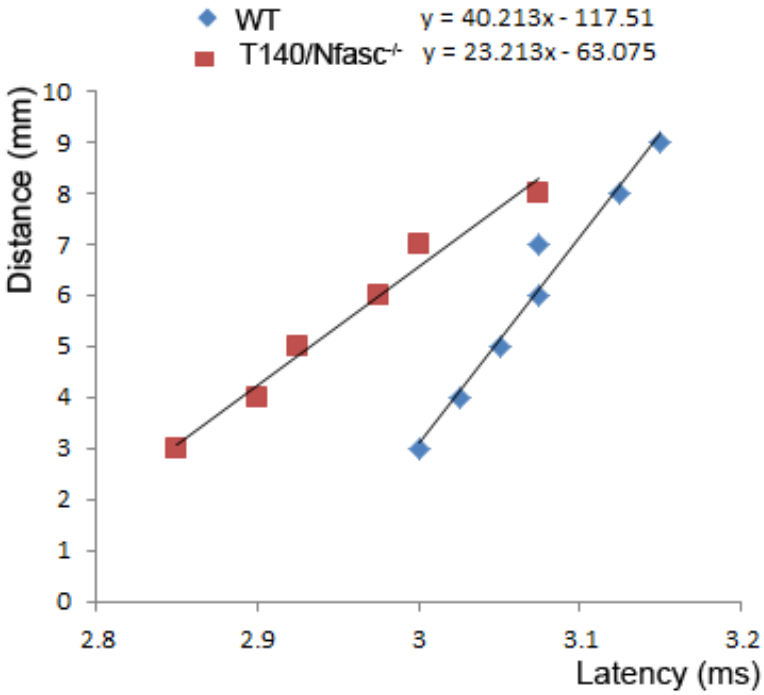
WT
y = 40.213x - 117.51
T140/Nfasc-/-
y = 23.213x - 63.075
Distance (mm)
10
9
8
7
6
5
4
3
2
1
0
2.8
2.9
3
3.1
3.2
Latency (ms)

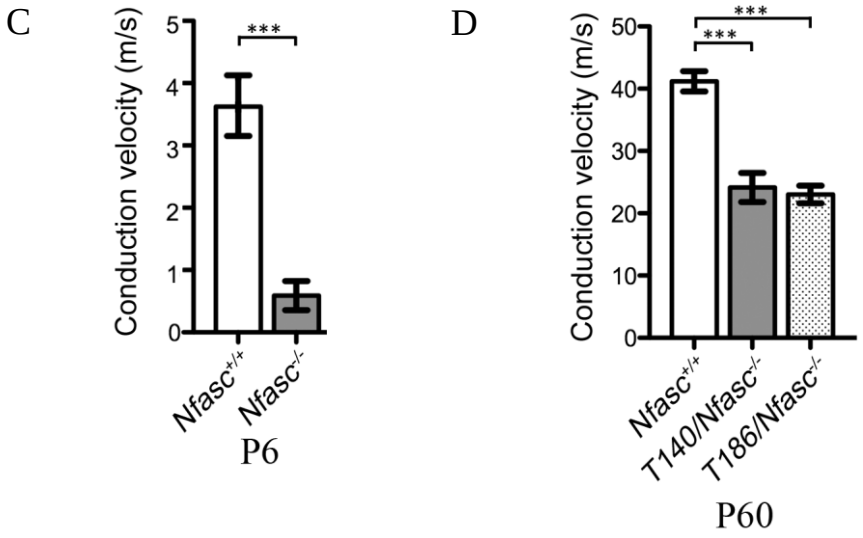

Figure 39. Nerve conduction velocity is partially rescued in transgenic animals.

A. The wave shape of the CAP of both WT and T140/Nfasc$^{-/-}$ are shown here, their shapes were very similar. CAP of T186/Nfasc$^{-/-}$ is almost the same as T140/Nfasc$^{-/-}$, which was not showing here.
B. The data of one quadriceps nerve from each WT and T140/Nfasc$^{-/-}$ is plotted on the chart. The conduction velocity is calculated as the slope of the trend line. The same method was used to calculate the conduction velocity of nerve from T186/Nfasc$^{-/-}$.
C. Data comes from Sherman et al., 2005. In Neurofascin transgenic animals, the conduction velocities of mutant peripheral sciatic nerves were drastically reduced from 3.7 ± 0.5 m/s (WT, Nfas$^{+/+}$) to 0.7 ± 0.2 m/s (Nfasc−/−) (means ± SEM; n = 3 for each).
D. Quadriceps nerves from P60 animals was used to measure the nerve conduction velocity. The conduction velocities are: 41.20 ± 1.64 m/s for WT, 24.13±2.32 for T140/Nfasc$^{-/-}$ and 23.02±1.42 for T186/Nfasc$^{-/-}$ animals. The conduction velocity of WT animals is almost twice of the transgenic animals. There was no significant difference between the two transgenic lines. Values are means ± SEM; n=6 mice for each condition; ∗∗∗, p <0.0001, one way ANOVA test is followed by Tukey's Multiple Comparison Test.

In my experiment, the CAP of both WT animals and mutants (in T140/Nfasc$^{-/-}$ and T186/Nfasc$^{-/-}$) was recorded and the conduction velocity of nerves was calculated using the distance divided by the latency (Fig. 39 A and B). To compare the shape of the CAP wave, the distances used for recording in Fig. 39 A are different between

WT and mutant, to ensure the duration of the CAP were similar. From the picture and the other CAP waves which I measured, I have the impression the potential difference is smaller in mutant comparing with WT. Because the voltage of the stimulations in my experiments is different between measurements, further study using similar stimulations is needed to confirm the existence of the differences.

Nerve conduction velocity analysis showed the nerve conduction velocity dropped from 41 to 23-24 m/s, this confirmed an almost 50% conduction velocity reduction in the transgenic animals (Fig. 39 D). However, this compares with an over 80% reduction in the peripheral nerves of mice lacking both paranodal junctions and Nfasc186 (Sherman et al. 2005) (Fig. 39 C). The faster nerve conduction velocity in transgenic animals comparing with Nfasc-null animals is likely to be the result of the rescued nodal components in T140/Nfasc$^{-/-}$ and T186/Nfasc$^{-/-}$ animals. Because in those animals the Na_v is concentrated at the nodes (Fig. 38); meanwhile, in Nfasc-null the Na_v is no longer targeted at nodes (Fig. 37).

Since the nerve conduction velocity was reduced by half in the transgenic animals, I determined if this would affect behaviour. The Rotarod was used here to analyse motor behaviour. Rotarod is a motor coordination test; however, in our animal model both the CNS and PNS are likely to malfunction. Hence our result was not an index of the motor neuron dysfunction but a quantifiable way of evaluating how worse the transgenic animals performed in a behavioural task. And the performance of the transgenic animals clearly showed they were worse than the wild type animal (Fig. 40). This is consistent with their gait abnormalities.

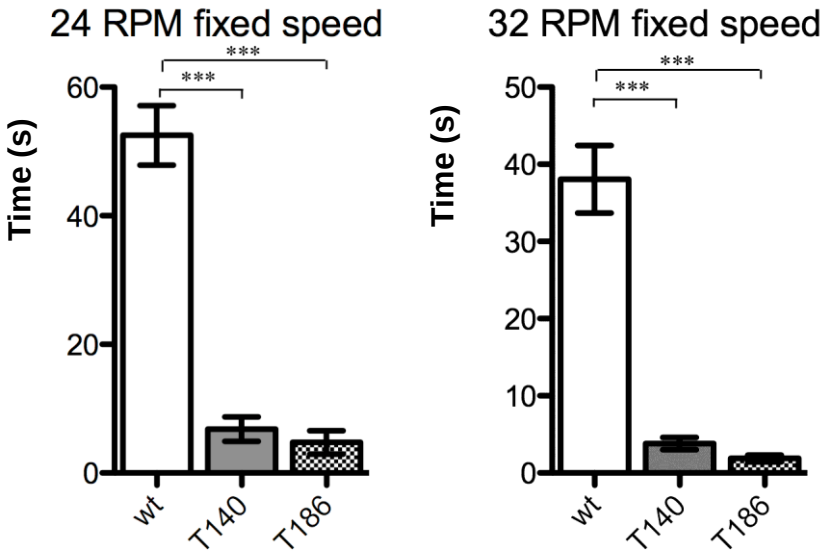

Figure 40. The transgenic animals have motor behavioural dysfunction.
T140/Nfasc$^{-/-}$ and *T186/Nfasc*$^{-/-}$ P60 animals were significantly worse than WT animals on the Rotarod. And the deficit comparing the two different transgenice animals was not significantly different. Values are means ± SEM where n=6 mice for each condition. ***, p <0.0001, one way ANOVA test is followed by Tukey's Multiple Comparison Test.

3.1.13 Summary of the first part of my study.

A third isoform of Neurofascin, Nfasc140, has been characterized in this study. By RT-PCR and DNA sequencing, I confirmed the amino acid sequence of Nfasc140. By comparing its sequence with Nfasc186 and Nfasc155, the domain structure of Nfasc140 was shown. Nfasc140 has the domains common to all known Neurofascins, it contains six IgG domains, A, B and D FnIII domains, the transmembrane region and the cytoplasmic domain.

The domain composition of Nfasc140 is almost identical to that of Nfasc166 in chick. It has been shown that Nfasc166 is predominantly expressed in dorsal root ganglia from E5 to E8 in chick and the level of expression decreases afterwards (Koticha et al., 2005). I found Nfasc140, like Nfasc166, is highly expressed at the early embryonic stages and down regulated at late embryonic stages.

Conditional deletion of Neurofascins in glial or neuronal cells revealed that Nfasc140 is expressed in neurons. When the Neurofascins are deleted from the nodes, neuronal proteins like AnkyrinG, NrCAM, Brevican and Gliomedin are no longer targeted to the nodes (Sherman et al., 2005, Zonta et al., 2008). This led me to compare the other neuronal Neurofascin, Nfasc186, with Nfasc140. The results showed that Nfasc140 alone, like Nfasc186, can recruit the nodal proteins to the nodes of Ranvier in both PNS and CNS.

3.2 Intact paranodal axoglial junctions can cluster Na_v channels in the absence of neuronal Neurofascin

In this second part, in order to explore the function of Nfasc155-Caspr-Contactin complex during the formation of nodes of Ranvier, especially to further explore the controversial relationship between the paranodal complex and Na_v clustering at the nodes, I intended to generate a transgenic line in which Nfasc186 could be deleted at a very early development stage. This would allow me to determine whether Nfasc155 and the axoglial junction alone can promote the clustering of Na_v at the nodes.

3.2.1 Generation of early deletion of Neuronal Neurofascins animals

In order to clarify the function of neuronal Neurofascins and how Na_v channels are targeted initially to the node, I generated a neuronal Cre-expressing line in which the Cre was expressed at an early age. In this mouse line the Cre recombinase is driven by the thymus cell antigen 1 (*Thy-1*) promoter and this was crossed with mice carrying *Nfasc* floxed alleles to generate mice in which Neurofascins were specifically inactivated in neuronal cells at an early development stage (*Thy-Cre/Nfasc*$^{fl/fl}$). In these studies Nfasc155 should continue to be expressed under the control of its normal promoter in myelin-forming glia.

I intended to generate a mouse model which can abolish neuronal Neurofascin expression before sodium channels are targeted to the nodes of Ranvier. So the Cre

needed to be activated before Na_v channel targeting and also have a high efficiency to delete the Neurofascins.

To check the age of Cre activation and the efficiency of Cre penetration in CNS, the expression levels of neuronal Neurofascins in spinal cord tissues at different ages were checked using NFC-1 antibodies. As the result showed, the Cre started to inactivate neuronal Neurofascin expression before E15 and at E18 the neuronal Neurofascins were undetectable by western blot (Fig. 41).

In the CNS, clustering of Na_v channels depends on specific axoglial contact (Rasband et al.,1999) . Previous studies have indicated that myelination in ventral spinal cord starts at E18, one day before birth (Foran et al., 1992). Moreover, our own studies on the cervical spinal cord show that at P3 nodes are undetectable by sodium channel staining (unpublished). So when neuronal Neurofascins were deleted at E18 the sodium channels were not yet clustered. Hence, our transgenic animal line fulfils the criteria for our experimental purpose.

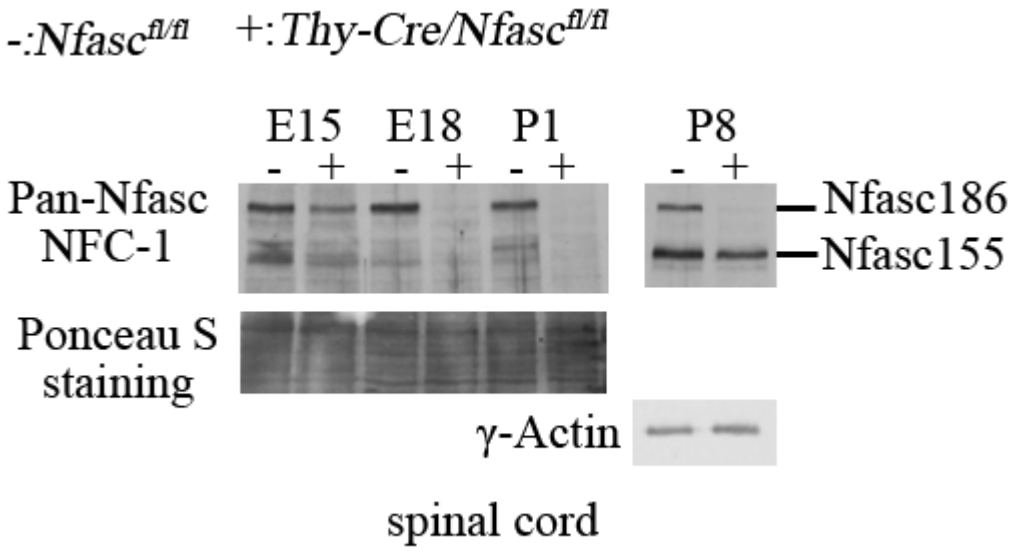

Figure 41. Nfasc186 is deleted from CNS from E18.
Western blots of spinal cords from different ages showed at E15 Nfasc186 was partially deleted. And from E18 to P8 Nfasc186 was undetectable by western blot. Normalized with Ponceau S at E15,E18 and P1, and γ-Actin at P8.

The western blot at P8 (Fig. 41) showed when Nfasc186 was deleted Nfasc155 was also slightly reduced. This may reflect a slight delay of Nfasc155 expression after deleting neuronal Neurofascins. This was suggested by the observation of Nfasc155 expression patterns in different ages in PNS sections (Fig. 42).

In order to examine Cre expression in PNS, sections of quadriceps femoral nerves from P1-P5 animals were used for immunostaining. Results showed at P3, when Neurofascins had located at both nodes and paranodes in wild type animals, there was almost no Neurofascin staining in transgenic animals (Fig. 42 A). This indicated that Cre is active in neurons. Although Nfasc155 appearance at paranodes was delayed in the transgenic mouse at P6, Nfasc155 appeared at many paranodes, and at the same time Na_v channel staining was observed.. The delay in the expression of Nfasc155 might be caused by a delayed myelination. To examine this possibility, sections from P3 when there were very few Nfasc155 positive paranodes were stained with MAG antibodies. Results showed the MAG staining was very similar in both WT and transgenic mice, so the myelination had occurred in both control and transgenic animals (Fig. 42 B). Hence, the later appearance of Nfasc155 was unlikely caused by impeded myelination. Hence, the delayed appearance of Nfasc155 is likely to reflect a delayed localization or expression of Nfasc155 itself. How Nfasc186 might influence Nfasc155 localization or expression is unknown.

Importantly, at P3 there was little Nfasc186 staining in the nerve sections and by P6 the Nfasc186 was missing from most of the nodes (Fig. 42 C). This suggested that Nfasc186 is deleted before the clustering of Na_v channels occur at nodes of Ranvier. The results also showed that at P3 there were Na_v channels positive nodes without neuronal Neurofascin. This supports the view that paranodal junctions can cluster sodium channels independently of Nfasc186.

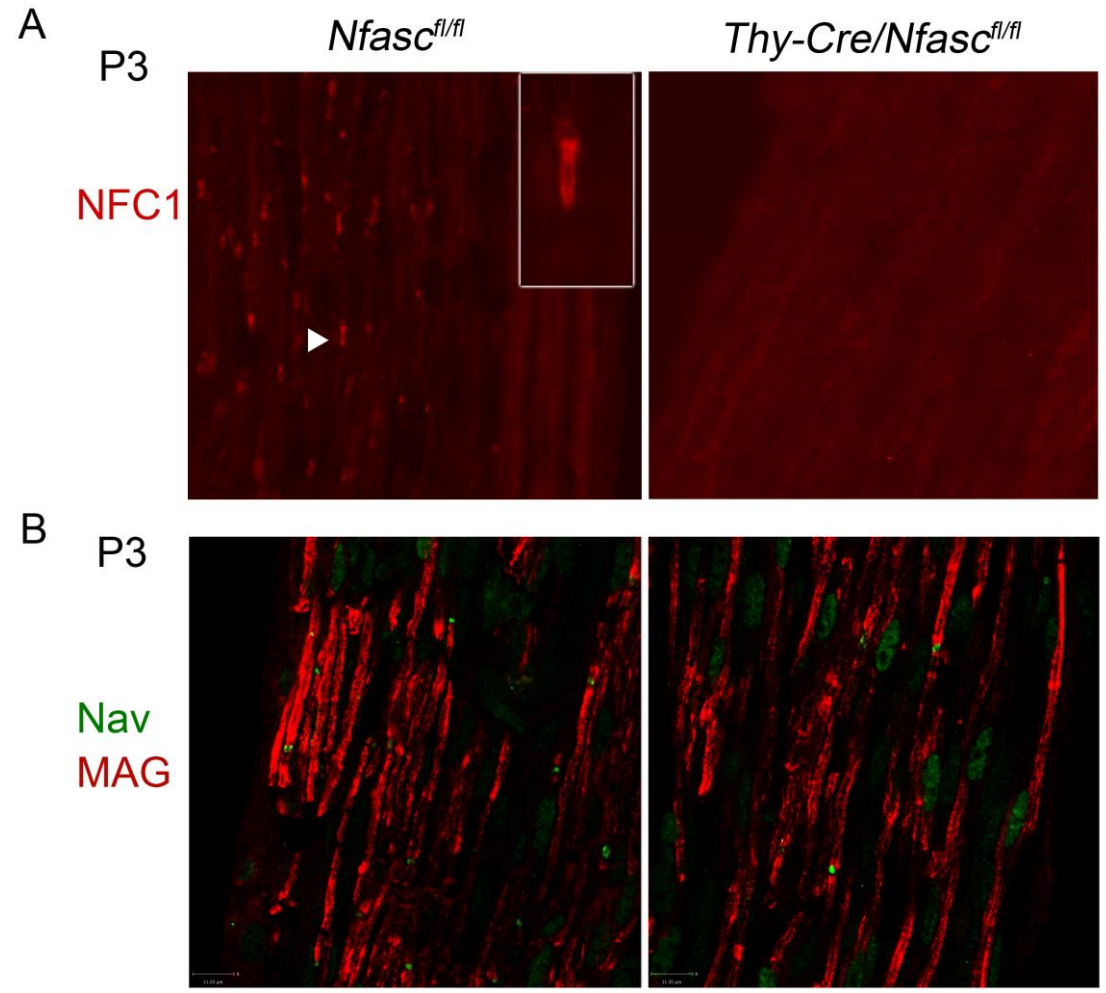
A
P3
Nfasc^fl/fl
Thy-Cre/Nfasc^fl/fl
NFC1
B
P3
Nav
MAG

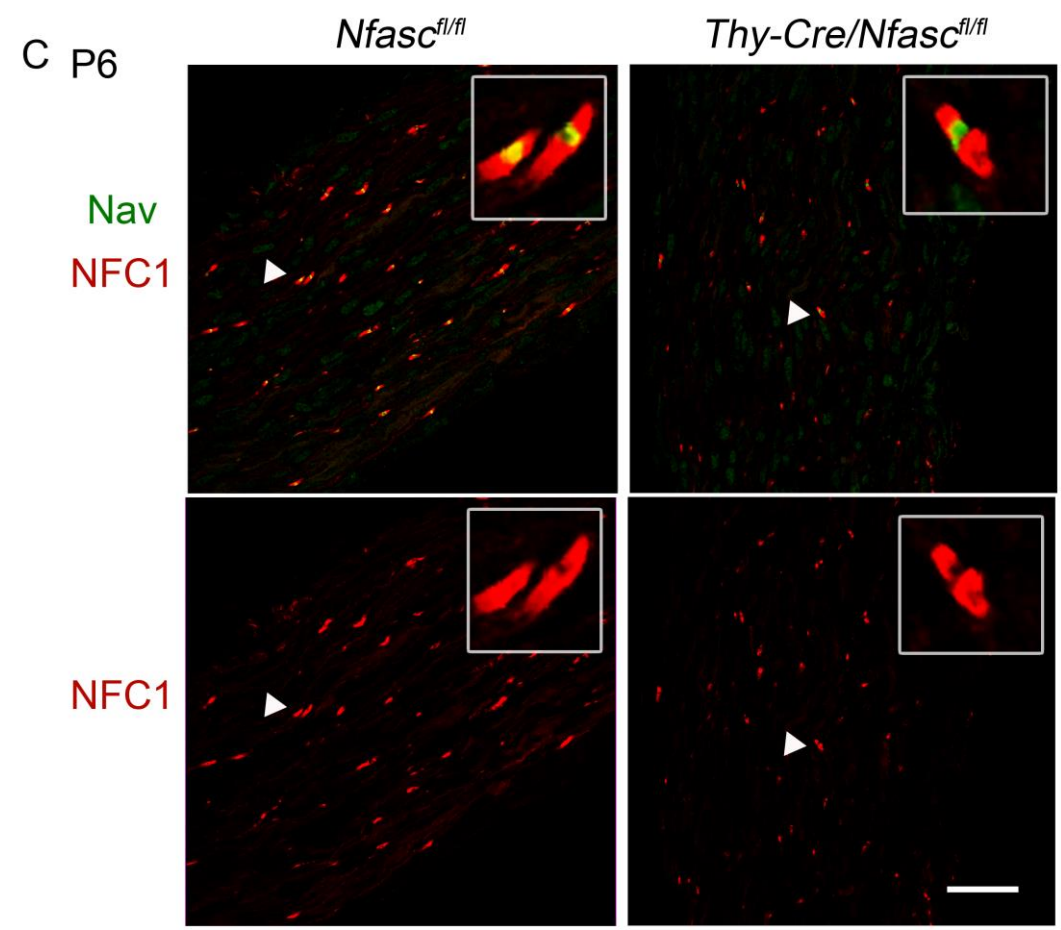

Figure 42. Nfasc155 expression is delayed in Thy-Cre/Nfasc$^{fl/fl}$ animals.

A. P3 PNS nerve sections showing Neurofascins detected by NFC1 antibody in WT. Neither Nfasc155 nor Nfasc186 positive nodes were present.
B. MAG staining in red showed axons at P3 were myelinated in both WT and transgenic animals.
C. At P6 Na_v channels were targeted at the nodes in the transgenic animals and Nfasc155 positive paranodes flanked the Na_v channels. Scale bar 15 µm.

3.2.2 Clustering of Na_v channels does not require neuronal Neurofascins.

To investigate the effect of Nfasc186 loss on Na_v channel targeting to the nodes, quantitative studies were done on P5 - P6 *Thy-Cre/Nfasc$^{fl/fl}$* animals. Results showed that while less than 1% of the nodes have Nfasc186, more than 90% of the nodes still have Na_v channels in CNS (Fig. 43). The high percentage of nodes which had Na_v channels without Nfasc186 showed that the clustering of Na_v channels is not obligately dependent on Nfasc186. A previous study (Sherman *et al.*, 2005) showed

that Na_v channels clustering did not happen in the Nfasc-null mouse, which showed that Neurofascins are indispensable for Na_v channel targeting to the nodes. In my study the high percentage of Na_v channels targeting to the nodes showed that the paranodal junction can cluster Na_v channels in the CNS. This confirmed previous observations that the clustering of Na_v channels in CNS does not require neuronal Neurofascins (Zonta *et al.*, 2008, Rasband *et al.*, 1999).

After the deletion of Nfasc186 from CNS nodes of Ranvier, its extracellular domain binding partner, Brevican (Hedstrom et al., 2007), was missing from the nodal area, but other major nodal components, like AnkyrinG and βIV-Spectrin, were still targeted to the nodes of Ranvier.

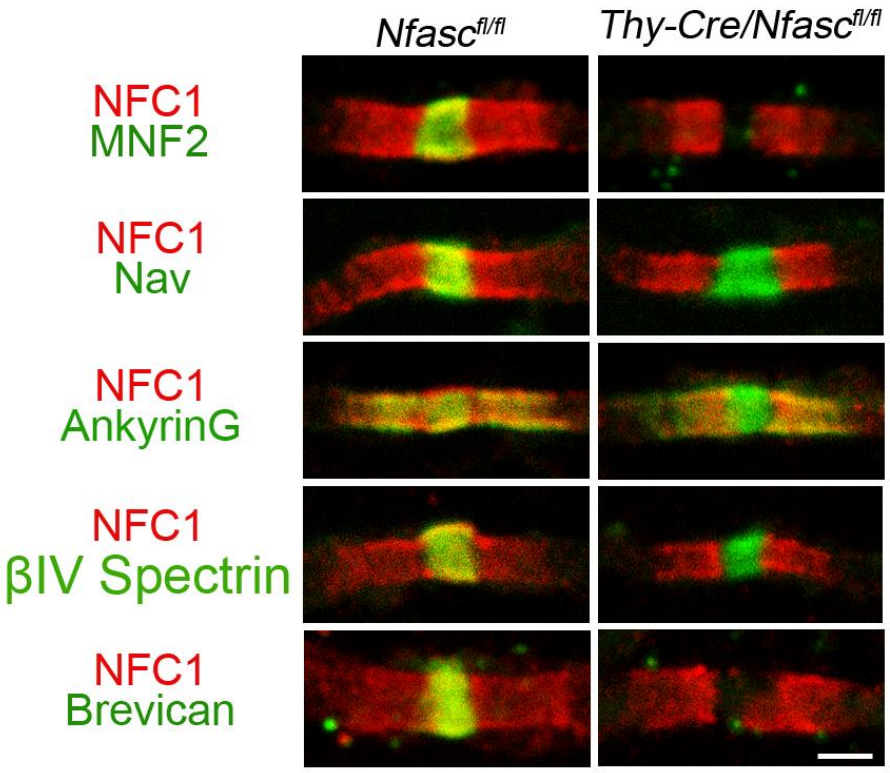

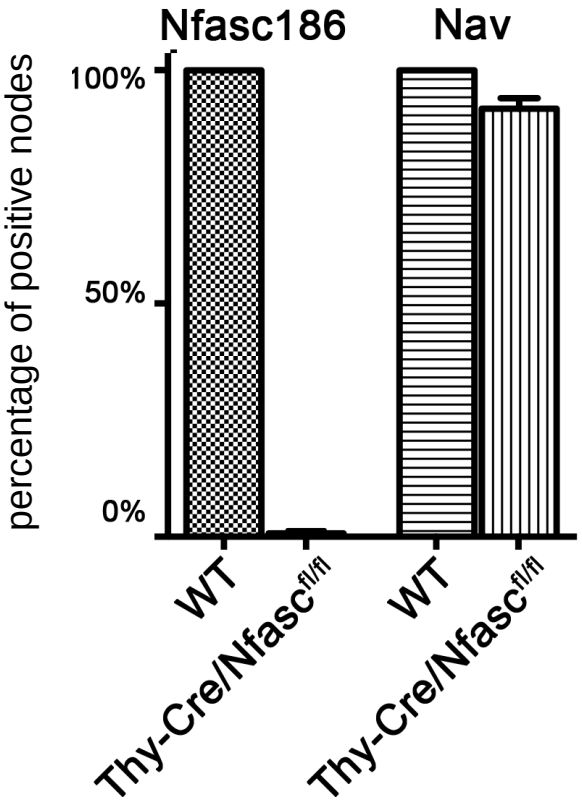

Figure 43. Na_v channel targeting without neuronal Neurofascins in CNS at P6
Immunoflorescence images of teased fibres from the ventral funiculus of the spinal cord in the CNS showed Nfasc186 and Brevican were not detected at the nodes at P6. Quantitation of the percentage of Nfasc186 positive nodes showed there was less than 1% Nfasc186 positive nodes left; meanwhile, quantitation of the Na_v positive nodes showed more than 90% nodes were targeted at the nodes of Ranvier. NFC1 recognises all forms of Neurofascin. Values are means ± SEM where n=3 mice for each condition. Scale bar 2 μm.

Similar results were observed in the PNS (Fig. 44). After the ablation of neuronal Neurofascins, the sodium channels could still target to the nodes. This finding differed from the result published by Sherman et al. (2005). In that study, transgenic mice $Nfasc^{-/-}/NfascΔIC^{+}$, which had a truncated form of Nfasc155 expressed in the glial cells on a Nfasc-null background, were used to address the question whether Nfasc155 alone could rescue Na_v channel clustering. They showed that when only the truncated form of Nfasc155 was expressed, no Na_v channel was clustered at the nodes in PNS. It seems likely that the cytoplasmic tail might have a key role in clustering Na_v channels; it is also possible that the *plp* promoter used might drive the truncated Nfasc155 expressing at a late time point which subsequently affects the normal clustering of Na_v channels.

Gliomedin which interacts with Nfasc186 at the node in the PNS was not targeted to the node, but other nodal proteins were targeted to the nodes. Nevertheless, the levels of expression of nodal proteins appeared to be lower than in the control group. This could be caused by the delayed Nfasc155 expression.

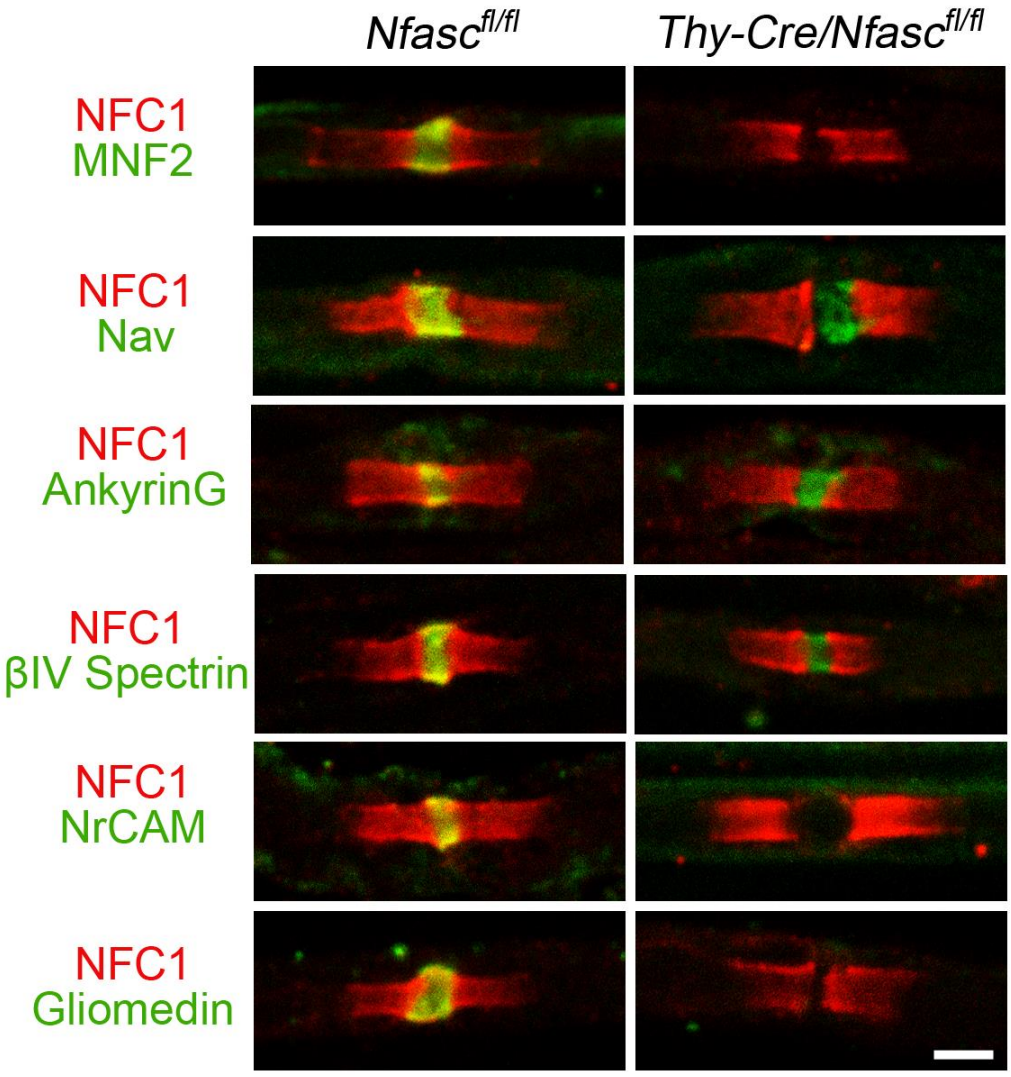

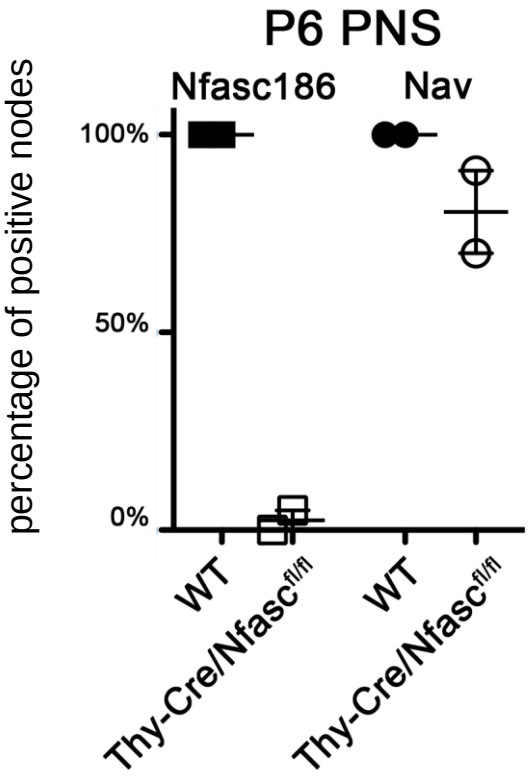

Figure 44. Na_v channel targeting without neuronal Neurofascins in PNS at P6
Immunoflorescence images of teased fibres of PNS showed that Nfasc186, NrCAM and Gliomedin were not detected at the nodes at P6. Quantitation of the percentage of Nfasc186 positive nodes showed that there were less than 3% Nfasc186 positive nodes left; quantitation of the Na_v positive nodes showed more than 80% nodes were targeted at the nodes of Ranvier. n=2 mice for each condition. Scale bar, 2 μm

3.2.3 Summary of the first part of my study.

A new neuronal Cre deletion mouse model was crossed with *Nfasc*$^{fl/fl}$ mice to generate *Tcre/Nfasc*$^{fl/fl}$,mice. So all the data above were gathered from animals on a CBA/C57 mixed background (F3 generation backcross to C57). At the F3 generation, neuronal Neurofascins, Nfasc186 and Nfasc140 were deleted as early as E18 in the CNS, before the start of myelination. In the PNS at P3, immunolabeling clearly showed Nfasc186 was not expressed in axons; surprisingly Nfasc155 was barely detectable and only very few Na_v channel-positive nodes were detected. However, at P6 many more Na_v channel-positive nodes and Nfasc155-positive paranodes appeared. This indicates a delayed targeting or expression of Nfasc155 in the absence of neuronal Neurofascins at an early age (before P3). Also because the appearance of Nfasc155 correlated with the increasing number of Na_v channels positive nodes from

P3 to P6. It indicates that the clustering of Na_v channels can be promoted by paranodal junctions.

Immunolabeling at P6 showed that less than 5% of the nodes have neuronal Neurofascins staining in either the PNS or CNS. However, more than 80% of the nodes in the PNS and more than 90% of CNS nodes have Na_v channels. This supports the view that Na_v channels can be clustered to the nodes of Ranvier by paranodal axoglial junctions only. In these experiments, only those nodes flanked symmetrically by Nfasc155 were counted. Some nodes only had Nfasc155 at one side, which may reflect the delayed expression of Nfasc155. And for some of those asymmetrical nodes, Na_v channels are also found targeted to the nodal area, next to Nfasc155 staining (data not shown).

3.2.3 The phenotypes changing from F3 to F6

When we generate Thy-Cre animals, we used CBA and C57 hybrid eggs to getting more fertilized eggs for micro injection and a better pregnancy rate. In order to eliminate the variations of the strain background I decided to backcross animals and put *Thy-Cre/Nfasc*$^{fl/fl}$ on a C57 background (F6 generation 98.375% congenic). Interestingly in F6 generation the phenotypes of the animals changed, the glial cells did not express Nfasc155 early in either PNS or CNS at P6 (Fig. 45). Also those animal die at P6 as all Neurofascins were not present, so they had the same phenotype as *Nfasc*$^{-/-}$ animals.

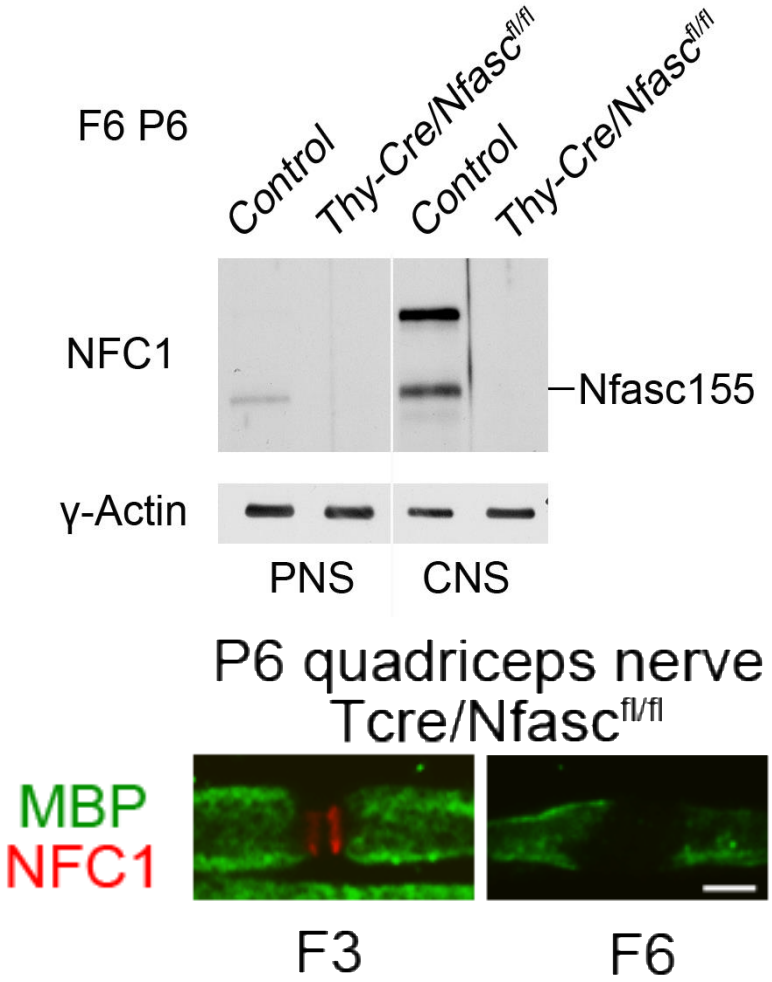

Figure 45. Nfasc155 is not expressed in F6 animals at P6
Western blot of quadriceps nerve and spinal cord tissues from F6 P6 animals showed that both Nfasc186 and Nfasc155 were deleted from *Thy-Cre/Nfasc*$^{fl/fl}$ animals. Normalized with γ-Actin. And immunoflorescent staining confirmed the ablation of Nfasc186 and Nfasc155 from the nodes of Ranvier in F6 P6 animals. . Scale bar, 2 µm

The Thy-1.2 promoter was shown to be able to drive the expression of Cre in non-neuronal tissues (Campsall et al., 2002). So loss of Nfasc155 might have been due to the fact that Cre was active in the glial cells on a C57 background, in this case it would delete all the Nfasc155 from glial cells. So we decided to check whether the change of background could cause the Cre to be expressed in glial cells and subsequently cause the ablation of the *Nfasc* gene and the Nfasc155 mRNA in glial cells. Hence, I checked Nfasc155 mRNA levels in peripheral nerves by semi-quantitative PCR. These should contain no neuronal mRNAs. Quadriceps nerves and the femoral branches from both WT and Thy-Cre/Nfasc$^{fl/fl}$ were taken and mRNA

was extracted. RT-PCRs with different numbers of cycles were shown below. Because there were no obvious differences between the expression levels of mRNA in WT and transgenic animals (Fig. 46), it was unlikely the Cre was active in the Schwann cells.

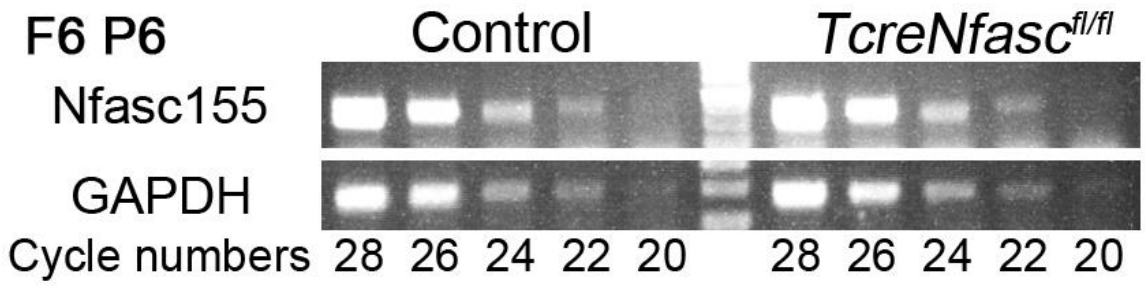

Figure 46. mRNA level of Nfasc155 is not altered in Thy-Cre/Nfasc$^{fl/fl}$ mice.
Semi-quantitative RT-PCR was performed to amplify Nfasc155mRNA. The levels of mRNA were not reduced in transgenic animals. Normalized with glyceraldehyde-3-phosphate dehydrogenase (GAPDH).

4. Conclusions and Discussion

4.1 OVERVIEW

A fully developed node of Ranvier permits the rapid propagation of action potentials in myelinated axons, this is critical for the function of the vertebrate nervous system.

Recently, there has been tremendous progress in our understanding of the events leading to the organization of the node and its environs along myelinated axons of the PNS and CNS. It has become increasingly clear that Neurofascins play a role in the localization of different channels in axons and that are required to establish saltatory conduction (Davis et al., 1993, Tait et al., 2000, Sherman et al., 2005, Burkarth et al., 2007, Zonta et al., 2008, Kriebel et al., 2011, Zonta et al., 2011).

Previous studies on two major isoforms of Neurofascins, Nfasc155 and Nfasc186, have shown they are functionally different and each of them has distinct roles in the nodal formation. A third isoform, Nfasc140, was also described by the group of Dr V. Bennett in 1995. I identified the protein domain composition of Nfasc140; using a transgenic approach I am able to characterize the possible functions of Nfasc140 *in vivo*. Here I will discuss and validate my data on my study of Nfasc140.

Even though the protein organizations at the nodes of Ranvier become more and more clear, the role of paranodal complex in clustering of nodes is still controversial. Two studies have showed that the targeting of Na_v channels to the mature nodes of Ranvier can occur independently of the expression of Nfasc186 (or Neuronal Neurofascins) (Zonta et al., 2008; Feinberg et al., 2011). However, in another study, Nfasc186 has been showed to be indispensable for the targeting of Na_v channels to the nodes of Ranvier and paranodes could not substitute (Thaxton *et al.*, 2011). I generated *Thy-Cre/Nfasc*$^{fl/fl}$ mouse line, which allows me to clarify the controversial theories. I found evidence showing the paranodal complex can target Na_v to the nodal area. Here, I will discuss my results and the differences comparing with other papers and point out the reasons for those differences.

4.2 Study of Nfasc140

4.2.1 Domain composition of Nfasc140

Western blot (Fig. 24, 25) result of the expression pattern of Nfasc140 showed the protein is highly expressed at embryonic stages, and is the predominate isoform of Neurofascin at the age of E13. Meanwhile, full length RT-PCR results revealed that at the age of both E13 (data not show) and E15 (Fig. 21) only one band was amplified and the sequencing results showed it is an isoform of Neurofascin which is smaller in size than Nfasc155. I think the amplified cDNA and the 140kD protein band detected on western blot is associated for four reasons. First, the estimated protein size based on RT-PCR and sequencing result is very similar to the Nfasc140 protein band on Western blot. Second, the appearing of only one band at E13 in both Western blot and one product of RT-PCR has been found at E13. Third, using one pan Neurofascin antibody and two isoform specific antibodies to probe the Nfasc140 protein on western blot, it confirmed the protein band on western blot has the same domains composition as the domains structure predicted by RT-PCR and sequencing result. Last, an adding or lacking of other domain will lead to an obvious change on protein size, which is unlikely happened in this case. So I think the association between cDNA and protein bands is well established here. To further confirm the protein sequence, protein sequencing can be conducted, Nfasc140 can be purified from animal brain tissue and digested into small pieces and subsequently sent to sequence. However, it would be very challenging to sequence the whole Nfasc140 protein. Because Nfasc140 has more than one thousand amino acids, that is very long for protein sequencing, and it is also not easy to purify Nfasc140 from animal brains using the anti-peptide antibody we have. While all the results were very convincing, I think it is unnecessary to sequence the whole Nfasc140 protein in my study.

Using primers to amplify all isoforms of transcripts of *Neurofascin*, at the age of E13.3 when only one isoform of Neurofascin was detectable by western blot, one cDNA was amplified (Fig. 21, 24). Using the same primers, when more than one isoforms of Neurofascin were detected on western bolt at the ages of E15.5, P17 and P30, but only one cDNA was amplified (Fig. 21, 24). Here, one cDNA product was

amplified instead of multiple products could be caused by the mRNA concentration differences among tissues from different ages, therefore, only the isoform which has the highest mRNA concentration in the tissue at a specific age was preferably amplified under the RT-PCR condition. In other experiment, different PCR primers which only amplify a small segment of *Neurofascin* can yield more than one bands from the mRNA (cNDA) extract from P17 and P30 animals which indicates the transcripts of other isoforms of *Neurofascin* is also presented in animals brain tissues when multiple protein bands were detected on western blots.

The domain composition of Nfasc140 was determined by using three different Neurofascin antibodies to probe the Nfasc140 band on western blots. And the results demonstrated that Nfasc140 has no specific domains comparing with Nfasc186 and Nfasc155 (Fig. 23). Among those western blots, besides the three Neurofascins there were some uncharacterized bands, I will discuss them here. In the blot probed by NFC1 antibody, a faint band appearing above the Nfasc140 band in the lane of E15.5 is a non-specific band. Because in previous studies the same band was also detected from Neurofascin knockout animal tissues at E15.5. Meanwhile, a band was detected by both NFC1 and MNF2 below the Nfasc186 band in the lane of P60. Which I think is a break down products of Nfasc186 in old animal tissues. Because a band at similar size was also found in the transgenic animal in which only Nfasc186-flag was expressed (*T186/Nfasc*$^{-/-}$) (Fig. 37), and also it could be recognized by two different antibodies (Fig. 23). Due to the limited time for my study, I did not continue to characterize those proteins in my study.

The domain composition of Nfasc140 is very similar to Nfasc166, and it has been shown that Nfasc166 interacts with NF166-axonin-1 and increases neurite outgrowth (Koticha et al., 2005, Pruss et al., 2009). This suggested Nfasc140 could have a similar role in regulating neurite extension and outgrowth in mouse. All these neurite outgrowth experiments were based on *in vitro* studies which have their limitations. It is known that the cell environment and cell-cell interactions in vitro differ from *in vivo*. In my study, I wanted to use *in vivo* system to answer this question, but I found there is not a well-established experimental procedure to evaluate the changes of

neurite outgrowth in vivo, so I've checked the gross brain size and cortex thickness of control and transgenic animals but no obvious difference were found. Meanwhile, it is suggested Nfasc186 which has the Mucin like domain which can depress the neurite outgrowth. But when comparing the transgenic mice which only Nfasc140 or Nfasc186 was expressed, I did not find any obvious difference between brain size and cortex thickness. So I did not conduct further experiments to characterize the possible roles for Nfasc140 related to neurite outgrowth. Hence whether Nfasc140 has a role in regulating neurite outgrowth *in vivo* is unclear, further studies are needed to answer this question.

4.2.2 Nfasc140 is differentially expressed during CNS development

Like the embryonic isoform Nfasc166 in chick, Nfasc140 is highly expressed at early embryonic stages. Also Nfasc140 is the predominate isoform in WT murine brain at E13 and E15 (Fig. 24). Interestingly, in contrast to Nfasc166 in chick, the expression level of Nfasc140 is up-regulated at later ages, around P12, which interestingly correlates with increasing MBP expression. Meanwhile, in the paper of Pomicter et al. (2010) they found a Neurofascin isoform (Nfasc155L) , which has a size similar to Nfasc140 is altered in multiple sclerosis plaque tissues. These observations suggest a possible role of Nfasc140 in myelination. However, in the study of Pomicter et al. they claimed the protein at the size of 140kD is a glial isoform after finding the protein was deleted from spinal card of glial specific Neurofascin knock out animals at P16. I think at the age of P16, the 140kD protein level in their control is very low (in my study the Nfasc140 also appears as a faint band at the age of P14 (Fig. 24)), and the glial specific Neurofascin knock out animals are smaller and sick comparing with control at the age of P16. Hence the lower expression level and the bad state of animals might be the reasons that the 140kD band was undetectable in the study of Pomicter et al. rather than because the protein is deleted from the animals. To study this, brain tissues from MS patient and animals can be run on a western blot side by side and probed with Neurofascin antibody to confirm whether the 140kD band described by Pomicter et al. is correspond to Nfasc140 isoform. And also one can check the changes of the expression level of Nfasc140 in plaque tissues of MS patient. Also brain tissues from animal demyelination and remyelination

models can be used to check whether the change is related to the changes in myelination states.

4.2.3 Nfasc140 is differentially glycosylated

Nfasc140 is differentially phosphorylated in pons and cerebellum of murine brains (Fig. 26). Reversible phosphorylation often results in a conformational change in the structures of enzymes and receptors, which can activate or inhibit the enzymes and receptors. We know Neurofascin are CAMs and Nfasc140 isoform can help the targeting of nodal proteins like NrCAM, Gliomedin and Brevican. However, there is no evidence that Nfasc140 can regulate their expression levels, for example, NrCAM is still expressed and the level of expression is not changed in Neurofascin knockout mice observed by Sherman et al. (2005). It is possible that through phosphorylation the interaction between Nfasc140 and AnkyrinG is altered, which is suggested by the observation that the phosphorylated FIGQY motif of Neurofascin is able to bind to AnkyrinG (Kriebel et al., 2012) and Nfasc140 has the same FIGQY motif as the Neurofascin used in the study of Kriebel et al.. But the reason for the differential phosphorylation of Nfasc140 in different parts of brain is still unclear.

4.2.4 Nfasc140 is a neuronal protein

In *CNP-Cre/Nfasc*$^{fl/fl}$ animals, Nfasc140 is still presented when Nfasc155 is deleted from the murine brain lysates (Fig. 28 left). In *PLP-CreERT2/ Nfasc*$^{fl/fl}$ animals there was still a trace of Nfasc155 detected on western blot. Because the animals were sick, we did not keep them longer before all the Nfasc155 got deleted. Meanwhile, the Nfasc186 seems to be stronger this could be caused by the fact that the Nfasc186 band is at the top of SDS-page gel, which means the proteins have not been separated well enough, this could lead to an artificial difference. The same samples were used for more than 3 repeats, but the Nfasc186 bands always looked different between WT and *PLP-CreERT2/ Nfasc*$^{fl/fl}$. The Nfasc140 band is still clearly showed on the western blot (Fig. 28 right). The intensity of the Nfasc140 band looks reduced but it is clear the change of expression of Nfasc140 is not as affected as Nfasc155. Because Nfasc155 is the glial isoform and both mouse lines showed the loss of Nfasc155 in

the presence of Nfasc140, I think it is clear that Nfasc140 is not a glial isoform of Neurofascin. Transgenic line, *Thy1-CreER2T/ Nfasc*$^{fl/fl}$, was used to check whether Nfasc140 is a neuronal isoform. Results showed when neuronal Nfasc186 is deleted in adult tissue, Nfasc140 is highly reduced (Fig. 29). There was a light band of Nfasc140 still present on the western blot. This could suggest that Nfasc140 has a lower turnover rate than Nfasc186. I think by using all three different lines, it is sufficient to prove Nfasc140 is a neuronal isoform of Neurofascin. To further confirm this conclusion, more experiments can be added, For example, neurons and glial cells can be cultured separately and western bolt of only neuron or glial cells can show the different composition of Neurofascin isoforms in different cell types.

4.2.5 Nfasc140 is highly concentrated in the developing cerebellum

Western blot of mouse brain lysates suggested the expression level of Nfasc140 is very high in brains of murine embryos (Fig 27). To check where the Nfasc140 localizes in the whole brain, sagittal sections were stained with pan-Neurofascin antibody NFC1. MNF2 antibody can recognize Nfasc186 only, to distinguish Nfasc140 from Nfasc186 also MNF2 antibody were also used. Cerebellums of embryonic brains were found to have strong NFC1 signal also little MNF2 signal (Fig. 30). Hence, I focused my study on wild type animal cerebellum to check the possible function of Nfasc140. Immunofluorescence pictures of brain sections of animals showed at all ages, E13.5, E15.5 and E17. 5, NFC1 signals were detectable (Fig. 29). At the age of E15.5 the NFC1 signal is very strong, and the strongest NFC1 signal comes from the DCN of the cerebellum. Because studies on the developing cerebellum often on cellular migration, cell migration was examined by immunofluorescence studies. Results showed no obvious effects of Nfasc140 on cellular migration were found in the cerebellum. And also because the Nfasc186 isoform start to express at between E13.3 and E15.5 (Fig. 24), it becomes hard to dissect the effect of Nfasc140 at a later age. To better understand the role of Nfasc140 alone, I was planning to compare the Neurofascin knockout animal with the transgenic animals (T140/Nfasc$^{-/-}$) which expressing Nfasc140 only. However, I did not have enough time to conduct this experiment during my study, because I focused my study on exploring the possible role of Nfasc140 involved in myelination.

4.2.6 Nfasc140-flag can organise the nodal complex

When the Neurofascins are deleted from the nodes, neuronal proteins like AnkyrinG, NrCAM and βIV-Spectrin are no longer targeted to the nodes (Sherman et al., 2005, Zonta et al., 2008). Conditional deletion of Neurofascins in glial or neuronal cells revealed that Nfasc140 is expressed in neurons. This led me to study the role of Nfasc140 during nodal formation and also compare the other neuronal Nfasc186 with Nfasc140. The results showed that Nfasc140 alone, like Nfasc186, can recruit the nodal proteins to the nodes of Ranvier. Also the Gliomedin and Brevican which were suggested to interact with Nfasc186 are also found to be targeted at the node of Ranvier (Fig. 38).

Compared with Nfasc186, the domain composition of Nfasc140 lacks the Mucin and FnIIIE domains (Fig. 21). But in my study I have shown that both Nfasc140 and Nfasc186 can target Nav to the node of Ranvier (Fig. 38 and 39). This indicates the Mucin and FnIIIE domains are not necessary for Na_v clustering. It is interesting that in nerves both Nfasc140 and Nfasc186 are expressed and have the same role of clustering Na_v. This suggests Nfasc140 is a second neuronal Neurofascin, in addition to Nfasc186, with a role in the formation of nodes of Ranvier. Because the Na_v clustering at the nodes is the foundation of the action potential propagation, it is possible animals evolved this two proteins having the same role to make the Na_v clustering mechanism more stable and reliable.

4.2.7 Expression of Nfasc140-flag or Nfasc186-flag partially restores nerve function

In the study of Sherman et al. (2005), it was shown that total Neurofascin knockout mice have a reduction of peripheral nerve conduction velocity to less than 20% of WT mice (Fig. 39 left). Meanwhile, my electrophysiological study showed that, in mice only expressing Nfasc140 or Nfasc186, peripheral nerve conduction velocity is reduced to almost half of the WT animals, which, in both cases, is higher than the total Neurofascin knockout (Fig. 39). Dr D. Sherman from our lab examined the

myelination profile of the peripheral nerves of these transgenic animals and no difference was found between them and WT mice. Which includes normal myelination in semithin cross sections of quadriceps nerves and no statistical difference between internodal distance. Also in previous studies of Neurofascin, there is no evidence that the Neurofascin will affect the nerve size. So there are two possible explanations for the decreased conduction velocity. First the Na_v is not targeted very well at some of the nodes in the transgenic mice. The Na_v might have decreased concentration at the nodes, this could slow down the depolarization and take more time for the active nodes to reach threshold potential. To clarify this, a statistical study of the intensity and size of Na_v can be conducted. Second, the loss of Nfasc155 in these animals means the lack of the paranodal complex. This will lead to the loss of the physical connection between glial cells and axons at the paranodes. Hence a higher threshold potential is needed to activate the following nodes of Ranvier. In both cases I think the threshold potential will be hard to reach. So the active node will need more time to get enough depolarization before the action potential travels to the next node of Ranvier.

4.2.8 Possible reasons for the behavioral abnormalities of mouse lines, T140/Nfasc$^{-/-}$ and T186/Nfasc$^{-/-}$

Both transgenic animal lines, T140/Nfasc$^{-/-}$ and T186/Nfasc$^{-/-}$, show signs of abnormalities such as tremor and weak hindlimbs, and the motor coordination test confirmed those animals are abnormal in a motor behaviour test. My study is mainly focused on the nervous system, and I know Neurofascin could have other functions in different organs. Hence, the real reason for the behavioral abnormality is unclear. But I suspect the change in the distribution of K_v and the slower nerve conduction velocity could contribute to the abnormality. If the K_v redistribution caused a prolonged time of repolarization, it could lead to a longer refractory period, and the nerves may miss or not transmit some of the signals through the axons. Meanwhile, slower nerve conduction velocity in CNS could lead to the malfunction of coordination center, the cerebellum. This will compromise the coordination, precision and accurate timing of movement. At the same time, in PNS, slow nerve

conduction of motor neurons will mean the signals from the CNS can not reach the muscles at the right time so the different groups of muscle can not contract at the pace they should; low nerve conduction of sensory neurons could affect the signals from all senses sending information back to CNS, which could also affect the coordination of movements.

Interestingly, Neurofascin knockout mice die at the age of P7, however, mice over-expressing Nfasc140 or Nfasc186 stay alive for more than 1 year, even though the animals have only have half of the nerve conduction velocity of WT nerves and show signs of abnormalities.

4.2.9 Potential role of Neurofascins in health and disease.

Nfasc140 could possibly promote neurite outgrowth because it has a similar domain composition as Nfasc166 which was shown to promote the neurite outgrowth (Kriebel et al., 2012). Also it doesn't have the Mucin and FNIIIE domains which are supposed to depress the neurite outgrowth in cell culture (Pruss et al., 2009). Meanwhile Nfasc186 has those domains. In my study, I have shown Nfasc140 and Nfasc186 could be expressed by the same neurons, which suggested they may be the candidate proteins which can regulate the development of neurons. Also the cell may express these two proteins at different level in order to control the growth or construction of the nervous system.

Antibodies specific to either Nfasc155 or Nfasc186 have been identified in patients with inflammatory neuropathy (Hughes et al., 2012). If the presence of neuronal Nfasc140 is taken into consideration, the patients which only have Nfasc186 specific antibodies might have a less severe abnormality, since I have found that Nfasc140 alone is sufficient to maintain the integrity of the nodes. Nevertheless, it is possible that once antibodies are generated against Nfasc186, further antibodies are also raised against Nfasc140. These would be expected to also recognize Nfasc155.

4.3 Intact paranodal axoglial junctions cluster Na_v channels in the absence of neuronal Neurofascins

4.3.1 Generation of early deletion of Neuronal Neurofascins animals

I generated a neuronal Cre-expressing line in which the Cre was expressed at an early age. After crossing with mice carrying *Nfasc* floxed alleles, *Thy-Cre/Nfasc*$^{fl/fl}$ mice were generated. In these mice, neuronal Neurofascins (Nfasc186 and Nfasc140) were specifically inactivated at an early development stage, and Nfasc155 continued to be expressed under the control of its normal promoter in myelin-forming glia. Western blots of WT and transgenic animals at E15 to P8 (Fig. 40) showed that the Nfasc186 band was reduced at E15 and became undetectable afterwards. At E15 the Nfasc140 is also reduced comparing with WT. Because the Nfasc140 is down regulated at later ages, the Nfasc140 band is not clear in control and appears undetectable in transgenic animals. Those observations indicated the Cre is active from before E15 and neuronal Neurofascins (Nfasc186 and Nfasc140) were deleted in CNS. Meanwhile, at P8 when Nfasc155 appeared in the WT lanes, the Nfasc155 is still present. But the Nfasc155 band of transgenic has less intensity, which suggested Nfasc155 was affected. Two possibilities could contribute to the reduction of Nfasc155. First, the transgenic animals were smaller in size than litter mates. This indicated a possible delay on development, which could lead to a low level of expression of Nfasc155 in nerves. Second, because the Thy-1.2 promoter was shown to be able to drive the expression of Cre in non-neuron tissues (Campsall et al., 2002), it was possible that Cre was activated in some glial cells and deleted Nfasc155.

Meanwhile, in the PNS, because the nerves express low levels of Nfasc186, it is impossible to check the expression of Nfasc186 by western blot. Longitudinal sections of Quadriceps nerve were used in an immunofluorescence study to evaluate the deletion of neuronal Neurofascins. The results showed at P3 almost no Neurofascins were targeted at the nodes (Fig. 42A), the Neurofascins staining appeared at P6 which is mainly Nfasc155. These observations suggested that the neuronal Neurofascins were abolished and a delayed expression of glial Neurofascin (result form 3.2.2 showed the Neurofascin signal at P6 are mainly glial Nfasc155).

Although there was reduced or delayed expression of glial Nfasc155, paranodes can still be detected (Fig. 41c), hence, the animals can still be used to explore the relationship between paranodal axoglial junctions and Na_v channels.

4.3.2 Clustering of Na_v does not require neuronal Neurofascins.

When sampling the nodes flanked by paranodes an immunofluorescence and statistical study at P6 showed less than 3% neuronal Neurofascin positive nodes but more than 80% Na_v positive nodes in both PNS and CNS. The high reduction of neuronal Neurofascins and a high presence of Na_v showed the clustering of Na_v without neuronal Neurofascins. This supports the view that Na_v channels can be clustered to the nodes of Ranvier by paranodal axoglial junctions only. This is consistent with the studies of Zonta et al. (2008) and Feinberg et al. (2010). However, in my study of the PNS only two animals were used. Although the difference is clear, data from another animal is needed to get convincing results.

Some nodes only had Nfasc155 at one side, which may reflect the delayed expression of Nfasc155. And I noticed in my study for some of those asymmetrical nodes, Na_v channels are also found targeted to the nodal area, next to Nfasc155 staining. This needs detailed research and statistical studies to confirm. If this is true, it means when only one side of the node has the paranodal axoglial junctions, Na_v could still cluster to the node. This would suggest that the paranodal axoglial junctions are not a barrier to prevent the diffusion of $Na_{v,}$ but actively help the targeting of Na_v at nodes.

4.3.3 Explanations behind the difference between my results and the others.

The *in vitro* study of Dzhashiashvili et al.(2007) is the first paper to propose the idea that Nfasc155 alone is not sufficient to organize the Na_v channels. In their experiment they used shRNA knockdown of Nfasc186 in DRG co-culture. But their culture system resembled the condition of when Nfasc186 is deleted after the node was already formed. Hence, this probably led to the wrong conclusion. And also *in*

vitro system has a very different cell environment, which also can lead to anomalous results as well.

A recent paper (Thaxton et al., 2011) came to very different conclusions concerning the ability of paranodes to cluster sodium channels in the absence of neuronal Neruofascin in either CNS or PNS. The differences between the findings of Thaxton (Thaxton et al, 2011) on one hand and Zonta et al (Zonta et al., 2008), Feinberg (Feinberg et al., 2010) and my results on the other hand, may lie in the type of neuronal Cre line used by Thaxton et al to eliminate neuronal Nfasc186. In the case of Thaxton et al, their model was a Cre/LoxP animal model like ours, but they used the neuron-specific promoter *Neurofilament light chain* (*Nefl-Cre*) (Leconte et al., 1994; Schweizer et al., 2002) to drive Cre expression. Although *Nefl-Cre* has been used as an embryonic neuronal specific Cre, in their paper *Nefl-Cre* only deleted 20% of Nfasc186 at P11 suggesting that Cre was expressed either very late or very inefficiently. Also, in the paper of Thaxton Cre-mediated loss of Nfasc186 in the CNS was rather variable (Fig. 47).

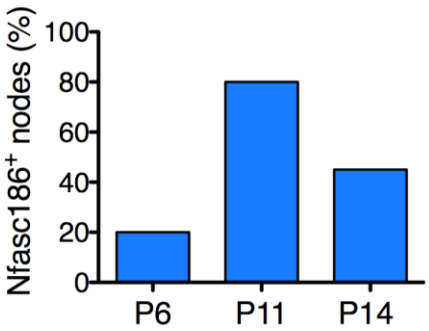

Figure 47. The loss of Nfasc186 is variable in different ages in the PNS.
Data from the paper of Thaxton et al. showed the *Nefl-Cre* eliminated Nfasc186 from almost 80% of the nodes but at P11 and P14 the Nfasc186 positive node rose to 80% and 20% (Thaxton et al., 2011).

So in their animal the later ablation or inefficient deletion of Nfasc186 means that before Nfasc186 ablation, the interaction of Nfasc186 with Na_v had already happened and the nodes of Ranvier were already formed with Nfasc186. So this animal model in fact included the scenario of studying sodium channel clustering after node formation, in other words, maintenance. Interestingly, from our unpublished data (Desmazieres, Zonta, Zhao et al.), deletion of Nfasc186 from a mature node is accompanied by the mislocalization of Na_v channels. Hence their animal model is more likely showing the deletion of Nfasc186 after Na_v targeting to the nodes, rather than the Na_v clustering without Nfasc186. This could explain why their observations were different from mine.

4.3.4 The phenotypes changing from F3 to F6

Unexpectedly, when we further back-crossed animals to the C57BL/6 background, the phenotype of the animals changed. The expression of Nfasc155 was no longer detectable by western blot or immunofluorescence. The Na_v channels were not detectable anymore and the animals died at P6. These mutant animals phenocopy Neurofascin knockout mice (Sherman et al., 2005, Zonta et al., 2008). However, the mRNA level of Nfasc155 was not changed in the PNS nerves of the mutant. This indicates that the loss of Nfasc155 protein localized at the paranode is not a result of ectopic expression of Cre in glial cells. Since we observed a delay in Nfasc155

expression in F3 generation animals, this delay could become more pronounced on a C57BL/6 background and leads to a more extreme phenotype with fatal effects on the mice.

4.4 Concluding remarks

This work adds substantial new evidence on the role of CAMs in the formation and stability of nodes of Ranvier.

The third isoform of Neurofascins, Nfasc140, was been studied and its characters were revealed. The domain composition of Nfasc140 has been identified. The pattern of expression of Nfasc140 is shown. Different from other Neurofascins, Nfasc140 is the predominate isoform in early embryonic stage, which suggested the importance of Nfasc140 during the nervous system development.

Nfasc140 is the only isoform of Neurofascins which has different post-translational modifications at different ages and in different tissues. It is differentially glycosylated in different part of the brain. These indicate it could have different roles at different development stage of animals and also in different part of the brain at the same age.

Expressing only Nfasc140-flag in animals showed Nfasc140 can cluster the Na_v and organise the other nodal components at the nodes of Ranvier. This subsequently forms functional nodes of Ranvier and permits rapid propagation of action potentials in myelinated axons. Comparing transgenic animals which express Nfasc140-flag or Nfasc186-flag only, suggested that Nfasc140 without the Mucin and FnIIIE has the same function as Nfasc186 in organising the node of Ranvier. Here, two similar proteins are involved in the same mechanism in nodal formation, which might indicate the importance of Neurofascins in the formation and maintenance of nodes of Ranvier.

Besides the study of Nfasc140, an early neuronal Neurofascins deletion animal modal has also been established in this study. Using this animal model, I revealed

that clustering of Na_v does not require neuronal Neurofascins; in another words Na_v channels can be clustered to the nodes of Ranvier by paranodal axoglial junctions only. This should clarify the controversial theories about whether paranodal axoglial junctions have a role in sodium clustering.

Because more and more research starts to focus on the Neurofascins and other nodal protein during neurological diseases, I think my study can lay down our basic understanding of the formation and maintenance of nodes of Ranvier. This can help us and other researchers to analysis the changes of proteins which are associated with Neurofascins during diseases and explore new treatment for neurological diseases.

5. Future directions

5.1 Characterization of Nfasc140

It has been shown that the expression of Nfasc155 alone can promote oligodendrocyte process migration in the CNS during myelination; moreover, Neurofascin knockout mice or mice with only Nfasc186 show a delay in oligodendrocyte process migration (Zonta et al., 2008). Since the expression level of Nfasc140 during the early postnatal period is correlated with the expression of MBP, it would be interesting to investigate whether Nfasc140 can affect oligodendrocyte process migration *in vivo*.

In transgenic animals expressing either Nfasc140 or Nfasc186, the expression level of Nfasc140 and Nfasc186 is very high as judged by Western blot comparing with WT animals at the same age (Fig. 35). However, the intensity of immunostaining of Neurofascins at the AIS is relatively weak in transgenic animals. This suggested that there might be a possible interaction between Nfasc140 and Nfasc186 which stabilizes at the AIS. If Nfasc140-flag (FLAG-tagged) and Nfasc186-HA (HA tagged) were expressed in the same mouse it would be possible to check whether the flag staining at the AIS is stronger than in mice only expressing Nfasc140-flag. The two proteins could also be investigated for co-immunoprecipitation.

Although there are major differences between avians and mammals, because Nfasc166 has been shown to increase the neurite outgrowth in chick, Nfasc140 might have a similar function. This could be investigated using cultured mouse neurons to check whether Nfasc140 can promote neurite outgrowth.

5.2 Intact paranodal axoglial junctions cluster Na_v channels in the absence of neuronal Neurofascins

I generated two different founders for the *Tcre* line. Only one founder has been analysed at the F3 generation, and now backcrossed with C57BL/6 mice to the F6

generation. It is still unclear whether all the changes of the phenotype of the F6 animals are caused by the change of background of animals. Hence, if we compare the same founder and found the same phenotype changes, then we can confirm the animal background affects the phenotype of mutants. So it will be interesting to determine whether paranodal axoglial junctions are also missing when Nfasc186 is deleted using the second founder. In parallel, it will be of interest to put those animals back on to CBA background again (the original transgenic founders were CBA x C57BL/6 F1 hybrids), in order to determine if the phenotype I observed at F3 is restored.

In my study, I found that when neuronal Neurofascins were deleted from the nodes the expression of Nfasc155 is also affected (Fig. 37 and 38). And I proposed the idea that the Nfasc155 has a delayed expression time when neuronal Neurofascins are not present. To further study whether the loss of neuronal Neurofascins can delay the expression or targeting of Nfasc155, it would be interesting to check by immunofluorescence whether the paranodes at a later time point will appear. However, *Tcre/Nfasc*$^{fl/fl}$ animals die at P6. Hence, DRG and Schwann cell co-cultures of *Tcre/Nfasc*$^{fl/fl}$ animals could be set up to study later stages of myelination *in vitro*. After myelination the co-cultures would be maintained for as long as possible to determine when Nfasc155 is expressed at later stages of myelination. Also, since I found that after overexpression of Nfasc186 or Nfasc140 the mice survive very well, even in the absence of intact paranodes. Therefore, it would be interesting to check by immunostaining and western blot whether transgenic Nfasc186 or Nfasc140 in *Tcre/Nfasc*$^{fl/fl}$ mice at F6 generation regain the expression of the endogenous Nfasc155.

Although sodiumchannels have a vital role in permitting saltatory conduction at the nodes of Ranvier, the precise mechanisms of how they are targeted to the nodes of Ranvier still require further study. If what I proposed in my study is true, that paranodal axoglial junctions can cluster Na_v. It would be interesting to identify the downstream molecules which link the Na_v and proteins which form paranodal complex to eventually reveal the mechanism of how Na_v is clustered.

REFERENCES

Alan Peters, Sanford L. Palay, Henry deF. Webster(1991) *The Fine Structure of the Nervous System: the Neuron and the Supporting Cells*. (Oxford Univ. Press, Oxford, UK).

Altevogt, B. M., Kleopa, K. A., Postma, F. R., Scherer, S. S., & Paul, D. L (2002). Connexin29 is uniquely distributed within myelinating glial cells of the central and peripheral nervous systems *The Journal of neuroscience : the official journal of the Society for Neuroscience*, *22*(15), 6458-70.

Arbuthnott, E. R., Boyd, I. A., & Kalu, K. U (1980). Ultrastructural dimensions of myelinated peripheral nerve fibres in the cat and their relation to conduction velocity *The Journal of Physiology*, *308*, 125-57.

Bartsch, U., Pesheva, P., Raff, M., & Schachner, M (1993). Expression of janusin (J1-160/180) in the retina and optic nerve of the developing and adult mouse *Glia*, *9*(1), 57-69.

Barnett MW, Larkman PM (June 2*007). "The action potential". Pract Neurol 7 (3): 192–7. PMID 17515599.*

Bekku, Y., Rauch, U., Ninomiya, Y., & Oohashi, T (2009). Brevican distinctively assembles extracellular components at the large diameter nodes of Ranvier in the CNS *J. Neurochem.*, *108*(5), 1266-76.

Bennett, V., & Baines, A. J (2001). Spectrin and ankyrin-based pathways: metazoan inventions for integrating cells into tissues *Physiological reviews*, *81*(3), 1353-92.

Bennett, V., & Lambert, S (1999). Physiological roles of axonal ankyrins in survival of premyelinated axons and localization of voltage-gated sodium channels *Journal of neurocytology*, *28*(4-5), 303-18.

Berglund, E. O., & Ranscht, B (1994). Molecular cloning and in situ localization of the human contactin gene (CNTN1) on chromosome 12q11-q12 *Genomics*, *21*(3), 571-82.

Bhat, M A, Rios, J. C., Lu, Y., Garcia-Fresco, G. P., Ching, W., Martin, M. S., Li, J., et al (2001). Axon-glia interactions and the domain organization of myelinated axons requires neurexin IV/Caspr/Paranodin *Neuron*, *30*(2), 369-83.

Boyle, M E, Berglund, E. O., Murai, K. K., Weber, L., Peles, E., & Ranscht, B (2001a). Contactin orchestrates assembly of the septate-like junctions at the paranode in myelinated peripheral nerve *Neuron*, *30*(2), 385-97.

Boyle, M. E., Berglund, E. O., Murai, K. K., Weber, L., Peles, E., & Ranscht, B (2001b). Contactin orchestrates assembly of the septate-like junctions at the paranode in myelinated peripheral nerve *Neuron*, *30*, 385-97.

Brümmendorf, T., Wolff, J. M., Frank, R., & Rathjen, F. G (1989). Neural cell recognition molecule F11: homology with fibronectin type III and immunoglobulin type C domains *Neuron*, *2*(4), 1351-61.

Buck, T. M., Eledge, J., & Skach, W. R (2004). Evidence for stabilization of aquaporin-2 folding mutants by N-linked glycosylation in endoplasmic reticulum *American journal of physiology. Cell physiology*, *287*(5), C1292-9.

Burkarth, N., Kriebel, M., Kranz, E. U., & Volkmer, H (2007). Neurofascin regulates the formation of gephyrin clusters and their subsequent translocation to the axon hillock of hippocampal neurons *Mol. Cell. Neurosci.*, *36*(1), 59-70.

Butt, A. M., Colquhoun, K., Tutton, M., & Berry, M (1994). Three-dimensional morphology of astrocytes and oligodendrocytes in the intact mouse optic nerve *Journal of neurocytology*, *23*(8), 469-85.

Campsall, K. D., Mazerolle, C. J., de Repentingy, Y., Kothary, R., & Wallace, V. A (2002). Characterization of transgene expression and Cre recombinase activity in a panel of Thy-1 promoter-Cre transgenic mice *Developmental dynamics : an official publication of the American Association of Anatomists*, *224*(2), 135-43.

Chang, S., Rathjen, F. G., & Raper, J. A (1987). Extension of neurites on axons is impaired by antibodies against specific neural cell surface glycoproteins *J. Cell Biol.*, *104*(2), 355-62.

Charles, P., Tait, S., Faivre-Sarrailh, C., Barbin, G., Gunn-Moore, F., Denisenko-Nehrbass, N., Guennoc, A., et al (2002). Neurofascin is a glial receptor for the paranodin/Caspr-contactin axonal complex at the axoglial junction *Current biology : CB*, *12*(3), 217-20.

Clark, B. D., Goldberg, E. M., & Rudy, B (2009). Electrogenic tuning of the axon initial segment *The Neuroscientist : a review journal bringing neurobiology, neurology and psychiatry*, *15*(6), 651-68.

Colbert, C. M., & Pan, E (2002). Ion channel properties underlying axonal action potential initiation in pyramidal neurons *Nature Neuroscience*, *5*(6), 533-8.

Custer, A. W., Kazarinova-Noyes, K., Sakurai, T., Xu, X., Simon, W., Grumet, M., & Shrager, P (2003). The role of the ankyrin-binding protein NrCAM in node of Ranvier formation *J. Neurosci.*, *23*(31), 10032-9.

Davis, J. Q., & Bennett, V (1994). Ankyrin binding activity shared by the neurofascin/L1/NrCAM family of nervous system cell adhesion molecules *The Journal of biological chemistry*, *269*(44), 27163-6.

Davis, J. Q., Lambert, S., & Bennett, V (1996). Molecular composition of the node of Ranvier: identification of ankyrin-binding cell adhesion molecules neurofascin (mucin+/third FNIII domain-) and NrCAM at nodal axon segments *The Journal of cell biology*, *135*(5), 1355-67.

Davis, J. Q., McLaughlin, T., & Bennett, V (1993). Ankyrin-binding proteins related to nervous system cell adhesion molecules: candidates to provide transmembrane and intercellular connections in adult brain *J. Cell Biol.*, *121*(1), 121-33.

De Col, R., Messlinger, K., & Carr, R. W (2008). Conduction velocity is regulated by sodium channel inactivation in unmyelinated axons innervating the rat cranial meninges *The Journal of Physiology*, *586*(4), 1089-103.

Denisenko-Nehrbass, N., Oguievetskaia, K., Goutebroze, L., Galvez, T., Yamakawa, H., Ohara, O., Carnaud, M., et al (2003). Protein 4.1B associates with both Caspr/paranodin and Caspr2 at paranodes and juxtaparanodes of myelinated fibres Eur. *J. Neurosci.*, 17(2), 411-6.

Desmazières A., Sol-Foulon N. and Lubetzki C. (2012). Changes at the nodal and perinodal axonal domains: a basis for multiple sclerosis pathology? *Mult Scler* 18(2):133-7

Durbec, P., Gennarini, G., Goridis, C., & Rougon, G (1992). A soluble form of the F3 neuronal cell adhesion molecule promotes neurite outgrowth *J. Cell Biol.*, *117*(4), 877-87.

Dzhashiashvili, Y., Zhang, Y., Galinska, J., Lam, I., Grumet, M., & Salzer, J. L (2007). Nodes of Ranvier and axon initial segments are ankyrin G-dependent domains that assemble by distinct mechanisms. *The Journal of cell biology*, *177*, 857-870.

Einheber, S., Zanazzi, G., Ching, W., Scherer, S., Milner, T. A., Peles, E., & Salzer, J. L (1997). The axonal membrane protein Caspr, a homologue of neurexin IV, is a component of the septate-like paranodal junctions that assemble during myelination *J. Cell Biol.*, *139*(6), 1495-506.

Eshed, Y., Feinberg, K., Carey, D. J., & Peles, E (2007). Secreted gliomedin is a perinodal matrix component of peripheral nerves *J. Cell Biol.*, *177*(3), 551-62.

Eshed, Y., Feinberg, K., Poliak, S., Sabanay, H., Sarig-Nadir, O., Spiegel, I., Bermingham, J. R., et al (2005). Gliomedin mediates Schwann cell-axon interaction and the molecular assembly of the nodes of Ranvier *Neuron*, *47*, 215-29.

Feil, R., Wagner, J., Metzger, D., & Chambon, P (1997). Regulation of Cre recombinase activity by mutated estrogen receptor ligand-binding domains *Biochem. Biophys. Res. Commun.*, *237*(3), 752-7.

Feinberg, K., Eshed-Eisenbach, Y., Frechter, S., Amor, V., Salomon, D., Sabanay, H., Dupree, J. L., et al (2010). A Glial Signal Consisting of Gliomedin and NrCAM Clusters Axonal Na+ Channels during the Formation of Nodes of Ranvier. *Neuron*, *65*(4), 490-502.

Fernando, M. S., Simpson, J. E., Matthews, F., Brayne, C., Lewis, C. E., Barber, R., Kalaria, R. N., et al (2006). White matter lesions in an unselected cohort of the elderly: molecular pathology suggests origin from chronic hypoperfusion injury *Stroke; a journal of cerebral circulation*, *37*(6), 1391-8.

Fleidervish, I. A., Lasser-Ross, N., Gutnick, M. J., & Ross, W. N (2010). Na+ imaging reveals little difference in action potential-evoked Na+ influx between axon and soma *Nature Neuroscience*, *13*(7), 852-60.

Foran, D. R., & Peterson, A. C (1992). Myelin acquisition in the central nervous system of the mouse revealed by an MBP-Lac Z transgene *J. Neurosci.*, *12*(12), 4890-7.

Gao, Y., & Mehta, K (2007). N-linked glycosylation of CD38 is required for its structure stabilization but not for membrane localization *Molecular and cellular biochemistry*, *295*(1-2), 1-7.

Garver, T. D., Ren, Q., Tuvia, S., & Bennett, V (1997). Tyrosine phosphorylation at a site highly conserved in the L1 family of cell adhesion molecules abolishes

ankyrin binding and increases lateral mobility of neurofascin *The Journal of cell biology*, *137*(3), 703-14.

Gennarini, G., Cibelli, G., Rougon, G., Mattei, M. G., & Goridis, C (1989). The mouse neuronal cell surface protein F3: a phosphatidylinositol-anchored member of the immunoglobulin superfamily related to chicken contactin *J. Cell Biol.*, *109*(2), 775-88.

Gennarini, G., Durbec, P., Boned, A., Rougon, G., & Goridis, C (1991). Transfected F3/F11 neuronal cell surface protein mediates intercellular adhesion and promotes neurite outgrowth *Neuron*, *6*(4), 595-606.

Grubb, M. S., & Burrone, J (2010). Activity-dependent relocation of the axon initial segment fine-tunes neuronal excitability *Nature*, *465*(7301), 1070-4.

Hedstrom, K. L., Xu, X., Ogawa, Y., Frischknecht, R., Seidenbecher, C. I., Shrager, P., & Rasband, M. N (2007a). Neurofascin assembles a specialized extracellular matrix at the axon initial segment. *The Journal of cell biology*, *178*, 875-886.

Hedstrom, Kristian L, Ogawa, Y., & Rasband, M. N (2008). AnkyrinG is required for maintenance of the axon initial segment and neuronal polarity *The Journal of cell biology*, *183*(4), 635-40.

Hedstrom, Kristian L, Xu, X., Ogawa, Y., Frischknecht, R., Seidenbecher, C. I., Shrager, P., & Rasband, M. N (2007b). Neurofascin assembles a specialized extracellular matrix at the axon initial segment *The Journal of cell biology*, *178*(5), 875-86.

Hodgkin AL, Huxley AF. *Action potentials recorded from inside a nerve fibre. Nature1939;144:710–11*.

Hockfield, S., Kalb, R. G., Zaremba, S., & Fryer, H (1990). Expression of neural proteoglycans correlates with the acquisition of mature neuronal properties in the mammalian brain *Cold Spring Harbor symposia on quantitative biology*, *55*, 505-14.

Hille B. 2001. *Ion channels of excitable membranes*.: Sinauer Associates. xviii, 814.

Howell, O. W., Palser, A., Polito, A., Melrose, S., Zonta, B., Scheiermann, C., Vora, A. J., et al (2006). Disruption of neurofascin localization reveals early changes preceding demyelination and remyelination in multiple sclerosis *Brain*, *129*(Pt 12), 3173-85.

Hu, W., Tian, C., Li, T., Yang, M., Hou, H., & Shu, Y (2009). Distinct contributions of Na(v)1.6 and Na(v)1.2 in action potential initiation and backpropagation *Nature Neuroscience*, *12*(8), 996-1002.

Hughes, R. A., & Willison, H. J (2012). Neurofascin antibodies in inflammatory neuropathy: how many needles make a haystack *Neurology*, *79*(23), 2224-5.

Huxley A.F., Stämpfli R. Evidence for saltatory conduction in peripheral myelinated nerve fibres. J. Physiol. 1949;108:315–339.

Imai, T., Jiang, M., Chambon, P., & Metzger, D (2001). Impaired adipogenesis and lipolysis in the mouse upon selective ablation of the retinoid X receptor alpha mediated by a tamoxifen-inducible chimeric Cre recombinase (Cre-ERT2) in adipocytes *Proc. Natl. Acad. Sci. U.S.A.*, *98*(1), 224-8.

Jenkins, S. M., & Bennett, V (2001). Ankyrin-G coordinates assembly of the spectrin-based membrane skeleton, voltage-gated sodium channels, and L1 CAMs at Purkinje neuron initial segments *J. Cell Biol.*, *155*(5), 739-46.

Kirschbaum, K., Kriebel, M., Kranz, E. U., Pötz, O., & Volkmer, H (2009). Analysis of non-canonical fibroblast growth factor receptor 1 (FGFR1) interaction reveals regulatory and activating domains of neurofascin *The Journal of biological chemistry*, *284*(42), 28533-42.

Kobayashi, K., Nakahori, Y., Miyake, M., Matsumura, K., Kondo-Iida, E., Nomura, Y., Segawa, M., et al (1998). An ancient retrotransposal insertion causes Fukuyama-type congenital muscular dystrophy *Nature*, *394*(6691), 388-92.

Kole, M. H., Ilschner, S. U., Kampa, B. M., Williams, S. R., Ruben, P. C., & Stuart, G. J (2008). Action potential generation requires a high sodium channel density in the axon initial segment *Nature Neuroscience*, *11*(2), 178-86.

Komada, M., & Soriano, P (2002). [Beta]IV-spectrin regulates sodium channel clustering through ankyrin-G at axon initial segments and nodes of Ranvier *J. Cell Biol.*, *156*(2), 337-48.

Kordeli, E., Lambert, S., & Bennett, V (1995). AnkyrinG. A new ankyrin gene with neural-specific isoforms localized at the axonal initial segment and node of Ranvier *J. Biol. Chem.*, *270*(5), 2352-9.

Koticha, D., Babiarz, J., Kane-Goldsmith, N., Jacob, J., Raju, K., & Grumet, M (2005a). Cell adhesion and neurite outgrowth are promoted by neurofascin NF155 and inhibited by NF186 *Molecular and cellular neurosciences*, *30*, 137-48.

Koticha, Darshan, Babiarz, J., Kane-Goldsmith, N., Jacob, J., Raju, K., & Grumet, M (2005b). Cell adhesion and neurite outgrowth are promoted by neurofascin NF155 and inhibited by NF186 *Mol. Cell. Neurosci.*, *30*(1), 137-48.

Koticha, Darshan, Maurel, P., Zanazzi, G., Kane-Goldsmith, N., Basak, S., Babiarz, J., Salzer, J., et al (2006). Neurofascin interactions play a critical role in clustering sodium channels, ankyrin G and beta IV spectrin at peripheral nodes of Ranvier *Developmental biology*, *293*(1), 1-12.

Kriebel, M., Wuchter, J., Trinks, S., & Volkmer, H (2012). Neurofascin: a switch between neuronal plasticity and stability *The international journal of biochemistry & cell biology*, *44*, 694-7.

Kriebel, Martin, Metzger, J., Trinks, S., Chugh, D., Harvey, R. J., Harvey, K., & Volkmer, H (2011). The cell adhesion molecule neurofascin stabilizes axo-axonic GABAergic terminals at the axon initial segment *J. Biol. Chem.*, *286*(27), 24385-93.

Kuba, H., Oichi, Y., & Ohmori, H (2010). Presynaptic activity regulates Na(+) channel distribution at the axon initial segment *Nature*, *465*(7301), 1075-8.

Kuhn, T. B., Stoeckli, E. T., Condrau, M. A., Rathjen, F. G., & Sonderegger, P (1991). Neurite outgrowth on immobilized axonin-1 is mediated by a heterophilic interaction with L1(G4) *The Journal of cell biology*, *115*(4), 1113-26.

Labasque, M., Devaux, J. J., Lévêque, C., & Faivre-Sarrailh, C (2011). Fibronectin type III-like domains of neurofascin-186 protein mediate gliomedin binding and its clustering at the developing nodes of Ranvier *The Journal of biological chemistry*, *286*, 42426-34.

Lambert, S, Davis, J. Q., & Bennett, V (1997). Morphogenesis of the node of Ranvier: co-clusters of ankyrin and ankyrin-binding integral proteins define early developmental intermediates *J. Neurosci.*, *17*(18), 7025-36.

Leconte, L., Semonin, O., Zvara, A., Boisseau, S., Poujeol, C., Julien, J. P., & Simonneau, M (1994). Both upstream and intragenic sequences of the human

neurofilament light gene direct expression of lacZ in neurons of transgenic mouse embryos *Journal of molecular neuroscience : MN*, *5*(4), 273-95.

Lemaillet, G., Walker, B., & Lambert, S (2003). Identification of a conserved ankyrin-binding motif in the family of sodium channel alpha subunits *The Journal of biological chemistry*, *278*(30), 27333-9.

Li, J., Chen, C., & Liu-Chen, L (2007). N-Glycosylation of the human kappa opioid receptor enhances its stability but slows its trafficking along the biosynthesis pathway *Biochemistry*, *46*(38), 10960-70.

Lonigro, A., & Devaux, J. J (2009). Disruption of neurofascin and gliomedin at nodes of Ranvier precedes demyelination in experimental allergic neuritis *Brain*, *132*(Pt 1), 260-73.

Lustig, M., Zanazzi, G., Sakurai, T., Blanco, C., Levinson, S. R., Lambert, S., Grumet, M., et al (2001). Nr-CAM and neurofascin interactions regulate ankyrin G and sodium channel clustering at the node of Ranvier *Current biology : CB*, *11*(23), 1864-9.

Lüthi, A., Mohajeri, H., Schachner, M., & Laurent, J. P (1996). Reduction of hippocampal long-term potentiation in transgenic mice ectopically expressing the neural cell adhesion molecule L1 in astrocytes *J. Neurosci. Res.*, *46*(1), 1-6.

Maertens, B., Hopkins, D., Franzke, C., Keene, D. R., Bruckner-Tuderman, L., Greenspan, D. S., & Koch, M (2007). Cleavage and oligomerization of gliomedin, a transmembrane collagen required for node of ranvier formation *J. Biol. Chem.*, *282*(14), 10647-59.

Mathey, E. K., Derfuss, T., Storch, M. K., Williams, K. R., Hales, K., Woolley, D. R., Al-Hayani, A., et al (2007a). Neurofascin as a novel target for autoantibody-mediated axonal injury *The Journal of experimental medicine*, *204*, 2363-72. doi:10.1084/jem.20071053

Mathey, Emily K, Derfuss, T., Storch, M. K., Williams, K. R., Hales, K., Woolley, D. R., Al-Hayani, A., et al (2007b). Neurofascin as a novel target for autoantibody-mediated axonal injury *The Journal of experimental medicine*, *204*(10), 2363-72.

Melendez-Vasquez, C. V., Rios, J. C., Zanazzi, G., Lambert, S., Bretscher, A., & Salzer, J. L (2001). Nodes of Ranvier form in association with ezrin-radixin-

moesin (ERM)-positive Schwann cell processes *Proc. Natl. Acad. Sci. U.S.A.*, *98*(3), 1235-40.

Menegoz, M., Gaspar, P., Le Bert, M., Galvez, T., Burgaya, F., Palfrey, C., Ezan, P., et al (1997). Paranodin, a glycoprotein of neuronal paranodal membranes *Neuron*, *19*(2), 319-31.

Michaely, P., & Bennett, V (1995). Mechanism for binding site diversity on ankyrin. Comparison of binding sites on ankyrin for neurofascin and the Cl-/HCO3- anion exchanger *J. Biol. Chem.*, *270*(52), 31298-302.

Milev, P., Meyer-Puttlitz, B., Margolis, R. K., & Margolis, R. U (1995). Complex-type asparagine-linked oligosaccharides on phosphacan and protein-tyrosine phosphatase-zeta/beta mediate their binding to neural cell adhesion molecules and tenascin *J. Biol. Chem.*, *270*(42), 24650-3.

Morell P, Quarles RH. The Myelin Sheath. In: Siegel GJ, Agranoff BW, Albers RW, et al., (1999) *Basic Neurochemistry: Molecular, Cellular and Medical Aspects. 6th edition.* Philadelphia: Lippincott-Raven

Neher EJ, *Sakmann B.* Single channels currents recorded from the membrane of denervated frog muscle fibres. *Nature1976;260:779–802.*

Ng, J. K., Malotka, J., Kawakami, N., Derfuss, T., Khademi, M., Olsson, T., Linington, C., et al (2012). Neurofascin as a target for autoantibodies in peripheral neuropathies *Neurology*, *79*(23), 2241-8.

Oohashi, T., Hirakawa, S., Bekku, Y., Rauch, U., Zimmermann, D. R., Su, W., Ohtsuka, A., et al (2002). Bral1, a brain-specific link protein, colocalizing with the versican V2 isoform at the nodes of Ranvier in developing and adult mouse central nervous systems *Molecular and cellular neurosciences*, *19*(1), 43-57.

Ornitz D. M. and Itoh N. (2001). Fibroblast growth factors *Genome Biol*. 2, REVIEWS3005

Pacharra, S., Hanisch, F., & Breloy, I (2012). Neurofascin 186 is O-mannosylated within and outside of the mucin domain *Journal of proteome research*, *11*(8), 3955-64.

Peles, E, Nativ, M., Campbell, P. L., Sakurai, T., Martinez, R., Lev, S., Clary, D. O., et al (1995). The carbonic anhydrase domain of receptor tyrosine phosphatase beta is a functional ligand for the axonal cell recognition molecule contactin *Cell*, *82*(2), 251-60.

Peles, E, Nativ, M., Lustig, M., Grumet, M., Schilling, J., Martinez, R., Plowman, G. D., et al (1997). Identification of a novel contactin-associated transmembrane receptor with multiple domains implicated in protein-protein interactions *EMBO J.*, *16*(5), 978-88.

Pesheva, P., Gennarini, G., Goridis, C., & Schachner, M (1993). The F3/11 cell adhesion molecule mediates the repulsion of neurons by the extracellular matrix glycoprotein J1-160/180 *Neuron*, *10*(1), 69-82.

Peters A, Palay SL, Def WH. (1991) *The Cellular Sheaths of Neurons in the Fine Structure of the Nervous System: The Neurons and Supporting Cells*. W. B. Saunders; Philadelphia.

Pillai, Anilkumar M, Thaxton, C., Pribisko, A. L., Cheng, J., Dupree, J. L., & Bhat, M. A (2009). Spatiotemporal ablation of myelinating glia-specific neurofascin (Nfasc NF155) in mice reveals gradual loss of paranodal axoglial junctions and concomitant disorganization of axonal domains *J. Neurosci. Res.*, *87*(8), 1773-93.

Poliak, S., & Peles, E (2003). The local differentiation of myelinated axons at nodes of Ranvier *Nature reviews. Neuroscience*, *4*(12), 968-80.

Pomicter, A. D., Shroff, S. M., Fuss, B., Sato-Bigbee, C., Brophy, P. J., Rasband, M. N., Bhat, M. A., et al (2010). Novel forms of neurofascin 155 in the central nervous system: alterations in paranodal disruption models and multiple sclerosis *Brain : a journal of neurology*, *133*, 389-405.

Pruss, T., Kranz, E. U., Niere, M., & Volkmer, H (2006). A regulated switch of chick neurofascin isoforms modulates ligand recognition and neurite extension *Mol. Cell. Neurosci.*, *31*(2), 354-65.

Prüss, H., Schwab, J. M., Derst, C., Görtzen, A., & Veh, R. W (2011). Neurofascin as target of autoantibodies in Guillain-Barre syndrome *Brain : a journal of neurology*, *134*, e173; author reply e174.

Raine, C. S (1984). Morphology of myelin and myelination. In P. Morell (ed.), *Myelin*, 2nd ed. New York: Plenum, pp. 1–41.

Ranscht, B (1988). Sequence of contactin, a 130-kD glycoprotein concentrated in areas of interneuronal contact, defines a new member of the immunoglobulin supergene family in the nervous system *J. Cell Biol.*, *107*(4), 1561-73.

Rasband, M N, Peles, E., Trimmer, J. S., Levinson, S. R., Lux, S. E., & Shrager, P (1999). Dependence of nodal sodium channel clustering on paranodal axoglial contact in the developing CNS *J. Neurosci.*, *19*(17), 7516-28.

Rasband, M N, Trimmer, J. S., Schwarz, T. L., Levinson, S. R., Ellisman, M. H., Schachner, M., & Shrager, P (1998). Potassium channel distribution, clustering, and function in remyelinating rat axons *The Journal of neuroscience : the official journal of the Society for Neuroscience*, *18*(1), 36-47.

Rasband, Matthew N. (2010). The axon initial segment and the maintenance of neuronal polarity *Nature reviews. Neuroscience*, *11*(8), 552-62.

Rasband, Matthew N, Park, E. W., Zhen, D., Arbuckle, M. I., Poliak, S., Peles, E., Grant, S. G., et al (2002). Clustering of neuronal potassium channels is independent of their interaction with PSD-95 *J. Cell Biol.*, *159*(4), 663-72.

Rathjen, F. G., Wolff, J. M., Chang, S., Bonhoeffer, F., & Raper, J. A (1987). Neurofascin: a novel chick cell-surface glycoprotein involved in neurite-neurite interactions *Cell*, *51*(5), 841-9.

Reimer, M. M., McQueen, J., Searcy, L., Scullion, G., Zonta, B., Desmazieres, A., Holland, P. R., et al (2011). Rapid disruption of axon-glial integrity in response to mild cerebral hypoperfusion *J. Neurosci.*, *31*(49), 18185-94.

Rhodes, K. J., Strassle, B. W., Monaghan, M. M., Bekele-Arcuri, Z., Matos, M. F., & Trimmer, J. S (1997). Association and colocalization of the $K_v$beta1 and $K_v$beta2 beta-subunits with K_v1 alpha-subunits in mammalian brain K+ channel complexes *The Journal of neuroscience : the official journal of the Society for Neuroscience*, *17*(21), 8246-58.

Robert F. Hevner (2008). Reelin and the Cerebellum *Reelin Glycoprotein*. 141-158

Robertson WF 1900. A microscopic demonstration of the normal and pathological histology of mesoglia.cells. *J. Ment. Sci.* 46: 733-752.

Roots, B.I. 2009. The phylogeny of invertebrates and the evolution of myelin. *Neuron Glia Biol.* **4**(2): 101-109.

Rios, J C, Melendez-Vasquez, C. V., Einheber, S., Lustig, M., Grumet, M., Hemperly, J., Peles, E., et al (2000). Contactin-associated protein (Caspr) and contactin form a complex that is targeted to the paranodal junctions during myelination *J. Neurosci.*, *20*(22), 8354-64.

Rios, Jose C, Rubin, M., Martin, M. S., Downey, R. T., Einheber, S., Rosenbluth, J., Levinson, S. R., et al (2003). Paranodal interactions regulate expression of sodium channel subtypes and provide a diffusion barrier for the node of Ranvier *J. Neurosci.*, *23*(18), 7001-11.

Saito, F, Masaki, T., Kamakura, K., Anderson, L. V., Fujita, S., Fukuta-Ohi, H., Sunada, Y., et al (1999). Characterization of the transmembrane molecular architecture of the dystroglycan complex in schwann cells *The Journal of biological chemistry*, *274*(12), 8240-6.

Saito, Fumiaki, Moore, S. A., Barresi, R., Henry, M. D., Messing, A., Ross-Barta, S. E., Cohn, R. D., et al (2003). Unique role of dystroglycan in peripheral nerve myelination, nodal structure, and sodium channel stabilization *Neuron*, *38*(5), 747-58.

Salzer, J L. (1997). Clustering sodium channels at the node of Ranvier: close encounters of the axon-glia kind *Neuron*, *18*(6), 843-6.

Salzer, James L, Brophy, P. J., & Peles, E (2008). Molecular domains of myelinated axons in the peripheral nervous system *Glia*, *56*(14), 1532-40.

Schafer, D. P., Bansal, R., Hedstrom, K. L., Pfeiffer, S. E., & Rasband, M. N (2004). Does paranode formation and maintenance require partitioning of neurofascin 155 into lipid rafts *The Journal of neuroscience : the official journal of the Society for Neuroscience*, *24*(13), 3176-85.

Scherer, S. S., Xu, T., Crino, P., Arroyo, E. J., & Gutmann, D. H (2001). Ezrin, radixin, and moesin are components of Schwann cell microvilli *J. Neurosci. Res.*, *65*(2), 150-64.

Schweizer, U., Gunnersen, J., Karch, C., Wiese, S., Holtmann, B., Takeda, K., et al (2002). Conditional gene ablation of Stat3 reveals differential signaling requirements for survival of motoneurons during development and after nerve injury in the adult *The Journal of cell biology*, *156*(2), 287-97.

Shenoy, A. M., Markowitz, J. A., Bonnemann, C. G., Krishnamoorthy, K., Bossler, A. D., & Tseng, B. S (2010). Muscle-Eye-Brain disease *Journal of clinical neuromuscular disease*, *11*(3), 124-6.

Sherman, D. L., Tait, S., Melrose, S., Johnson, R., Zonta, B., Court, F. A., Macklin, W. B., et al (2005). Neurofascins are required to establish axonal domains for saltatory conduction *Neuron*, *48*(5), 737-42.

Shibata, M., Ohtani, R., Ihara, M., & Tomimoto, H (2004). White matter lesions and glial activation in a novel mouse model of chronic cerebral hypoperfusion *Stroke; a journal of cerebral circulation*, *35*(11), 2598-603.

Simons M, Trotter J (October 2007). "Wrapping it up: the cell biology of myelination". *Curr. Opin. Neurobiol.* 17 (5): 533–40.

Sistani, L., Rodriguez, P. Q., Hultenby, K., Uhlen, M., Betsholtz, C., Jalanko, H., Tryggvason, K., et al (2013). Neuronal proteins are novel components of podocyte major processes and their expression in glomerular crescents supports their role in crescent formation *Kidney Int.*, *83*(1), 63-71.

Sotelo, C (2004). Cellular and genetic regulation of the development of the cerebellar system *Progress in neurobiology*, *72*(5), 295-339.

Squinto, S. P., Aldrich, T. H., Lindsay, R. M., Morrissey, D. M., Panayotatos, N., Bianco, S. M., Furth, M. E., et al (1990). Identification of functional receptors for ciliary neurotrophic factor on neuronal cell lines and primary neurons *Neuron*, *5*(6), 757-66.

Srinivasan, Y., Elmer, L., Davis, J., Bennett, V., & Angelides, K (1988). Ankyrin and spectrin associate with voltage-dependent sodium channels in brain *Nature*, *333*(6169), 177-80.

Susuki, K., & Rasband, M. N (2008). Molecular mechanisms of node of Ranvier formation. *Current Opinion in Cell Biology*, *20*(6), 616-623.

Tait, S., Gunn-Moore, F., Collinson, J. M., Huang, J., Lubetzki, C., Pedraza, L., Sherman, D. L., et al (2000). An oligodendrocyte cell adhesion molecule at the site of assembly of the paranodal axo-glial junction *J. Cell Biol.*, *150*(3), 657-66.

Thaxton, C., Pillai, A. M., Pribisko, A. L., Dupree, J. L., & Bhat, M. A (2011). Nodes of Ranvier Act as Barriers to Restrict Invasion of Flanking Paranodal Domains in Myelinated Axons. *Neuron*, *69*(2), 244-257.

Traka, M., Dupree, J. L., Popko, B., & Karagogeos, D (2002). The neuronal adhesion protein TAG-1 is expressed by Schwann cells and oligodendrocytes and is

localized to the juxtaparanodal region of myelinated fibers *J. Neurosci.*, *22*(8), 3016-24.

Trapp, B. D., Peterson, J., Ransohoff, R. M., Rudick, R., Mörk, S., & Bö, L (1998). Axonal transection in the lesions of multiple sclerosis *The New England journal of medicine*, *338*(5), 278-85.

Vabnick, I., Trimmer, J. S., Schwarz, T. L., Levinson, S. R., Risal, D., & Shrager, P (1999). Dynamic potassium channel distributions during axonal development prevent aberrant firing patterns *The Journal of neuroscience : the official journal of the Society for Neuroscience*, *19*(2), 747-58.

Voas, M. G., Glenn, T. D., Raphael, A. R., & Talbot, W. S (2009). Schwann cells inhibit ectopic clustering of axonal sodium channels *J. Neurosci.*, *29*(46), 14408-14.

Volkmer, H, Leuschner, R., Zacharias, U., & Rathjen, F. G (1996). Neurofascin induces neurites by heterophilic interactions with axonal NrCAM while NrCAM requires F11 on the axonal surface to extend neurites *J. Cell Biol.*, *135*(4), 1059-69. Retrieved from

Volkmer, H, Zacharias, U., Nörenberg, U., & Rathjen, F. G (1998). Dissection of complex molecular interactions of neurofascin with axonin-1, F11, and tenascin-R, which promote attachment and neurite formation of tectal cells *J. Cell Biol.*, *142*(4), 1083-93. Retrieved from

Wang, H., Kunkel, D. D., Martin, T. M., Schwartzkroin, P. A., & Tempel, B. L (1993). Heteromultimeric K+ channels in terminal and juxtaparanodal regions of neurons *Nature*, *365*(6441), 75-9.

William F Brown; Charles Francis Bolton; Michael J Aminoff (2002). *Neuromuscular function and disease : basic, clinical, and electrodiagnostic aspects*. Publisher Saunders

Xiao, Z. C., Bartsch, U., Margolis, R. K., Rougon, G., Montag, D., & Schachner, M (1997). Isolation of a tenascin-R binding protein from mouse brain membranes. A phosphacan-related chondroitin sulfate proteoglycan *The Journal of biological chemistry*, *272*(51), 32092-101.

Xu, M., Cao, R., Xiao, R., Zhu, M. X., & Gu, C (2007). The axon-dendrite targeting of Kv3 (Shaw) channels is determined by a targeting motif that associates with the

T1 domain and ankyrin G *The Journal of neuroscience : the official journal of the Society for Neuroscience*, *27*(51), 14158-70.

Yamaguchi, Y (2000). Lecticans: organizers of the brain extracellular matrix *Cellular and molecular life sciences : CMLS*, *57*(2), 276-89.

Yan, Y., Scott, D. J., Wilkinson, T. N., Ji, J., Tregear, G. W., & Bathgate, R. A (2008). Identification of the N-linked glycosylation sites of the human relaxin receptor and effect of glycosylation on receptor function *Biochemistry*, *47*(26), 6953-68.

Yap, C. C., Vakulenko, M., Kruczek, K., Motamedi, B., Digilio, L., Liu, J. S., & Winckler, B (2012). Doublecortin (DCX) mediates endocytosis of neurofascin independently of microtubule binding *J. Neurosci.*, *32*(22), 7439-53.

Zhou, D., Lambert, S., Malen, P. L., Carpenter, S., Boland, L. M., & Bennett, V (1998a). AnkyrinG is required for clustering of voltage-gated Na channels at axon initial segments and for normal action potential firing *The Journal of cell biology*, *143*(5), 1295-304.

Zhou, F., Su, J., Le Fu, Yang, Y., Zhang, L., Wang, L., Zhao, H., et al (2008). Unglycosylation at Asn-633 made extracellular domain of E-cadherin folded incorrectly and arrested in endoplasmic reticulum, then sequentially degraded by ERAD *Glycoconjugate journal*, *25*(8), 727-40.

Zhou, L., Zhang, C. L., Messing, A., & Chiu, S. Y (1998b). Temperature-sensitive neuromuscular transmission in $K_v1.1$ null mice: role of potassium channels under the myelin sheath in young nerves *The Journal of neuroscience : the official journal of the Society for Neuroscience*, *18*(18), 7200-15.

Zonta, B., Desmazieres, A., Rinaldi, A., Tait, S., Sherman, D., Nolan, M., & Brophy, P (2011). A Critical Role for Neurofascin in Regulating Action Potential Initiation through Maintenance of the Axon Initial Segment. *Neuron*, *69*(5), 945-956.

Zonta, B., Tait, S., Melrose, S., Anderson, H., Harroch, S., Higginson, J., Sherman, D. L., et al (2008). Glial and neuronal isoforms of Neurofascin have distinct roles in the assembly of nodes of Ranvier in the central nervous system *J. Cell Biol.*, *181*(7), 1169-77.

de Bernabé, D. B., Currier, S., Steinbrecher, A., Celli, J., van Beusekom, E., van der Zwaag, B., Kayserili, H., et al (2002). Mutations in the O-mannosyltransferase

gene POMT1 give rise to the severe neuronal migration disorder Walker-Warburg syndrome *American journal of human genetics*, *71*(5), 1033-43.

van den Steen, P. E., Opdenakker, G., Wormald, M. R., Dwek, R. A., & Rudd, P. M (2001). Matrix remodelling enzymes, the protease cascade and glycosylation *Biochimica et biophysica acta*, *1528*(2-3), 61-73.